A Study on Surface Nano-Modification by Dopant Ion Irradiation

ドーパントイオン照射による表面ナノ改質の素過程に関する研究

February 2009

Waseda University
Faculty of Science and Engineering
Nanoscience-Nanoelectronics

Takefumi Kamioka

Contents

1 Introduction **1**

1.1 Background and Motivation 1

1.2 Overview of Dissertation 9

2 Development of the System for Real-time Scanning Tunneling Microscope Observation of Dopant Ion Irradiation Effects on Solid Surface **14**

2.1 Development of Liquid-Metal-Ion-Source Low-Energy Ion Gun / High-Temperature Ultrahigh Vacuum Scanning Tunneling Microscope Combined System (LMIS-IG/STM) 15

2.1.1 Description of the System 15

2.1.2 Preliminary Observations of the Irradiated Si(111)-7 × 7 Surface with Si^{2+} Ions at High Temperature 23

2.2 Development of an Ion Beam Alignment System for Real-Time Scanning Tunneling Microscope Observation of Dopant-Ion Irradiation Effects 27

2.2.1 Ion Beam Alignment System Using Absorbed Current Image 28

2.2.2 Preliminary Results of Real-Time STM Observation of Si Surfaces Irradiated with P^{+} Ions 34

2.3 Summary of Chapter 2 39

3 Real-Time Scanning Tunneling Microscope Observation of Silicon Sur-

face Modified by Gold Ion Irradiation 41
3.1 Introduction 41
3.2 Experiment 44
3.3 Results and Discussion 46
3.4 Summary of Chapter 3 57

4 Real-Time Scanning Tunneling Microscope Observation of Silicon Surface Modified by Phosphorus Ion Irradiation 61
4.1 Experiment 63
4.2 Modification on Si(111) Surface 65
4.2.1 Morphological Change by Ion Irradiation and During Heat Treatment 65
4.2.2 Surface Modification by Additional Ion Irradiation onto the Same Surface 72
4.2.3 Behavior of Point Defects 80
4.3 Modification on Si(001) surface 94
4.3.1 Morphological Change by Ion Irradiation and During Heat Treatment 94
4.3.2 Segregation of Phosphorus Atoms toward Surface 98
4.4 Summary of Chapter 4 101

5 Conclusion 104

ACKNOWLEDGMENTS 106

List of Publications 108

List of Figures

1.1 Architecture of Si-based MOS transistor (n-type). 6

1.2 Implantation-induced defects. 7

1.3 Real-time STM observation of ion irradiation effects. Real-time observation means that (a) the surface modification with ions can be observed just after ion irradiation, and (b) the observation area can be kept before and after ion irradiation. 8

1.4 Purpose of this work. By realizing real-time STM observation for dopant ion irradiation effects such as morphological and electrical change on surface, the atomistic behavior of implanted atoms and point defects are addressed. 11

2.1 Schematic diagram of the LMIS-IG/STM. 18

2.2 Picture of the LMIS-IG/STM. 19

2.3 Our home-made LMIS. (a) Illustration of an LMIS, and (b) an actual LMIS (P-Pt-Ni). 20

2.4 Accelerating voltage dependence of an ion beam current at a sample position of LMIS-IG/STM. 21

2.5 Successive STM images of the Si(111) surface at 510℃; (a) 80 s before, (b) during, and (c) 80 s after 500 eV Si^{2+} ion irradiation. The images were taken with constant current mode and at a scan speed of 80 s/image (Dose: about $3 \times 10^{14} cm^{-2}$, It: 0.06 nA, Vs: 1 V). 25

2.6 Successive STM images of the Si(111) surface at 500℃; 80 s, 240 s, 720 s, 880 s, and 960 s after 500 eV Si^{2+} ion irradiation (Constant current mode, It: 0.03 nA, Vs: 1V, Dose: $1.3 \times 10^{12} cm^{-2}$). 26

2.7 Schematic of the ion beam alignment system. The developed ion beam alignment system is composed of two setups: the absorbed current image (AEI) unit to visualize an ion-irradiated area and the dummy-target as an ion beam alignment mark. 31

2.8 Experimental setups and the AEI images viewed from the direction of the axis of ion gun; (a) arrangement of a sample and STM tip and (b) their actual AEI images. (c) The dummy sample positioned in front of the sample, and (d) an AEI image of the alignment mark on the dummy sample. The inset shows the magnified drawing of the alignment mark. The dashed line in the image corresponds to the slot on the head of the screw. 32

2.9 Experimental procedures for real-time STM observation of ion irradiation process; (a) the improved and (b) the conventional protocol. The experiment proceeds two steps: the preparation and the observation steps. In the conventional protocol, ion beam is interrupted after ion beam alignment. After waiting for recovery of UHV, a sample is prepared by heat treatment. Then ion beam is re-emitted and STM observation is started. In the improved protocol, a sample is prepared at first and ion beam is aligned. Then STM observation is started without interruption of ion beam. 33

2.10 Sequential STM images of Si(111)-7×7 surface (a) before, (b) during and (c) after the 5 keV-P^+ ion irradiation taken at R.T. Each image was taken with constant-height mode (current images); sample bias: 1.1 V, tunneling current: 0.2 nA, scan speed: 12 s/image, ion dose: $2.5 \times 10^{14} cm^{-2}$. 37

2.11 Sequential STM images of Si(111)-7×7 surface (a) before, (b) during and (c) after the 5 keV-P^+ ion irradiation taken at 500℃. Each image was taken with constant-height mode (current images); sample bias: 0.3 V, tunneling current: 0.2 nA, scan speed: 23 s/image, ion dose: $2 \times 10^{14} cm^{-2}$. 38

3.1 Experimental procedure of real-time STM observation of Au^+ ion irradiation effects on high-temperature Si surface. 45

3.2 Sequential STM images of Si(111)-7 × 7 surface kept at 500℃ (a) before, (b) during and (c) after Au^+ ion irradiation (Ion energy: 3 keV, Dose: $3 \times 10^{14} cm^{-2}$. Each image was taken with constant height mode (current image); sample bias: 1.5 V, tunneling current: 0.2 nA, scan speed: 12 s/image. 51

3.3 Sequential STM images of Au^+ ion irradiated Si(111) surface kept at 500℃; (a) 79 s, (b) 111, and (c) 731 s after the ion irradiation. Some modified sites on the surface are labeled by the alphabet " a " ∼" h" 52

3.4 (a) STM image of a modified site formed by Au ion irradiation taken at RT (current image, sample bias: 1.2 V, tunneling current: 0.1 nA), (b) its partial magnified image ($4nm \times 4nm$), and (c) atomic arrangement of 5 × 2-Au structure proposed by Erwin's model (ref. [19]). 53

3.5 Comparison of 5×2-Au area size by ion energy. Au^+ ions are irradiated onto Si(111)-7×7 surfaces kept at 500℃ with different ion energies; (a) 500 eV, (b) 1 keV and (c) 5 keV. The image (a) is taken at 500℃, 10 s after ion irradiation; The images (b) and (c) are taken at R.T. after being quenched 10 s after ion irradiation. Each ion dose is about $2 \times 10^{14} cm^{-2}$. Below each STM image ($80nm \times 80nm$), 7×7 and 5×2-Au areas are indicated as white area and hatched area, respectively. 54

3.6 Time evolution of size of a 5×2-Au area and each vacancy cluster after ion irradiation. The origin of the time scale corresponds to the beginning of the ion irradiation. Circle mark indicates the 5×2-Au area on terrace corresponding the structure " h " in Fig. 3.2(a), and the other marks indicates each vacancy cluster corresponding to the defects " a "∼ "g " in Fig. 3.2(a), respectively. 55

3.7 Distribution of Au ion calculated by TRIM (ref. [27]). (a) Ion tracks formed by Au ion implantation; Target material: amorphus-Si, Incident angle of ions: 60°, Ion energy: 3 keV, Numer of incident ions (simulated times of ion incidents): 10000. (b) Existing probability of Au ion as a function of depth. 56

4.1 Experimental procedure of real-time STM observation of P^+ ion irradiation effects on high-temperature Si surface. 64

4.2 Sequential STM images of 600℃-Si(111)-7×7 surface taken (a) before, (b) during, and (c) after the ion irradiation. Ion species is P^+ with 5 keV and dose is $5.4 \times 10^{13} cm^{-2}$. Each image was scanned with constant height mode at a scan speed of 60 s/image. Sample bias is +1 V and tunneling current is 0.2 nA. 67

4.3 Comparison of ion-irradiated surfaces between R.T. and high-temperature [Referred in *T. Kamioka et al., Rev. Sci. Technol.* ***79*** *(2008) 073707*]. Ion species: 5 keV-P$^+$, Dose: $2.5 \times 10^{14} cm^{-2}$ at R.T. and $2 \times 10^{14} cm^{-2}$ at 500℃. 68

4.4 Sequential STM images of 600℃-Si(111)-7×7 surface taken at (a) 108 s after, (b) 466 s after, and (c) 1576 s after the ion irradiation. Each image was scanned with constant height mode at a scan speed of 60 s/image. Sample bias is +1 V and tunneling current is 0.2 nA. 69

4.5 Time development of the number density of vacancy islands. The sample area size is $734 nm \times 867 nm$. Vacancy islands smaller than about $10 nm^2$ are not counted. 70

4.6 Step motion and evolution of vacancy islands before, after ion irradiation. 71

4.7 STM images of Si(111) surface at 600℃ before and after the second ion irradiation. Dose is $5.4 \times 10^{13} cm^{-2}$. Kinks sites are indicated by arrows. 74

4.8 Step motion and evolution of vacancy islands before, after the second ion irradiation. Dotted circle indicates the overlapped vacancy islands between before and after the ion irradiation. 75

4.9 STM images of Si(111) surface at 500℃ before and after the second ion irradiation. Dose is $6.3 \times 10^{13} cm^{-2}$. 76

4.10 STM images of Si(111) surface kept at 500℃ modified with intermittent ion irradiations. Dose at each time: $6.3 \times 10^{13} cm^{-2}$, Vs: +1 V, It: 0.2 nA. 77

4.11 Transition of the step edges and vacancy islands just after each ion irradiation. (a) 1590 s after the first ion irradiation, (b) 56 s after the second ion irradiation, and (c) 64 s after the fourth ion irradiation. . 78

4.12 Magnified images of vacancy islands near the step edge taken before and after the ion irradiation. Scan area size is $141nm \times 141nm$. 5 keV-P$^+$ ions were irradiated on to 500℃-Si(111) surface to a dose of $6.3 \times 10^{13} cm^{-2}$. 79
4.13 Time evolution of surface vacancies after the first ion irradiation at 600℃. 83
4.14 Time evolution of surface vacancies after ion irradiation at 600℃. Note that $t = 0$ corresponds to at the end of the second ion irradiation. 84
4.15 Time evolution of surface vacancies after ion irradiation at 500℃. Note that $t = 0$ corresponds to at the end of the second ion irradiation. 85
4.16 $\Delta N_{surfvac}$ denotes the net increase in the number of surface vacancies introduced by each ion irradiation. This value eliminates the variation in the number of surface vacancies during the time interval between each ion irradiation. 86
4.17 Density of atoms reached surface as a function of ion dose. 87
4.18 The density of surface vacancies in each segment on the terrace. Regions “ A ”, “ B ”, and ”C ” correspond to the regions in the above image, respectively. 88
4.19 Possible mechanisms of decay of vacancy islands; (a) supply of adatoms from the step edge, (b) emission of vacancies from the vacancy island, and (c) supply of interstitials from the bulk. 89
4.20 Preparation of TEM sample. A Si(001) substrate is irradiated with 5keV-P$^+$ ions at 500℃ and then quenched at 180 s after the ion irradiation. 90

4.21 Cross-section TEM images of (110) plane of Si(001) substrate. (a) Ion-irradiated sample with 5 keV-P^+ ions to a dose of about $10^{15}-10^{16} cm^{-2}$ at 500℃. The sample was quenched at 150 s after the ion irradiation. (b) Sample without ion irradiation. 91

4.22 Magnified cross-section TEM images of (110) plane of the ion-irradiated Si(001) substrate. The sample was irradiated with 5 keV-P^+ ions to a dose of about $10^{15}-10^{16} cm^{-2}$ at 500℃, then was quenched at 150 s after the ion irradiation. 92

4.23 Sequential STM images of 500℃-Si(001)-2×1 surface taken (a) before, (b) during, and (c) after the ion irradiation. Ion species is P^+ with 5 keV and dose is $4\times 10^{13} cm^{-2}$. Each image was scanned with constant height mode at a scan speed of 60 s/image. Sample bias is -2.6 V, and tunneling current is 0.08 nA. 96

4.24 Sequential STM images of 500℃-Si(001)-7×7 surface taken (a) 60 s after, and (b) 1631 s after the ion irradiation. Each image was scanned with constant height mode at a scan speed of 60 s/image. Sample bias is +1 V and tunneling current is 0.08 nA. 97

4.25 Growth rate of surface defect size along perpendicular and parallel to Si(001)-2×1 dimmer. “ A ”- ”E ” are sampled vacancy islands in the observation area. The Black and blue lines correspond to the components of each vacancy size parallel and perpendicular to the dimmer on the terrace. 99

4.26 Si(001) surface modified with 3 keV-P^+ ions taken at R.T. Sample surface was first irradiated at 500℃ and annealed at the same temperature, then was quenching to R.T. Observation mode: Topography, Vs: -2.4 V, It: 0.5 nA. 100

List of Tables

2.1 Comparison of LMIS-IG/STM with IG/STM. 22

4.1 Comparison of density of observed surface vacancies after the ion irradiation with ion dose and estimated sputtered atoms. 93

Chapter 1

Introduction

1.1 Background and Motivation

In the silicon (Si) based metal-oxide-semiconductor (MOS) technology (Fig. 1.1), dopant atoms are implanted into Si substrates for a variety of purposes, such as fabrication of p-wells and n-wells in complementary-MOS (CMOS) devices, adjustment of conductivity of channel regions, and formation of source/drain electrodes. Today ion implantation is the most commonly used technique for the doping method because of the high reproducibility in the position and dose of dopants, which is determined by host materials, acceleration energy of ions, and ion beam current. Since the device performance depends on the distribution of activated dopants, precise control of doping is needed.

As the dimensions of the MOS device are scaled down, several issues have emerged in regard to the control of the doping. In order to avoid short-channel effects, the junction depth of source/drain extension must be reduced. The required junction depth is about 10 nm for CMOS transistor for 22-nm generation as stated in the International Technology Roadmap for Semiconductors (ITRS) edition 2007 [1]. Different techniques have been proposed to improve the junction

depth, such as low-energy ion implantation and cluster-ion implantation followed by flash and laser thermal annealing. Also, decrease of the total number of dopants in the channel region could cause statistical fluctuation of each device performance. One of the cutting edge technology demonstrated that the threshold voltage (V_T) can be controlled by the precise control in the number and position of dopants [2].

During ion implantation, dopants are scattered by the collision with host atoms. Postimplant thermal process, which is required to recover the implantation damages and to electrically activate the implanted dopants, also causes significant diffusion of dopants. In addition, more size related effects such as dopant behavior in the vicinity of surface become prominent since dopants tend to segregate in the vicinity of surface. Thus, the interaction between implanted atoms and host materials need to be understood in atomic and nm scale.

Dopant behavior is influenced by the presence of defects in the substrates. For instance, diffusion of dopants in Si is mediated by point defects such as vacancies and interstitials. When ions are implanted into a substrate, excess point defects are generated (Fig. 1.2), so that the dopant diffusion is much affected by them. This phenomenon is well known as transient enhanced diffusion (TED) [3], which causes the unintentional spreading of the initial dopant profile. Also, dopants interact with point defects to form complex defects. During thermal treatment, excess point defects generated by ion implantation clusterize to form extended defects such as 311 defects [1–5], dislocation loops [4], vacant type cavities [6], etc. These defects act as trap sites for dopants, which prevent a complete electrical activation. Furthermore solid surface is regarded as a sink for point defects, so that the dopants could be trapped or segregated there. In order to address the dopant behavior, it is therefore important to reveal the behavior of point defects as control agents of dopants.

Recently there have been many studies to investigate behaviors of point defects. So far to observe point defects directly has been believed to be hardly possible.

However, when point defects agglomerate to form clusters, they are visible by microscopy methods such as transmission electron microscope (TEM), scanning reflection electron microscope (SREM), and scanning tunneling microscope (STM). The evolution and disappearance of implantation induced defects in bulk such as 311 defects, dislocation loops were observed using TEM [3–5]. Cross-section and plan-view microscopy revealed the microstructure of the defects and the evolution of the defects during annealing. Combination of the TEM observations and other analysis such as secondary ion mass spectroscopy (SIMS) clarified the strong interaction between point defects and dopants. Watanabe 's group [7, 8] observed the motion of atomic steps and vacancy islands during argon (Ar) ion irradiation using high-resolution SREM. The kinetics of vacancy diffusion and annihilation on the surfaces were derived from the behavior of defect structures such as retreat of steps and evolution of vacancy islands on the surface. Invention of STM has contributed to reveal the atomistic features of individual nm-size defects on solid surfaces. STM is a powerful tool to investigate solid surface in real space with atomic resolution. This probing technique has been used for direct observation of ion irradiation effects on solid surfaces modified with energetic He, Ar and Xe ions. Observations in atomic scale reveal the detailed features of vacant-type surface defects (vacancy clusters) such as shape and size and their evolution after thermal treatments [9–17]. The sizes of vacancy clusters correspond to the number of vacancies near the surfaces, so that their changes by heat treatment can be attributed to migration of point defects [16].

These pioneering works, however, did not focus on the surfaces modified by dopant irradiation. In addition, their STM observations are not in real-time but after the ion irradiations. In order to start STM observation following ion irradiation, it usually takes a few tens of minutes at least until the STM tip reaches the thermal equilibrium with the sample surface. STM observation can not be performed

during the period. This will obscure some of the dynamical aspects of behavior of implanted atoms and point defects.

In order to observe directly the dynamical changes in surface morphologies, our group [18] realized the real-time observation of ion-irradiation effects on solid surfaces by combining the ion-gun and STM (IG/STM) (see Fig. 1.3). The IG/STM with an ion source of rare gas has revealed various interesting features such as formation of vacancy type defects and Si islands on high-temperature Si(111)-7 $\times$ 7 surfaces [18, 19]. One of the most typical results is the direct observation of nucleation, growth, and decay of a vacancy type defect induced by a single Ar ion impact [18]. The evolution of such defects occur as a result of agglomeration and dissolution of vacancies and Si atoms on the surfaces, which are supplied by diffusion of point defects from clusters of point defects generated by ion irradiation. Consequently the IG/STM provided us with a mean to directly observe the behavior of point defects in the vicinity of the surfaces.

However, ion species used in our previous works using the IG/STM was limited to only gas elements such as Ar and Xe due to the lack of capability of implanting dopants, and real-time observation of doping effects had not been realized.

The purpose of the dissertation is to address the atomistic behavior of implanted atoms and point defects by realizing real-time STM observation method for dopant ion irradiation effects (Fig. 1.4). Three aims are included;

The first aim is to develop the system for real-time STM observation of dopant-ion irradiation effects. In order to observe in real-time solid surfaces modified by dopant ion beam, STM observation needs to be continued during the ion gun operation. In addition, dopant ion beam need to be aligned in the STM observation area. Therefore, we have implemented a liquid-metal-ion-source (LMIS) ion gun in the STM observation system, and we have also developed an alignment system suited for dopant-ion beam.

The second aim is to demonstrate that the developed real-time observation system is actually an effective tool for addressing the atomistic picture of implant atoms. In order to see directly the behavior of impurities, Si(111) substrates and gold (Au) atoms are chosen as host materials and impurities, respectively. Since Au atoms in Si diffuse rapidly and Au atoms chemically react with Si atoms on Si(111)-7×7 surface to form reconstructions such as Si(111)-5×2 and $\sqrt{3} \times \sqrt{3}$, behavior of implanted Au atoms can be expected to be distinguished within a short time after ion irradiation. Therefore, we have performed real-time observations of surfaces modified with Au atoms.

The third aim is to discuss the behavior of point defects in the vicinity of solid surfaces which are irradiated with dopant ions. Implantation induced defects provide an important clue to understand the behavior of point defects. The growth and decay of the defects during thermal treatment could be determined by the balance between vacancy flow and interstitial flow. We have observed phosphorus (P) ion irradiation effects on Si surfaces in real-time.

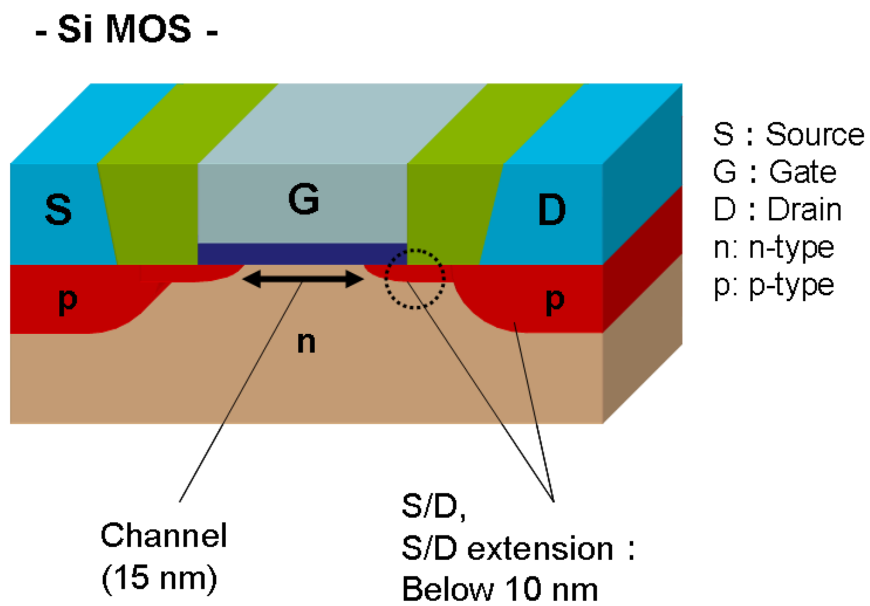

Figure 1.1: Architecture of Si-based MOS transistor (n-type).

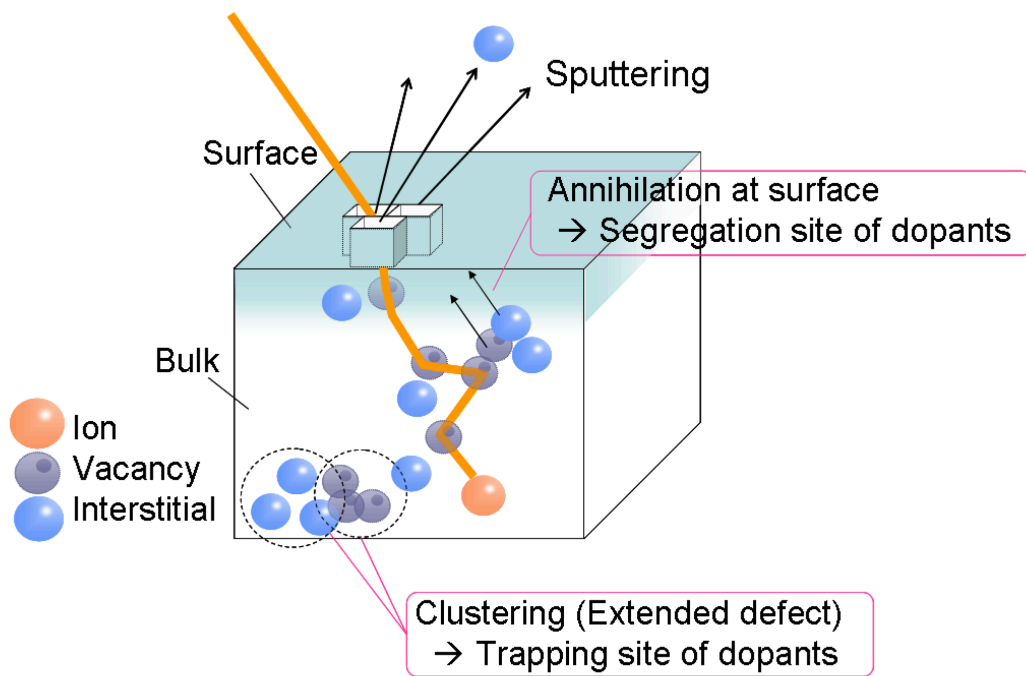

Figure 1.2: Implantation-induced defects.

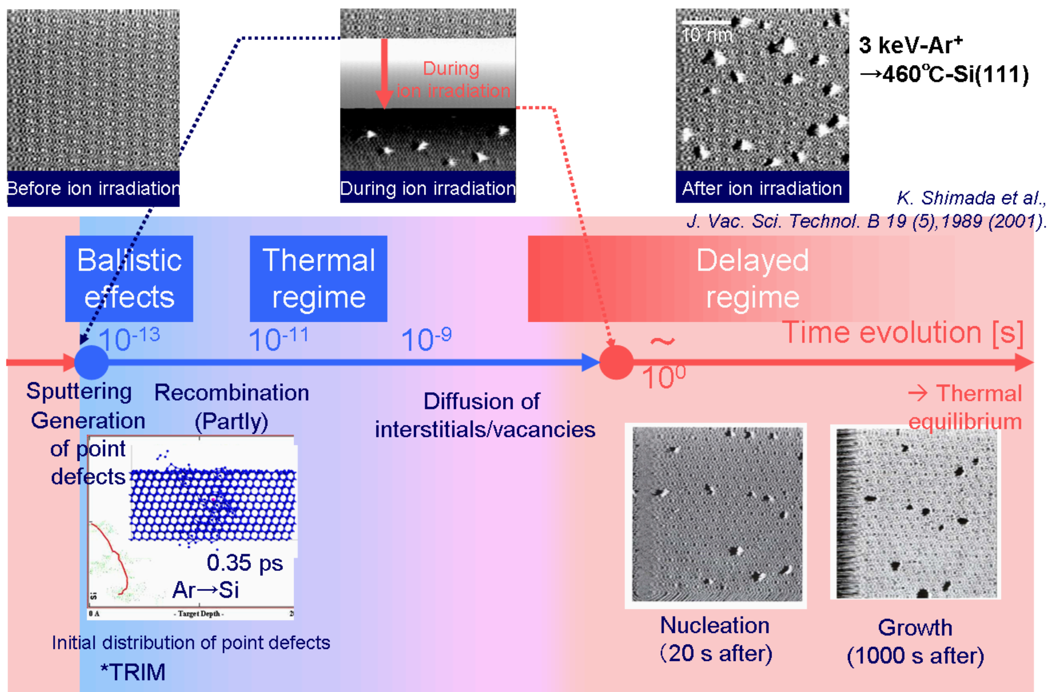

Figure 1.3: Real-time STM observation of ion irradiation effects. Real-time observation means that (a) the surface modification with ions can be observed just after ion irradiation, and (b) the observation area can be kept before and after ion irradiation.

1.2 Overview of Dissertation

The dissertation is composed of five chapters, which sum up our studies on addressing the atomistic behavior of dopants and point defects in nm scale by realizing real-time STM observation of dopant ion irradiation effects on Si surfaces.

In Chapter 2, a newly developed system for real-time scanning tunneling microscope (STM) observation of ion-irradiated solid surface is described: Development of a liquid-metal-ion-source ion gun and STM (LMIS-IG/STM) combined system, and development of a beam alignment system especially for " dopant-ion-beam " are explained in detail.

Our original LMIS-I/STM is composed of an ultra-high-vacuum high-temperature STM (UHV HT-STM) and a low-energy ion-gun with an LMIS. The ion gun is originally designed so that dopant ions are irradiated at the energies lower than 5 keV. After the description of the principle of operation, some basic performances are shown such as mass spectrum of ion beam using a gold (Au) and silicon (Si) LMIS and ion current at a sample position. In addition, as a preliminary experiment, a real-time STM observation of a high-temperature Si(111)-7 $\times$ 7 surface irradiated with Si^{2+} is demonstrated. Next, beam alignment system for " dopant " ion beam is described in detail as a key technique for real-time STM observation especially using LMISs containing dopant elements like P. Since such LMISs have low emission current and short lifetime, we faced a difficulty in aligning the dopant-ion beam in the STM observation area. The beam alignment system is composed of two setups: the absorbed current image (AEI) unit to visualize an ion-irradiated area, and the dummy target as an ion beam alignment mark. Installing the beam alignment system enables us not only to align a dopant-ion beam accurately but also to save the time for preparation of the experiment. Finally, the author realized a real-time STM observation of Si(111)-7 $\times$ 7 surfaces irradiated with P^{2+} for the first time.

In Chapter 3, the author will describe results of a real-time STM observation of Au^+ ion irradiation effects on Si surface. The STM based method enables us to track the change of the surface structures with atomic resolution. For example, Au atoms on Si(111)-7×7 dimer-adatom-stacking fault (DAS) surface are known to form several kinds of reconstructions such as 5×2 and $\sqrt{3} \times \sqrt{3}$ on topmost surface and the atomic arrangements and their composition per each unit cell are well defined. By using these reconstructions as the " rulers in nature ", we can estimate the number of Au atoms involved in the reconstructed domains.

In Chapter 4, some of our results archived up to now are summed up on the surfaces modified with P ion irradiation using Si(111) and Si(001) substrates. There are two major achievements. First, surface modification of Si(111)-7×7 with P ions are reported. Real-time STM observation of P ion irradiation effects are shown for the first time. Ion irradiation causes nucleation of vacancy islands and retreat of step edges, resulting in removal of surface atoms. Behavior of point defects is discussed in terms of number of diffused point defects toward surface. Second, surface modification of Si(001)-2×1 with P ions are reported. After the ion irradiation, vacancy islands and Si-P hetero-dimers seems to appeared on the surface. Since there is no signature of P on the initial surface, the observed P atoms is supplied from the substrate after the ion irradiation. Segregation of P atoms at surface and interface is generally supposed to degrade of device performance so that the mechanism needs to be clear from the technological view point. The results in the section are positioned as an early stage to address the atomistic behavior of dopants and a future subject is presented.

In Chapter 5, the author concludes the dissertation.

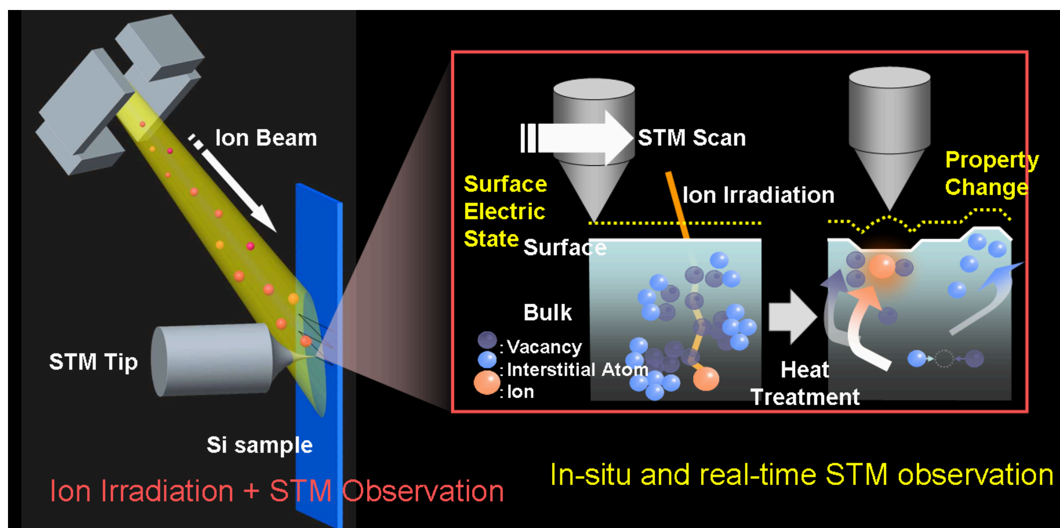

Figure 1.4: Purpose of this work. By realizing real-time STM observation for dopant ion irradiation effects such as morphological and electrical change on surface, the atomistic behavior of implanted atoms and point defects are addressed.

References

[1] 2007 ITRS JEITA (Japanese), p.37 in the Front End Process (FEP) section.

[2] T. Shinada, S. Okamoto, T. Kobayashi, and I. Ohdomari: Nature **437** (2005) 1128.

[3] P. A. Stolk, H. -J. Gossmann, D. J. Eaglesham, D. C. Jacobson, C. S. Rafferty, G. H. Gilmer, M. Jaraiz, J. M. Poate, H. S. Luftman, and T. E. Haynes: J. Appl. Phys. **81** (1997) 6031.

[4] F. Cristiano, Y. Lamrani, F. Severac, M. Gavelle, S. Boninelli, N. Cherkashin, O. Marcelot, A. Claverie, W. Lerch, S. Paul, and N. Cowern: Nucl. Instrum. Meth. B **253** (2006) 68.

[5] A. Agarwal, H. -J. Gossmann, D. J. Eaglesham, L. Pelaz, D. C. Jacobson, J. M. Poate, and T. E. Haynes: Mater. Sci. Eng. A **253** (1998) 269.

[6] G. Gaudina, F. Cayrela, C. Bongiornob, R. Jerisiana, C. Duboisc, V. Rainerib, and D. Alquiera: Mater. Sci. Eng. B **124-125** (2005) 266.

[7] H. Watanabe and M. Ichikawa: Appl. Phys. Lett. **68** (1996) 2514.

[8] H. Watanabe and M. Ichikawa: Phys. Rev. B **55** (1997) 9699.

[9] P. Bedrossian and T. Klitsner: Phys. Rev. B **44** (1991) 44.

[10] P. Bedrossian: Surf. Sci. **301** (1994) 223.

[11] B. S. Swartzentruber, C. M. Matzke, D. L. Kendall, and J. E. Houston: Surf. Sci. **329** (1995) 83.

[12] K. Yoneyama and K. Ogawa: Jpn. J. Appl. Phys. **35** (1996) 3719.

[13] Y. Wei, L. Li, and I. S. T. Tsong: Nucl. Instrum. Meth. B **115** (1996) 572.

[14] P. J. Bedrossian, M. -J. Caturla, and T. Diaz de la Rubia: Appl. Phys. Lett. **70** (1997) 176.

[15] K. Kyuno, D. G. Cahill, and R. S. Aveback: Phys. Rev. Lett. **83** (1999) 4788.

[16] T. Seki, T. Aoki, J. Matsuo, and I. Yamada: Nucl. Instrum. Meth. B **164-165** (2000) 650.

[17] J. C. Kim, D. G. Cahill, and R. S. Averback: Surf. Sci. **574** (2005) 175.

[18] K. Shimada, T. Ishimaru, T. Yamawaki, M. Uchigasaki, K. Tomiki, T. Matsukawa, and I. Ohdomari: J. Vac. Sci. Technol. B **19** (2001) 1989.

[19] M. Uchigasaki, K. Tomiki, T. Kamioka, E. Nakayama, T. Watanabe, and I. Ohdomari: Jpn. J. Appl. Phys. Part 2 **44** (2005) L313.

Chapter 2

Development of the System for Real-time Scanning Tunneling Microscope Observation of Dopant Ion Irradiation Effects on Solid Surface

In this chapter, a newly developed system for real-time observation of dopant ion irradiation effects of solid surfaces is described. We have added some new features to the original IG/STM. Development of a beam alignment system is also explained as a key technique for real-time STM observation especially using LMISs containing dopant elements such as P.

2.1 Development of Liquid-Metal-Ion-Source Low-Energy Ion Gun / High-Temperature Ultrahigh Vacuum Scanning Tunneling Microscope Combined System (LMIS-IG/STM)

The replacement of ion gun for rare gases with LMIS ion gun has enabled the implantation of various ion species. Improvement in ion optics and pumping system has made possible the low energy implantation and improved evacuation speed. In this section, development of our original liquid-metal-ion-source ion gun / high-temperature ultrahigh vacuum scanning tunneling microscope combined system (LMIS-IG/STM) is described. After the necessity for the LMIS-IG/STM is explained, the performance of the LMISIG/STM and the Si ion self-implantation effects, which as a preliminary experiment of P ion implantation, are reported.

2.1.1 Description of the System

The LMIS-IG/STM is composed of the low-energy LMIS ion gun (Biemtron Co. Ltd., UNSYS) and the high-temperature UHV STM unit (JEOL JSPM-4610S). A schematic and a picture of the LMIS-IG/STM are shown in Fig. 2.1 and Fig. 2.2, respectively. A special feature of this system is that LMIS-IG is installed. Our LMIS-IG has a “ U-shape ” refractory metal frame to which a sharp metal tip is spot welded (Fig. 2.3). The LMIS-IG can hold a metal alloy that contains dopant ion species. In the ionization chamber, an LMIS can emit various ions from a sharp metal tip by applying high voltage. The ion acceleration voltage is controlled within the range of 0-5 kV by changing the electrostatic potential of the cathode. The ions extracted from the ionization chamber are selected by an $E \times B$ mass separator, decelerated by the retarding lens system and irradiated onto a sample surface. A

Faraday cage is inserted into an ion beam path for measuring ion beam current. The ion incident angle is tilted to 60° with respect to the surface normal in order to minimize channeling in crystalline Si substrates. The implanted specimens can be flash annealed by resistive heating, and kept at a high temperature (400-600℃) during STM observation [1]. This system enables us to observe real-time STM images of sample surfaces at high temperatures during ion irradiation.

The special features of LMIS-IG/STM system are compared with the IG/STM as shown in Table 2.1.1. A variety of ions come from various alloys that contain required ion species. One special feature of the LMIS-IG/STM is the capability of hitting the selected target area with various ion species just by changing $E \times B$ parameters, which enables the in-situ investigation of, for example, co-doping effect of donor and acceptor ions. In addition, LMIS is effective in keeping the ionization chamber at high vacuum because a source gas is not necessary. Even better vacuum can be achieved by choosing a metal alloy for a particular ion species with keeping a proper vapor pressure, which results in higher ion emissivity. All these features have made a differential pumping unnecessary and made it possible to keep good vacuum without using turbo-molecular pump (TMP) and rotary pump (RP) that inevitably induce high mechanical noise. One more merit of the LMIS is the lower fluctuation in initial energy. Compared to a gas source type that has the fluctuation of 20-50 eV due to the fluctuation in ion position upon extraction, LMIS has eventually a point source and has the fluctuation of 10 eV or less.

The drawbacks of LMIS are the lower ion current and shorter life compared to a gas source. Lifetime of LMIS is one of our greatest concerns, because it is essential for long use without changing ion optics. The factors that deteriorate LMIS are the preferential sublimation of an element for particular ion species from the alloy and corrosion of filament frame metal by the alloying. Good choice of the alloys is the only solution to solve the problem.

In order to understand the mechanism of solid surface modification with each ion in terms of electrical activation of the implanted ions, shallow ion distribution is necessary for STM observation. We have designed the ion acceleration energy to be 100 eV and the ion incident angle to be 60° from surface normal. By doing it this way, the projected range (R_p) of most metal ions stays within a range of 0.3-1.1 nm. The low acceleration energy of 100 eV, however, tends to spread ion beam. For compatibility between low acceleration energy and not too wide spread of ion beam, we have electrically floated the whole ion optics and prepared a special ground in the ion gun [2–4]. This ground can be biased -5 kV to the earth potential. The potentials necessary for extraction, focusing, and deflection of the ion beam are supplied to the ground. This enables high-speed ion transport in the ion gun and the subsequent deceleration by the potential difference between the exit of ion gun and the target at the earth potential.

Figure 2.4 shows the ion beam current as a function of acceleration voltage, which is measured at a sample position of the LMIS-IG/STM. In order to observe the ion incidence and the subsequent phenomena in-situ with STM, one ion incidence per second in the area of $20 \times 20 nm^2$ is required. This corresponds to a dose rate of $2.5 \times 10^{11} cm^{-2} s^{-1}$ and the ion current of 1.2 nA. As shown in Fig. 2.4, the lowest Si^+ ion current exceeds the necessary value even at the extremely low acceleration voltage of 10 V. The beam diameter is about 3 mm at the acceleration voltage of 300 eV. This value is good enough for irradiating a whole target area. Observation of a selected target area with STM can also be done without any problems.

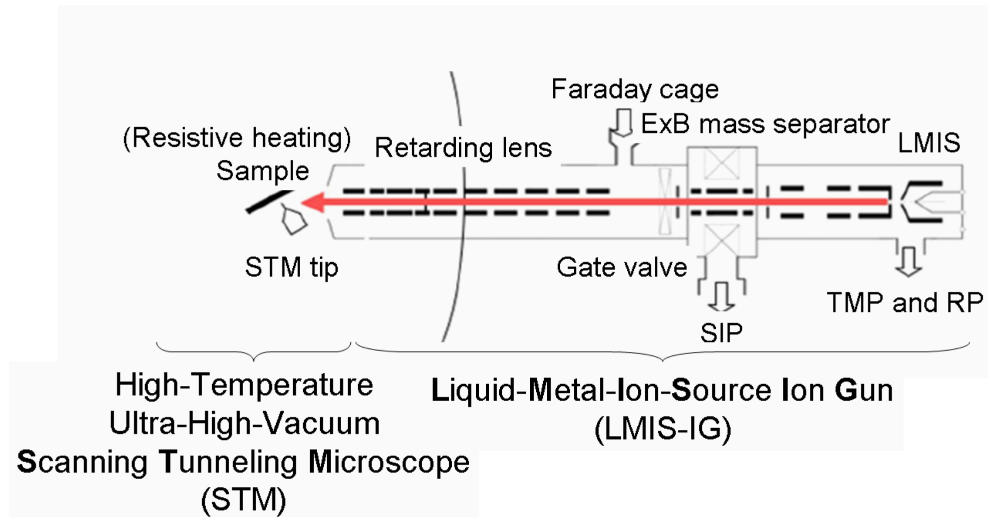

Figure 2.1: Schematic diagram of the LMIS-IG/STM.

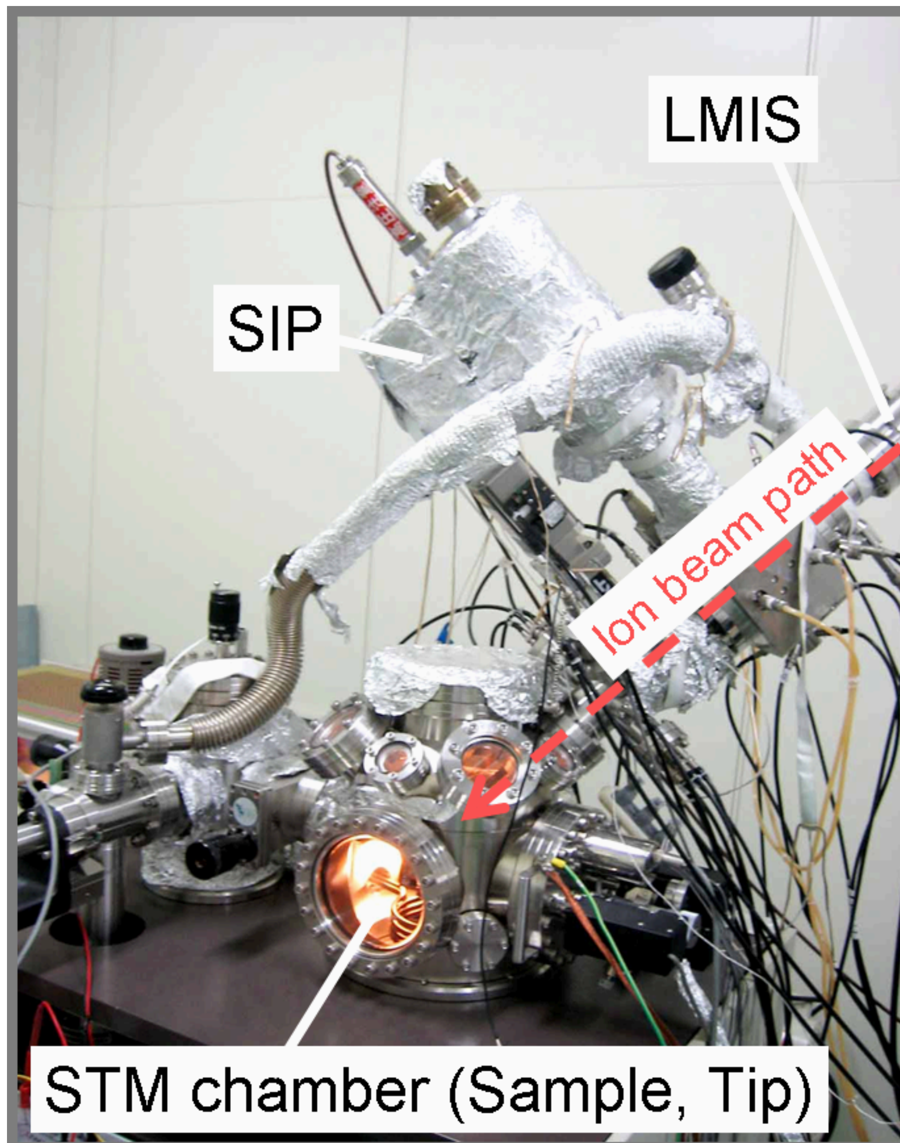

Figure 2.2: Picture of the LMIS-IG/STM.

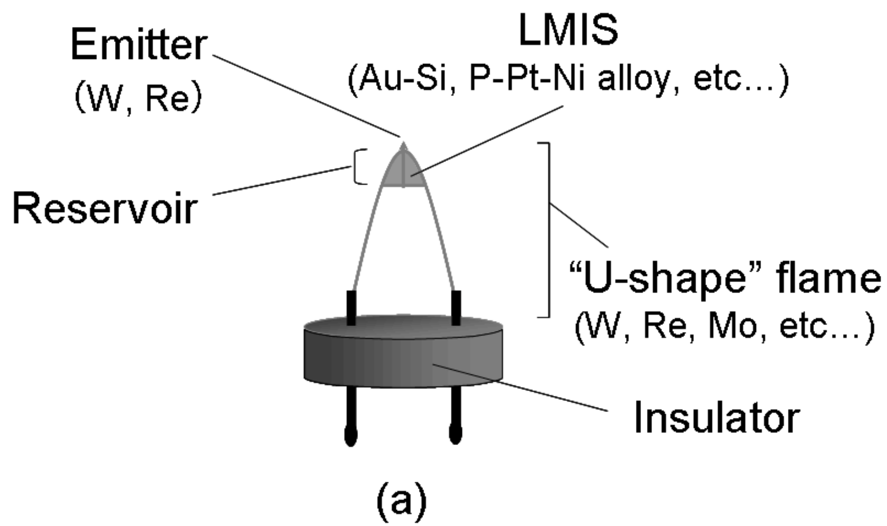

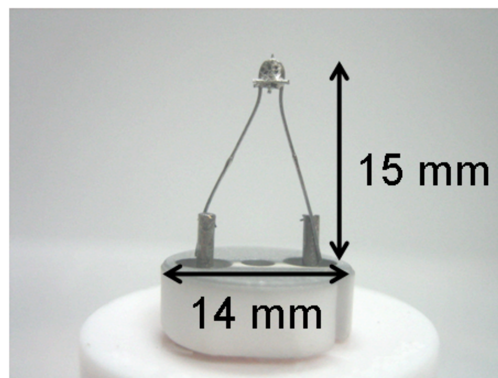

Figure 2.3: Our home-made LMIS. (a) Illustration of an LMIS, and (b) an actual LMIS (P-Pt-Ni).

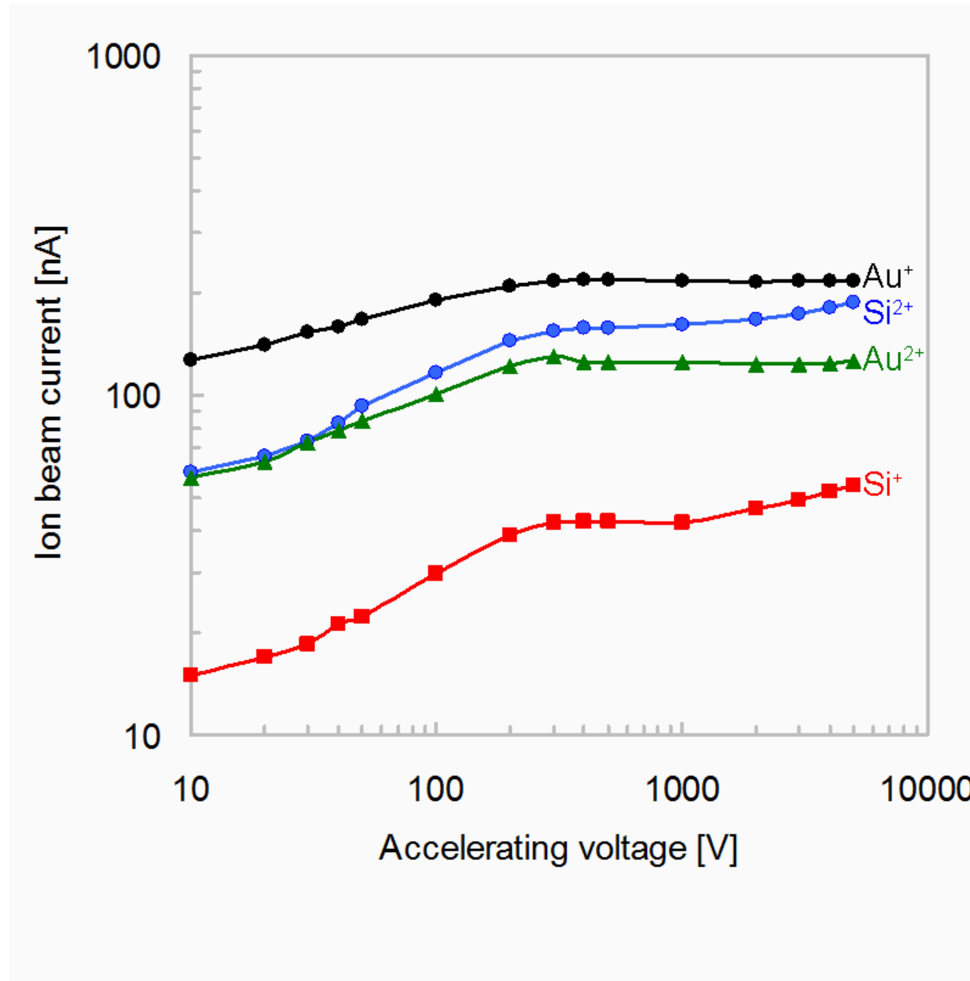

Figure 2.4: Accelerating voltage dependence of an ion beam current at a sample position of LMIS-IG/STM.

Table 2.1: Comparison of LMIS-IG/STM with IG/STM.

Ionization type	LMIS
Ion species	B, Si, P, Mn, Fe, Co, Ni, Cu, Ga, Ge, As, Pd, In, Sb, Pt, Au
Pressure of ionization chamber	10^{-5} Pa
TMP operation	OFF
Pressure of main chamber (during ion irradiation)	10^{-7} Pa
Ion acceleration voltage	10 V − 5 kV

2.1.2 Preliminary Observations of the Irradiated Si(111)-7×7 Surface with Si^{2+} Ions at High Temperature

There are two reasons for choosing Si as an implant species in the preliminary observation. Firstly a Si LMIS has a long lifetime and a high intensity, hence is convenient of experimental conditions such as ion optics and ion beam current. In order to ensure the observation of the irradiation effects, Si^{2+} ions with a high ion beam current (Fig. 2.4) were used instead of Si^{+} ions. Secondly Si has a similar mass with an important dopant, P, and the surface structural changes are expected to be similar. Figure 2.5 shows STM images of Si(111)-7×7 surface at 510℃ before, during and after Si^{2+} irradiation at 500 eV. In Fig. 2.5(a), three patches of lower terrace are seen together with step edges with irregular shapes. In Fig. 2.5(c), all the step edges retreat to the lower left direction. The initial edge distribution is overlapped in Fig. 2.5(c). The three patches disappear and result in deeply indented step edges. This indicates that the original patches are lower by one atomic layer.

Figure 2.6 shows the successive high resolution STM images of Si(111)-7×7 surface at 500 ℃ after Si^{2+} irradiation at 500 eV. The induced surface defects in the figure after 80 s is already reshaped, which can be seen by the fact that the bottom of the surface defects are one bilayer deep and the periphery tend to be parallel to dimer rows. One of the surface defects is annealed out after 960 s. All these STM figures indicate that the features of surface defects are similar to the ones found in the previous work based on the IG/STM [5]. One big advance is that a similar in-situ observation has been done using the novel LMIS-IG/STM.

In conclusion, we have developed an LMIS-IG/STM in order to investigate ion beam modification process *in-situ* based on our previous IG/STM. Various ion species from a liquid-metal-ion-source can be well separated with the $E \times B$ separation system. Current density is high enough for the successive STM observation. Preliminary observation of Si(111) surface irradiated with Si^{2+} ions has revealed the

similar behavior of surface defects induced by Ar^+ irradiation with IG/STM.

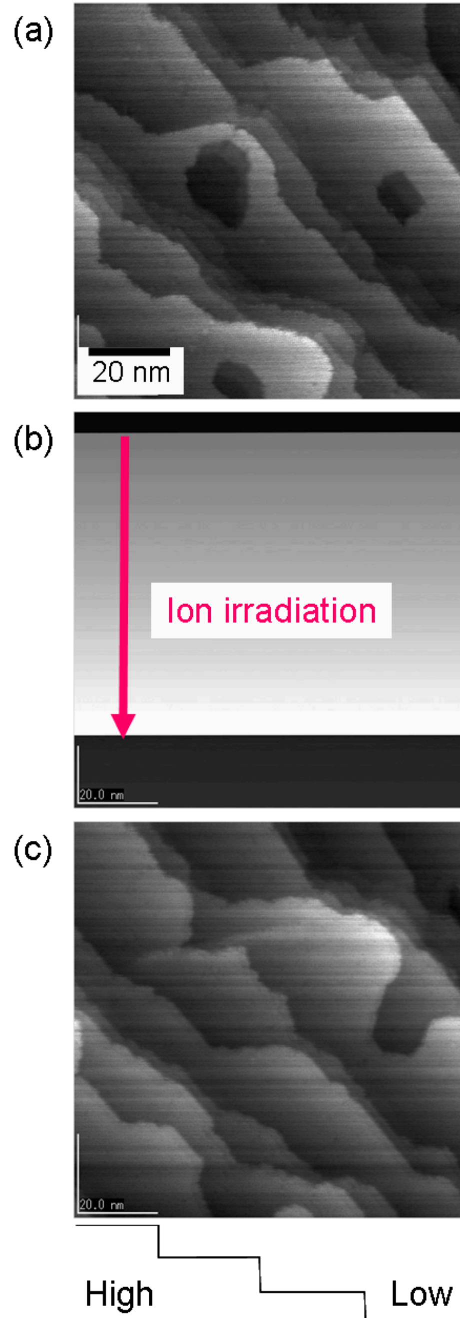

Figure 2.5: Successive STM images of the Si(111) surface at 510℃; (a) 80 s before, (b) during, and (c) 80 s after 500 eV Si^{2+} ion irradiation. The images were taken with constant current mode and at a scan speed of 80 s/image (Dose: about $3 \times 10^{14} cm^{-2}$, It: 0.06 nA, Vs: 1 V).

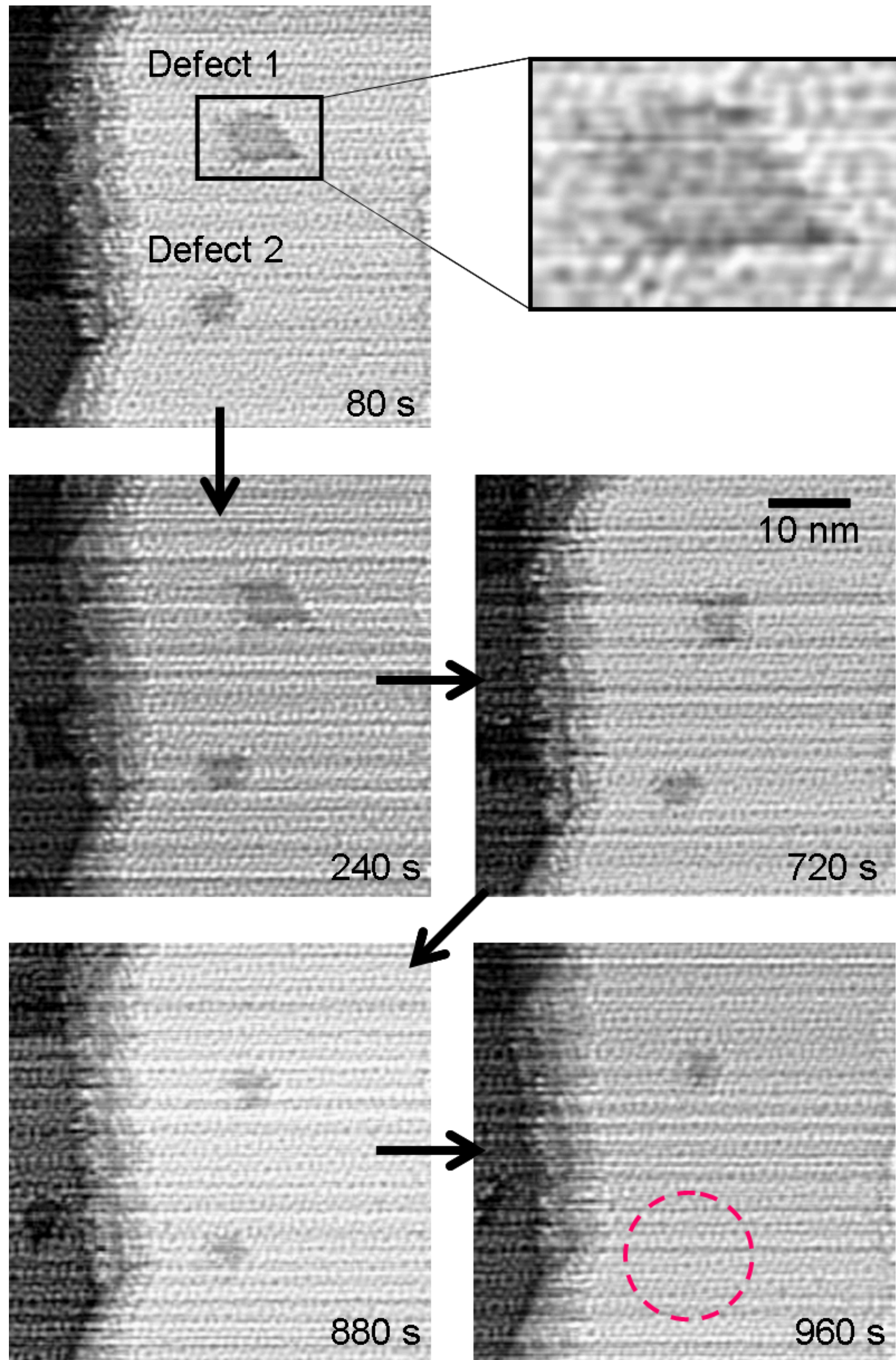

Figure 2.6: Successive STM images of the Si(111) surface at 500℃; 80 s, 240 s, 720 s, 880 s, and 960 s after 500 eV Si^{2+} ion irradiation (Constant current mode, It: 0.03 nA, Vs: 1V, Dose: $1.3 \times 10^{12} cm^{-2}$).

2.2 Development of an Ion Beam Alignment System for Real-Time Scanning Tunneling Microscope Observation of Dopant-Ion Irradiation Effects

In section 2.1 the author implemented the LMIS-IG/STM in order to aim at observing doping effects, and Si^{2+} ion irradiation effects on high-temperature Si surfaces were demonstrated as preliminary results [6]. However, real-time STM observation of " dopant " ion irradiation has not been realized yet because of the difficulty in aligning the dopant-ion beam in the STM observation area. This difficulty derives from the LMISs with low emission and short lifetime, which makes it difficult to align the beam just at a nano-scale region between an STM tip and a sample surface within the time limited by the short lifetime of the LMIS. Therefore, in order to realize the STM observation of dopant ion irradiation, it is required the quick and accurate ion beam alignment and the subsequent STM observation within a time as short as possible.

In this section, we report a highly improved ion-beam alignment system which enables us to aim accurately at an STM observation area in short time without damaging a sample surface. The author describes the details of the ion beam alignment system and demonstrate the results of real-time STM observation of P ion irradiation onto Si(111)-7×7 surfaces for the first time.

2.2.1 Ion Beam Alignment System Using Absorbed Current Image

We introduced a new ion beam alignment system into our original LMIS-IG/STM. The LMIS-IG/STM system is composed of an UHV high-temperature STM and a low-energy ion gun using an LMIS [6]. A variety of ions can be emitted by changing the metal alloys for the LMIS. The ion gun and an STM tip are facing a sample surface in the observation chamber, and the same observation area can be kept during ion irradiation. Each STM image is taken with time interval from 6 second to several tens seconds. This enables us to keep observing the ion irradiation effects with the time resolution of the STM scan period.

The newly developed ion beam alignment system is schematically shown in Fig. 2.7. The system is composed of two setups: (1) the absorbed current image (AEI) unit to visualize an ion-irradiated area and (2) the dummy-target as an ion beam alignment mark.

The AEI unit is a tool for visualizing the ion-irradiated region. The principle of operation is as follows. First, a raster-scan signal is output from the scan-signal generator and is sent to two paths: the ion gun and the oscilloscope. On the ion gun path, the signal is amplified by the voltage amplifier and applies to each x/y-deflection electrode of the ion gun. Thus the ion beam is raster-scanned with a frame rate of 12 or 24 frame/s. The area size of ion irradiation can be changed by controlling the amplitude of the deflection voltage from 0 to 300 voltage peak-to-peak (V_{p-p}). The number of the horizontal scanning line is 512 line and the area of raster-scan is designed to cover $10mm \times 10mm$ at maximum at the sample position. Then, the ion beam current absorbed into ion-irradiated objects such as a sample, an STM tip and the alignment mark, is detected and amplified by an I/V amplifier. Finally, the signal is input to an oscilloscope with applying the raster-scan signal as a synchronizing signal. In this way, the absorbed current is mapped on

the oscilloscope. The two-dimensional picture on the oscilloscope is the absorbed current image (AEI). The contrast of AEI reflects the difference in the absorbed current intensity. Fig. 2.8(a) illustrates the sample and the STM tip viewed from the direction of the axis of ion gun. The ion beam incident angle is tilted by 60 degrees with respect to the sample surface normal. Figure 2.8(b) shows an actual AEI of the sample and the STM tip taken by irradiation of P^+ ions with an acceleration voltage of 5 keV. The AEI clearly reflects the arrangement of the sample and STM tip. The beam spot size on the sample is estimated about 0.5 mm in diameter. This value is large enough for covering the areal interval of scanning lines (about 0.02 mm) so that ions are irradiated uniformly on the raster-scan area. Thus we can grasp the area to be irradiated with ions from the AEI.

The dummy-target is a movable metal plate with an alignment mark for the beam alignment. The dummy target can be inserted even when an STM tip is approached to the sample and protects the sample surface from the damage during the beam alignment. This enables us to align the beam after the preparation of the sample just before STM observation. Figure 2.8(c) illustrates the dummy-target inserted over the sample as the STM tip is approached. A head of a round head screw with a diameter of 2 mm is located in the center of the dummy-target as an alignment mark. The alignment mark is designed so that the center of a sample is positioned just behind it when it is viewed from the direction of the incident ion beam. Figure 2.8(d) shows an actual AEI of the alignment mark. It clearly reflects the alignment mark, and even the slot on the head of the screw is clearly observed as shown in the inset of Fig. 2.8(d).

By using the AEI unit and the dummy-target, experimental procedure is improved as shown in Fig. 2.9(a). In the new protocol, firstly the sample surface is prepared for observation. Next, the dummy-target is inserted over the sample, and the ion beam is emitted to get the AEI of the alignment mark. After the alignment

operation is completed, the ion beam is blanked electrically and the dummy-target is retracted. Thus the preparation of the real-time STM observation of ion irradiation process is completed. To start the observation, we have only to blank-off (restore) the ion beam.

The advantages of this method are summarized as follows. First, as illustrated in Fig. 2.9(a) and (b), the number of process steps is drastically decreased from the conventional procedure, and the time required for the beam alignment is much saved. In the conventional protocol as shown in Fig. 2.9(b), ion beam alignment was operated before sample preparation. The beam was aligned at the sample position using a sample for the alignment. In order to exchange the sample for the alignment for an observation-sample and prepare its surface by flash heating, about 3 h vacuuming are required after the ion beam interruption. In the new protocol as shown in Fig. 2.9(a), ion beam is aligned after the preparation of the observation-sample. By using the dummy-target, there is no need to exchange the sample, because the surface to be observed is already prepared before the ion irradiation. This protocol does not require the time for vacuuming. Additionally, the short time interval between the ion beam alignment operation and the STM observation without interrupting the ion beam accurizes the alignment of the ion beam.

There is another choice for imaging method such as secondary electron image (SEI) to visualize the ion-irradiated area. SEI method will be suitable in the case of extremely low dose (pA order), in which high detection sensitivity is needed. The imaging method of AEI, however, does not require a secondary electron detector and simplifies the system configuration.

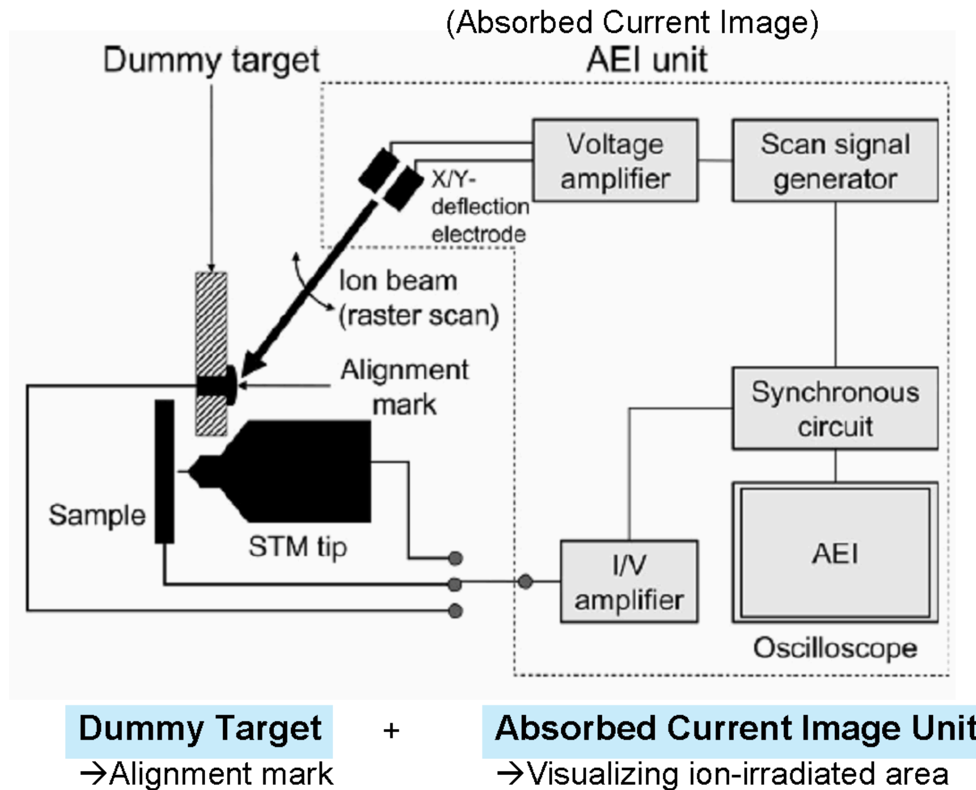

Figure 2.7: Schematic of the ion beam alignment system. The developed ion beam alignment system is composed of two setups: the absorbed current image (AEI) unit to visualize an ion-irradiated area and the dummy-target as an ion beam alignment mark.

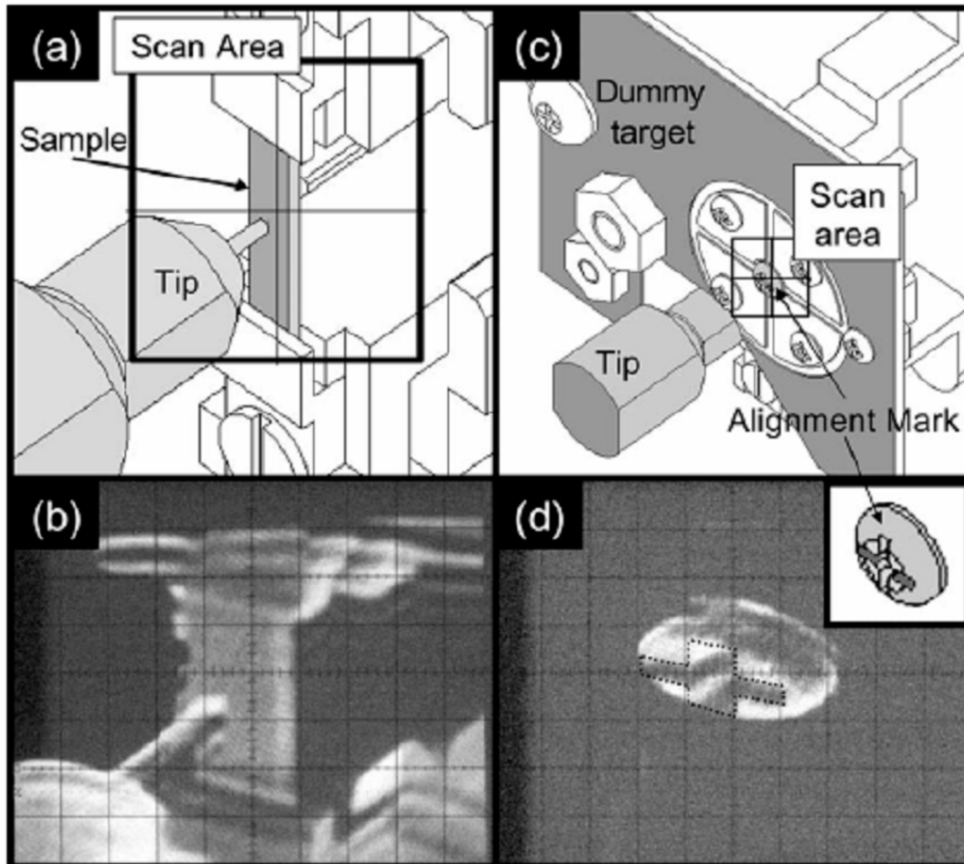

Figure 2.8: Experimental setups and the AEI images viewed from the direction of the axis of ion gun; (a) arrangement of a sample and STM tip and (b) their actual AEI images. (c) The dummy sample positioned in front of the sample, and (d) an AEI image of the alignment mark on the dummy sample. The inset shows the magnified drawing of the alignment mark. The dashed line in the image corresponds to the slot on the head of the screw.

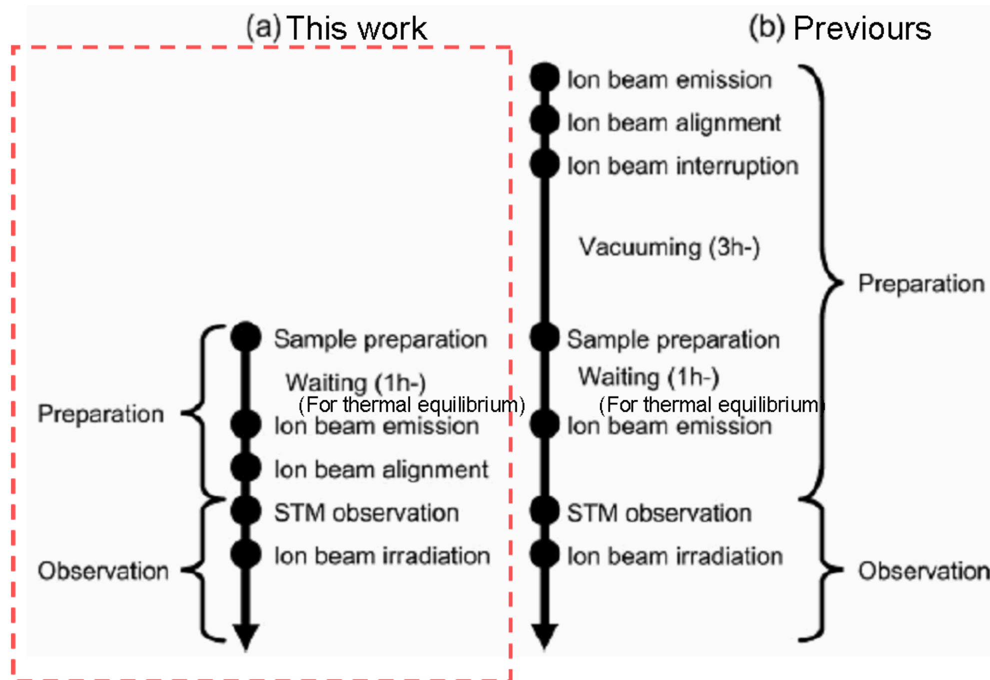

Figure 2.9: Experimental procedures for real-time STM observation of ion irradiation process; (a) the improved and (b) the conventional protocol. The experiment proceeds two steps: the preparation and the observation steps. In the conventional protocol, ion beam is interrupted after ion beam alignment. After waiting for recovery of UHV, a sample is prepared by heat treatment. Then ion beam is re-emitted and STM observation is started. In the improved protocol, a sample is prepared at first and ion beam is aligned. Then STM observation is started without interruption of ion beam.

2.2.2 Preliminary Results of Real-Time STM Observation of Si Surfaces Irradiated with P^+ Ions

According to the new procedure as shown in Fig. 2.9(a), we performed real-time observations of Si surfaces irradiated with P^+ ions at room temperature (R.T.) and a high temperature of 500℃. A sample cut from an n-Si(111) wafer was installed in the STM unit in UHV after chemical cleaning. The sample was degassed at 600℃ for more than 12 h, and was flashed repeatedly until the surface was covered with 7×7 dimer-adatom-stacking-fault (DAS) structure. The sample was then kept at observation temperature (R.T. or 500℃) for over 1 h until it reached thermal equilibrium with an STM tip. After preparation of the sample surface, the dummy-target was inserted as shown in Fig. 2.8(c) and the ion beam was aligned by capturing the AEI of the alignment mark. Then the ion beam was temporary deflected from the axis, and the dummy-target was retracted. Following the above mentioned procedure, STM observation was started. STM images of the surface were taken with constant-height mode. During the STM observation, P^+ ions with 5 keV were irradiated and the observation was continued in the same area. The ion doses are estimated by the following equation: $I \times t/S$, where I is average absorbed current, t irradiation time and S scan area size.

Figure 2.10 shows a series of STM images of Si(111)-7×7 surface before, during and after the ion irradiation at R.T. Before the ion irradiation as shown in Fig. 2.10(a), the whole surface is covered with 7×7 structure. Small dark spots on the surface are the atomic defects, which were already formed in the preparation of the sample surface before the ion irradiation. During the next image scan as shown in Fig. 2.10(b), the ion beam was irradiated. The ion dose is $2.5 \times 10^{14} cm^{-2}$. Upon the beam irradiation, it is unavoidable that the STM tip is also irradiated with the ions, so that the image turned white due to the incidence of positively charged P^+ ions into the STM tip. During this period, we can not observe the surface, but the

STM observation is rapidly reopened just after the end of ion irradiation. Figure 2.10(c) is the next image scanned after Fig. 2.10(b). In Fig. 2.10(c), we can see a drastic change in the surface morphology. The initial flat surface was destructed so that the 7×7 structure is hardly observed. The bright and dark regions frequently appear, which suggests that the surface is highly roughened. This kind of surface modification is considered to be induced by ion irradiation because it never happens without ion irradiation. The surface morphology of Fig. 2.10(c) did not change in the subsequent STM scans without the beam irradiation.

Figure 2.11 shows a series of STM images of Si(111)-7×7 surface before, during and after ion irradiation at 500℃. The ion dose is $2{\times}10^{14} cm^{-2}$. On the surface before ion irradiation as shown in Fig. 2.11(a), an atomic step is formed in the longitudinal direction. Just after the ion irradiation as shown in the bottom half of Fig. 2.11(b), small patches with a diameter of about 10 nm appeared as indicated with the black arrows. The defects are identified as the clusters of vacancy type point defects which are generated in the substrate by the ion irradiation. In the next image of Fig. 2.11(c), the step edge is roughened and the defects shrink. It is suggested that surface atom migration occurs at the step edge and Si atoms from the step edge fill up the vacancy clusters [5,7]. The density of surface defect is $3 \times 10^8 cm^{-2}$ (3 defect per $1000nm \times 1000nm$ area) and is much smaller than the ion dose. It is considered that although much more surface defects are formed by the ion irradiation, most of them recover by the time to reopen the surface observation. This result observed at high temperature is different from that at R.T. (see Fig. 2.10). At R.T. surface morphology remains to be roughened because of the insufficient thermal energy for migration of point defects such as vacancies and surface Si atoms.

In this way, we have succeeded in obtaining the sequential STM images of surface modification process by dopant ion irradiation at both R.T. and 500℃. By the new beam alignment procedure with the developed system, we have been able to

observe some changes in surface morphology at almost every experiment. Considering that in the conventional procedure 20-30 times of ion beam alignment was needed until some ion-irradiation effects was observed in real-time, the developed system has drastically improved the accuracy of the ion beam alignment. The developed system can be applicable to various types of LMISs. The LMIS-IG/STM equipped with the developed ion beam alignment system would be a powerful tool for microscopic investigation of the dynamic processes of ion irradiation.

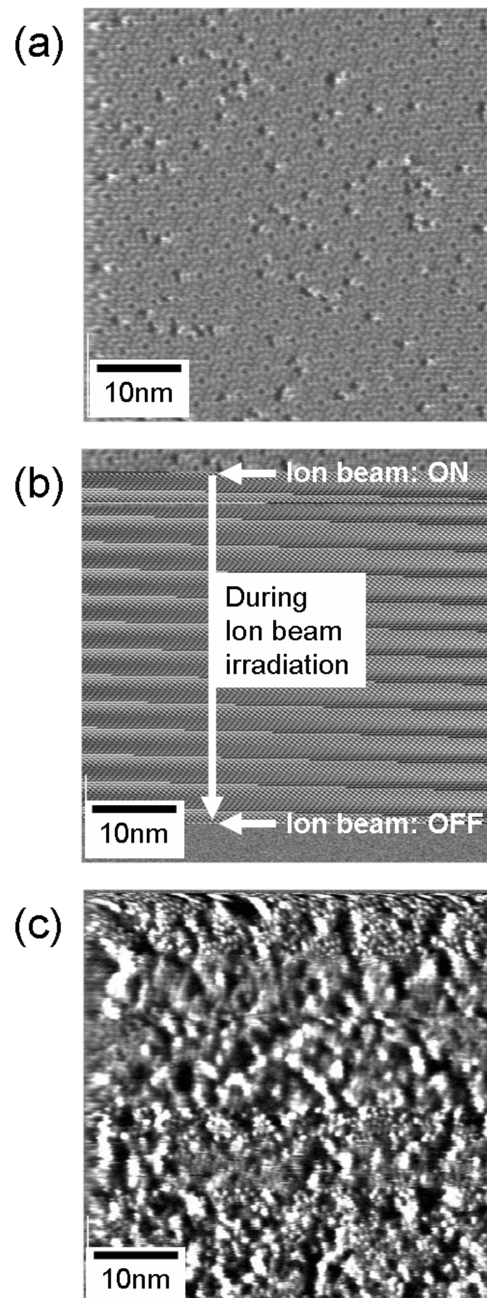

Figure 2.10: Sequential STM images of Si(111)-7×7 surface (a) before, (b) during and (c) after the 5 keV-P^+ ion irradiation taken at R.T. Each image was taken with constant-height mode (current images); sample bias: 1.1 V, tunneling current: 0.2 nA, scan speed: 12 s/image, ion dose: $2.5\times10^{14}cm^{-2}$.

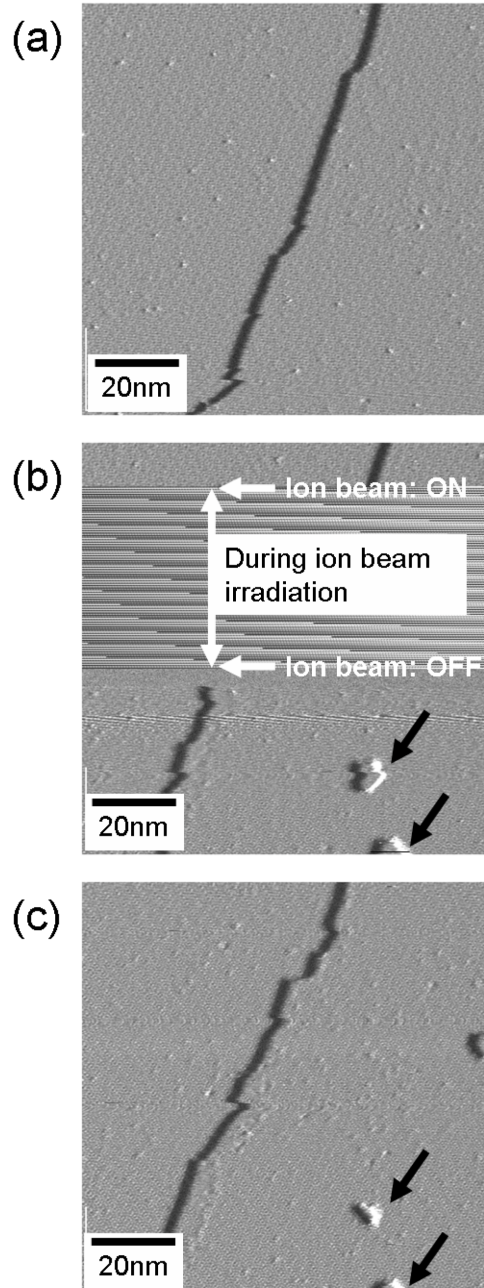

Figure 2.11: Sequential STM images of Si(111)-7×7 surface (a) before, (b) during and (c) after the 5 keV-P^+ ion irradiation taken at 500℃. Each image was taken with constant-height mode (current images); sample bias: 0.3 V, tunneling current: 0.2 nA, scan speed: 23 s/image, ion dose: $2 \times 10^{14} cm^{-2}$.

2.3 Summary of Chapter 2

In this chapter, a newly developed system for real-time STM observation of ion-irradiated solid surface is described; (1) Development of a liquid-metal-ion-source ion gun and STM (LMIS-IG/STM) combined system. (2) Development of a beam alignment system especially for " dopant-ion-beam " are explained in detail.

Our original LMIS-I/STM is composed of a high-temperature UHV STM and a low-energy ion-gun with an LMIS. The ion gun is originally designed so that dopant ions are irradiated at an energy lower than 5 keV. After the description of the principle of operation, some basic performances are shown such as mass spectrum of ion beam using a Au-Si LMIS and ion current at a sample position. In addition, as a preliminary experiment, a real-time STM observation of a high-temperature Si(111)-7×7 surface irradiated with Si^{2+} is demonstrated.

Next, a beam alignment system for " dopant " ion beam is described in detail as a key technique for real-time STM observation especially using LMISs composed of dopants such as P. Since such LMISs are low emission and short lifetime, we faced a difficulty in aligning the dopant-ion beam in the STM observation area. The beam alignment system is composed of two setups: the AEI unit to visualize an ion-irradiated area, and the dummy target as an ion beam alignment mark. Installing the beam alignment system enables us not only to align a dopant-ion beam accurately but also to save the time for preparation of the experiment.

Finally, we realized a real-time STM observation of Si(111)-7×7 surfaces irradiated with P^{+} for the first time.

References

[1] S. Kitamura, T. Sato, and M. Iwatsuki, Nature (London) **351** (1991) 215.

[2] T. Chikyow and N. Koguchi, J. Vac. Sci. Technol. B **16**, (1998) 2538.

[3] T. Chikyow, N. Koguchi, and A. Shikanai, Surf. Sci. **386**, (1997) 254.

[4] T. Chikyow (private communication).

[5] K. Shimada, T. Ishimaru, T. Yamawaki, M. Uchigasaki, K. Tomiki, T. Matsukawa, and I. Ohdomari, J. Vac. Sci. Technol. B **19**, (2001) 1989.

[6] M. Uchigasaki, T. Kamioka, T. Hirata, T. Shimizu, F. Lin, T. Shinada, and I. Ohdomari, Review of Scientific Instruments **76**, (2005) 126109.

[7] Y. Tanaka, K. Ishiyama, and A. Ichimiya, Surf. Sci. **357-358**, (1996) 840.

Chapter 3

Real-Time Scanning Tunneling Microscope Observation of Silicon Surface Modified by Gold Ion Irradiation

3.1 Introduction

Transport and reactions of gold (Au) atoms in silicon (Si) have been extensively studied owing to the technological importance such as contact matellization, lifetime control and a catalyst. Gold is a deep-level impurity in Si crystal and acts as an effective recombination center of minority carriers, so that Au impurities are utilized as so-called lifetime killer in high-speed Si devices such as *p*-*n* diodes and bipolar transistors [1, 2]. Recently, Au implantation is applied to the formation of a nanoparticle which is used as a nucleation site of a silicon nanowire in vapor-liquied-solid method [3, 4]. One important key in these techniques is to control behaviors of Au atoms in Si substrate. This is, however, difficult due to the rapid

diffusivity of Au in Si [5], and the complexity of the diffusion mechanism mediated point defects [6, 7]. Therefore, it is important to understand deeply the transport and reaction mechanisms of Au atoms in Si in nano-meter scale.

The Au atoms in Si substrate diffuse through exchange reactions between interstitial (Au_{int}) and substitutional (Au_{sub}) sites. The reaction from Au_{int} to Au_{sub} is considered to involve vacancies (V), which is called the Frank-Turnbull mechanism ($Au_{int}+V \leftrightarrow Au_{sub}$) [6]. The reverse reaction from Ausub to Auint is considered to involve a Si interstitial (I), which is called the kick-out mechanism ($Au_{sub}+I \leftrightarrow Au_{int}$) [7]. The Au_{int} diffuses much faster than Au_{sub}, so that the diffusion of Au atoms is promoted by Si interstitials and suppressed by vacancies. The Au atoms in Si substrate provide so-called " U-shape " profile [1, 8], in which both surface sides have high concentration of Au because surface acts as a sink of Si interstitials. Thus, the behavior of the Au atoms is known to be strongly affected by the distribution of point defects.

When Au atoms are introduced by ion implantation, behaviors of the Au atoms could be more complicated due to the interaction with excess point defects generated in the substrate. In particular, the heat treatment for the diffusion of implanted Au atoms leads to both a recovery of the crystal and a growth of defects due to the migration of the point defects. Therefore, it is crucial to understand the dynamical behavior of the implanted Au atoms during annealing just after ion irradiation. However, this is not completely clarified. Previous studies mainly focused on the thermal equilibrium or quasi-equilibrium distributions of Au atoms after the ion irradiation, which were obtained by Rutherford backscattering spectrometry (RBS) and transmission electron microscope (TEM) and so on, and the information on the behavior of each implanted Au atom under the nonequilibrium condition was obtained indirectly [9–14].

In order to address the atomistic picture of the interaction between implanted

impurities and substrate just after ion irradiation, our group developed the real-time observation system [15] (LMIS-IG/STM) as described in chapter 2. The system enables us to observe a sample surface during ion irradiation. From the sequential STM images of the sample surface, we can see the elemental steps of surface modification with the time interval of STM scan period.

In this chapter a real-time STM observation of Au^+ ion irradiation effects on Si surface is reported. The STM based method enables us to track the change of the surface structures with atomic resolution. For example, Au atoms on Si(111)-7×7 dimer-adatom-stacking fault (DAS) surface are known to form several kinds of reconstructions such as 5×2, $\sqrt{3} \times \sqrt{3}$ on the topmost surface [16] and the atomic arrangements and their composition per each unit cell are well defined. By using these reconstructions as the rulers in nature, we can estimate the number of Au atoms which are involved in reconstructed domains on surface.

3.2 Experiment

We performed the experiment using our original ion gun and STM combined system (LMIS-IG/STM), which is described in detail in Chapter 2 [15]. The system is composed of an UHV high-temperature STM and a low-energy ion gun using a liquid-metal-ion-source (LMIS). Various kinds of ions can be emitted by changing the metal alloys for the LMIS. In this experiment, an Au-Si alloy was used to extract Au ions. The ion gun and an STM tip are facing a sample surface in the observation chamber, and the same observation area can be kept during ion irradiation. Each STM image is taken with a time interval of several tens seconds. This enables us to keep observing the ion irradiation effects with the time resolution of the STM scan period.

Experimental procedure is shown in Fig. 3.1. A sample cut from an n-type Si(111) wafer was cleaned chemically and installed in the STM unit. The sample was degassed at 600℃ for about 12 h and flashed repeatedly at 1200℃ by resistive heating until whole surface was covered with 7×7 DAS structure. The thermally treated sample was kept at observation temperature (500℃) for over 1 h until it reached thermal equilibrium with an STM tip. After preparation of the sample surface, STM observation was started. STM images of the surface were taken with constant-height mode. During the STM observation, Au^+ ions were irradiated with 3 keV by spot irradiation, and the observation was continued in the same area. The beam spot size was about 0.5 mm in diameter and the ion doses was $3 \times 10^{14} cm^{-2}$, which is given by $I/e \times t/S$, where I, t, S stand for average current through the sample, irradiation time, beam spot size, and e is elemental charge, respectively.

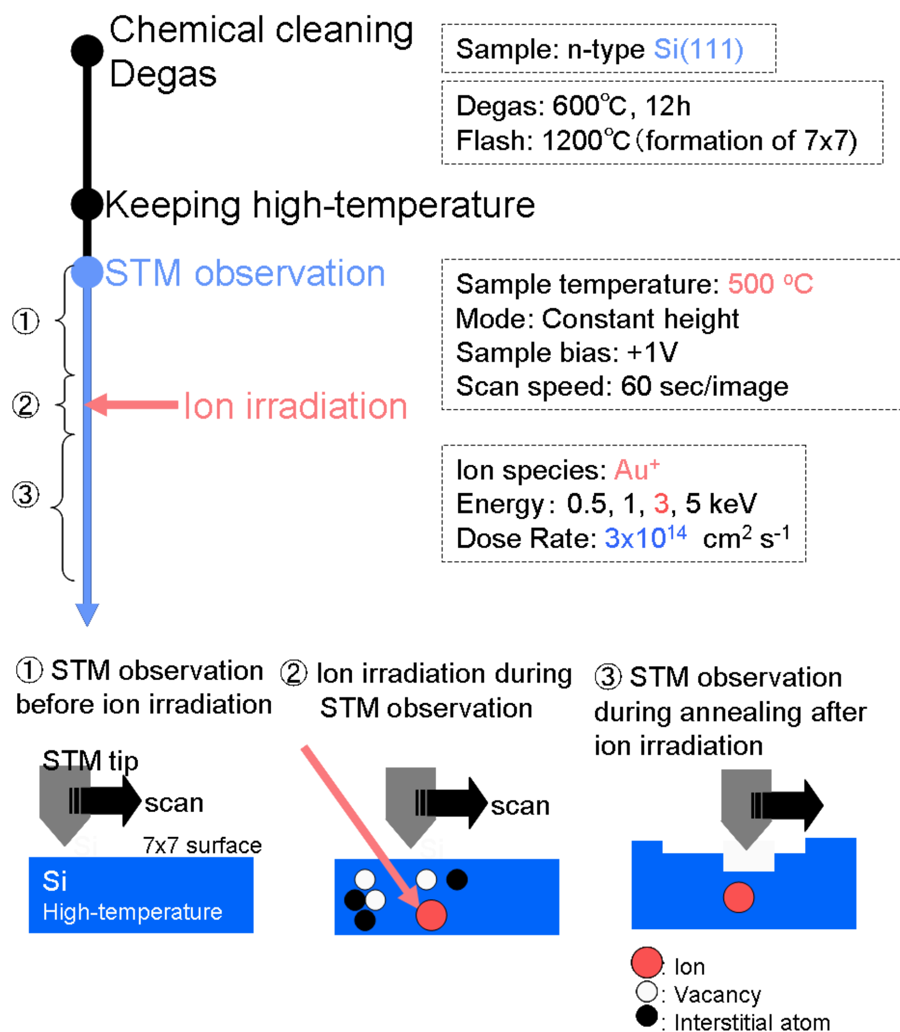

Figure 3.1: Experimental procedure of real-time STM observation of Au^+ ion irradiation effects on high-temperature Si surface.

3.3 Results and Discussion

Figure 3.2 shows a sequential STM images of Si(111)-7 × 7 surface kept at 500℃ ,which were taken (a) before, (b) during, and (c) after Au^+ ion irradiation. Before the ion irradiation, the whole surface was covered with 7×7 DAS structure as shown in Fig. 3.1(a). During the next scan, Au^+ ions were irradiated on the observation area as shown in Fig. 3.2(b). Upon the ion irradiation, it is unavoidable that the STM tip is also irradiated with the ions. During this period, the STM tip is retracted from the sample surface, so that we can not observe the atomic structure of the surface. However the STM observation is rapidly reopened just after the ion irradiation keeping the original observation area. After the ion irradiation, some new surface structures appeared as indicated by allows in Fig. 3.2(c). From the relation between the scan direction and the contrast change induced by the response of STM tip, these structures are identified to be indentations. Since they never form without ion irradiation, it is concluded that these structures are induced by the ion irradiation.

Figure 3.3 shows STM images of the Si(111) surface kept at 500℃, which were taken (a) 71 s, (b) 111 s, and (c) 731 s after the ion irradiation. The structure labeled " a " in Fig. 3.3(a) is a vacancy island, which is a two-dimensional cluster of surface vacancies. The same type of surface defects were observed in our previous work [17], in which Ar^+ ions were irradiated on a Si(111)-7×7 surface at 500℃. The vacancy islands are nucleated by ion impacts, and then they grew by incorporating vacancy-type point defects generated in the substrate upon the ion irradiation. The number density of the vacancy islands (about $1 \times 10^{11} cm^{-2}$) is much lower than expected from the ion dose ($3 \times 10^{14} cm^{-2}$). It is considered that although much more surface defects were formed by the ion irradiation, most of them have been annihilated or coalesced each other by the time to reopen the surface observation.

We also found that a chain structure, which is labeled " h " in Fig. 3.3(a), forms adjacent to a vacancy island. The periodic structure has a side length of $5a$, where

a is the lattice constant of Si(111) plane (0.381 nm). Since this structure has never been observed on Ar^+ ion irradiated Si(111)-7 × 7 surface [17], it is associated with incident Au^+ ions. Figure 3.4(a) shows a Si(111) surface image obtained in a separate experiment, which is taken at room temperature after ion irradiation at 500℃. Figure 3.4(b) is the magnified image of periodic bright spots observed in Fig. 3.4(a). This structure has $5a \times 2a$ periodicity (dashed parallelogram). Many studies of Au deposition on Si(111) surface reports 5 × 2-Au reconstruction forms at 500℃ when Au concentration on surface is lower than 0.7 monolayer (ML) [16, 18]. In the present experiment, surface concentration of Au atoms never exceeds 0.3 ML (corresponding ion dose is $3 \times 10^{14} cm^{-2}$), so that the condition for the appearance of the 5 × 2-Au is satisfied. One of the prevailing models of the 5 × 2-Au is shown in Fig. 3.4(c), which is known as ”Double Honeycomb Chain (DHC) ” model proposed by Erwin [19]. So far several model of 5 × 2 structure [20, 21] have been proposed and a firm consensus on the structure has not yet been reached. However, it is accepted, at least, that the 5 × 2 structure includes 4 Au atoms per unit cell in their models. As discussed later, the number of atoms involved in the structure can be estimated from the aerial size and the atomic configuration.

Since the 5 × 2-Au domain in Fig. 3.2 keeps growing after the ion irradiation, it is considered that the Au atoms were once implanted into the Si substrate and then diffused toward the surface. This picture is supported by ion energy dependency of 5 × 2-Au domain size. Figure 3.4 shows ion irradiated Si(111)-7 × 7 surfaces obtained 10 s after the ion irradiations with about the same dose ($2 \times 10^{14} cm^{-2}$), and at different ion energies (0.5, 1, and 5 keV). The coverage of 5 × 2-Au domain increases as the ion energy decreases. This is due to the difference in the initial distributions of Au ions; upon low energy ion implantation, the projected range (R_p) of ions is small so that more Au atoms reach the surface.

Our real-time observation reveals the interaction between Au atoms and defects

appeared on the surface. As shown in Fig. 3.3, it was found that 5×2-Au domains were formed at step edges and at a periphery of vacancy islands as indicated by arrows in Fig. 3.3(b). Formation of 5×2-Au at a step edge was also observed in other groups ' work on Au deposition [22–24]. This is because a step edge is a stable site for adsorption of Au atoms. In the present experiment, the periphery of vacancy islands induced by the ion irradiation also act as the nucleation site of 5×2-Au reconstructions as well as the step edges.

As seen in Fig. 3.3, the vacancy islands and the 5×2-Au domain change in their shape and size after the ion irradiation. Some vacancy islands shrink and disappear. The defect labeled " e " disappeared at 111 s after the ion irradiation as shown in Fig. 3.3(b), and after 731 s, the defects " b " and " g " also disappear as shown in Fig. 3.3(c). On the other hand, the 5×2-Au domain labeled " h " develops with time and finally reached the step edge as shown in Fig. 3.3(c). Figure 3.6 shows time evolution of the size of each vacancy island and the 5×2-Au domain after the ion irradiation. Size of vacancy islands are within about $10 - 50 nm^2$ just after the ion irradiation, then tend to slowly decrease as a whole. Contrarily, the 5×2-Au domain increases for about 2000 s after the ion irradiation.

The decrease in the vacancy island size means the recovery of the Si crystal. The same phenomena were also observed in our previous work of Ar^+ ion irradiation [17]. This is due to the diffusion of interstitial atoms toward the surface and the migration of surface atoms, resulting in filling the vacancy islands. This indicates that the vacancy island acts as a sink for Si interstitials.

The monotonic increase in the size of the 5×2-Au domain means that Au atoms are supplied from the substrate during heat treatment for 2000 s after the ion irradiation.

Diffusion coefficient of Au atom on the Si(111)-7×7 surface is estimated to be about $10^{-9} cm^2/s$ at 500℃ [25], which is much higher than those of in the substrate

by about four orders of magnitude [8, 26]. Therefore the rate-limiting process is considered to be the diffusion in the substrate. Based on this assumption, we calculate the number of Au atoms reached the surface. Number of Au atoms reached the surface is given by

$$N^{Surf}(t) = \frac{1}{2}\int_0^{+\infty} N_i(x) Erfc\left(\frac{x}{2Dt}\right) dx. \tag{3.1}$$

where N_i is the initial distribution of Au atoms as a function of depth x estimated by TRIM simulation [27], and D is the diffusion coefficient of Au atoms in the Si substrate. This equation means that the probability to reach the surface from depth x during the time t is given by the half of the co-error function [28]. According to the TRIM simulation, the R_p and the extent of the straggle (ΔR_p) for implanted Au atoms are 3.9 nm and 1.5 nm, respectively (Fig. 3.7). In eq. 3.1, we assume that an Au atom on the surface never return into the substrate, because they are stabilized by forming the 5×2-Au structure. According to literatures, the diffusion coefficient D of Au in dislocation-free Si crystal is $10^{-17} cm^2/s$ [7],8) and that in amorphous Si is $10^{-13} cm^2/s$ [26]. In the present experiment, the number of Au atoms appeared in the observation area ($100nm \times 100nm$) is estimated to be at most 1000 atoms. If we assume the diffusion coefficient in amorphous silicon, the time required for the 1000 atoms to reach the surface is only about 0.14 s, which is too short to explain the gradual increase of the Au domain size. If we assume the diffusion coefficient in dislocation-free Si crystal, the required time is about 1400 s, which corresponds roughly to the observed time scale. Therefore, it is considered that interactions in the substrate between Au atoms and excess point defects induced by the ion irradiation are almost negligible. In the present experimental condition, most of the defects in the substrate are likely to rapidly disappear by the heat treatment.

If experimental conditions such as temperature and ion dose are changed, the modulation of the diffusion speed may be expected. At lower temperatures, the excess point defects induced by the ion irradiation survive long time, and the inter-

action between Au atoms and the defects cannot be ignored. Also, higher dose leads to formation of complex defects which traps the Au atoms as reported by RBS and TEM studies [13, 14], so that the diffusivity would be slow down. By performing a more systematic study varying these conditions, various aspects of the behavior of the implanted Au atoms will be clarified.

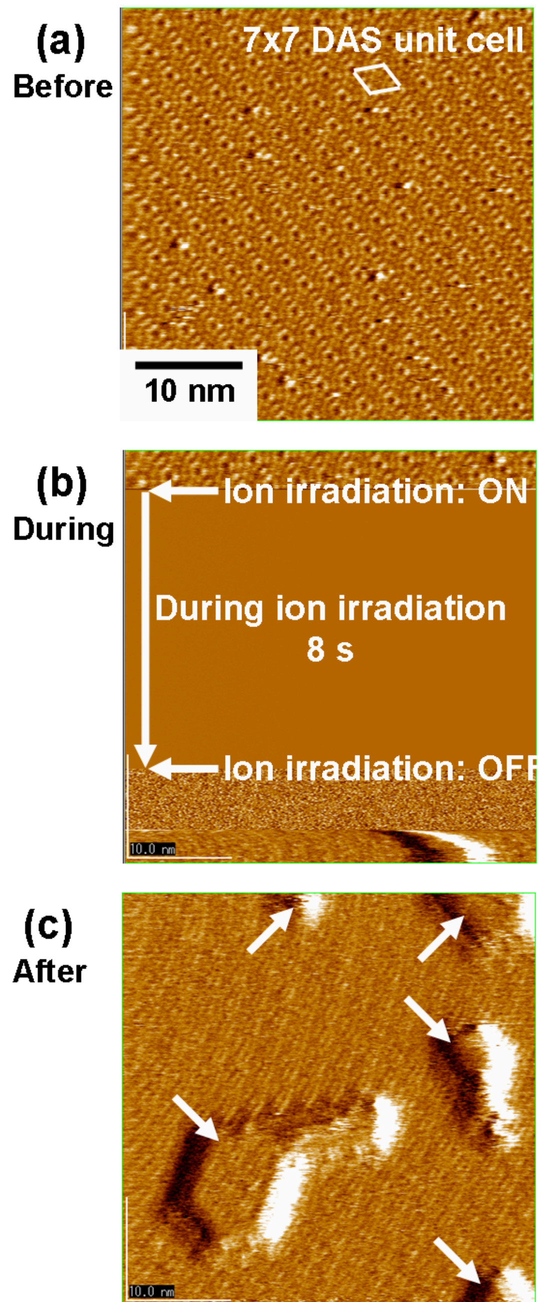

Figure 3.2: Sequential STM images of Si(111)-7×7 surface kept at 500C (a) before, (b) during and (c) after Au^+ ion irradiation (Ion energy: 3 keV, Dose: $3 \times 10^{14} cm^{-2}$. Each image was taken with constant height mode (current image); sample bias: 1.5 V, tunneling current: 0.2 nA, scan speed: 12 s/image.

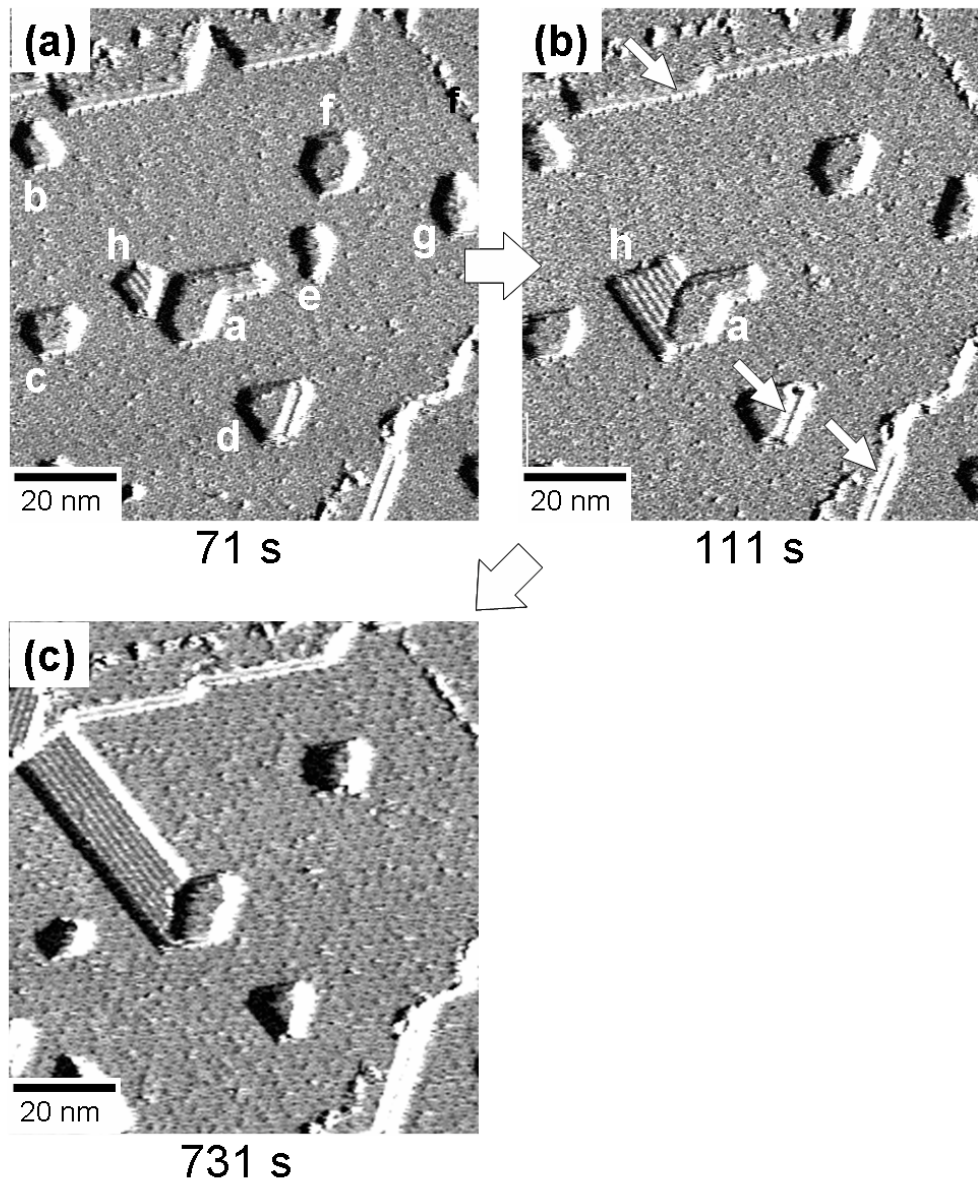

Figure 3.3: Sequential STM images of Au^+ ion irradiated Si(111) surface kept at 500℃; (a) 79 s, (b) 111, and (c) 731 s after the ion irradiation. Some modified sites on the surface are labeled by the alphabet " a "~" h" .

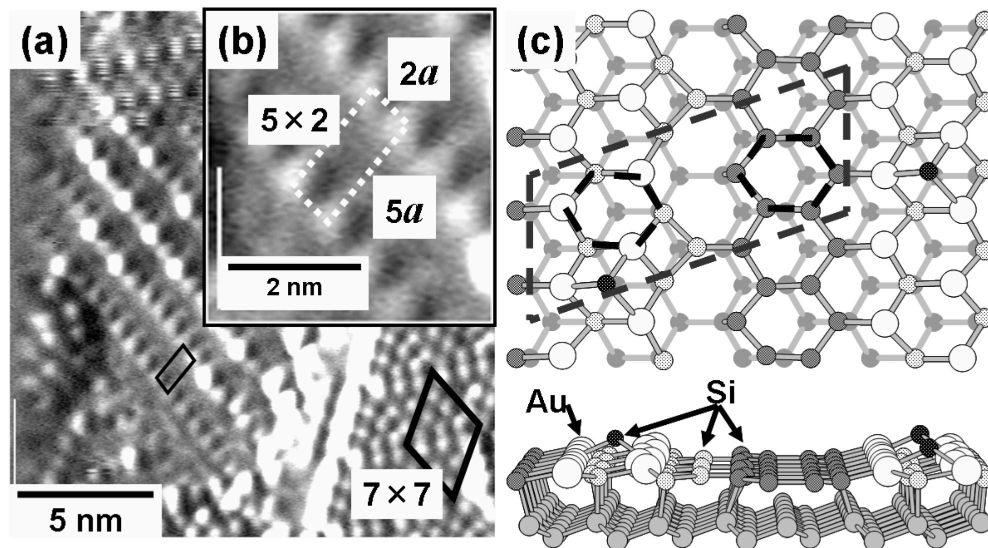

Figure 3.4: (a) STM image of a modified site formed by Au ion irradiation taken at RT (current image, sample bias: 1.2 V, tunneling current: 0.1 nA), (b) its partial magnified image ($4nm \times 4nm$), and (c) atomic arrangement of 5×2-Au structure proposed by Erwin's model (ref. [19]).

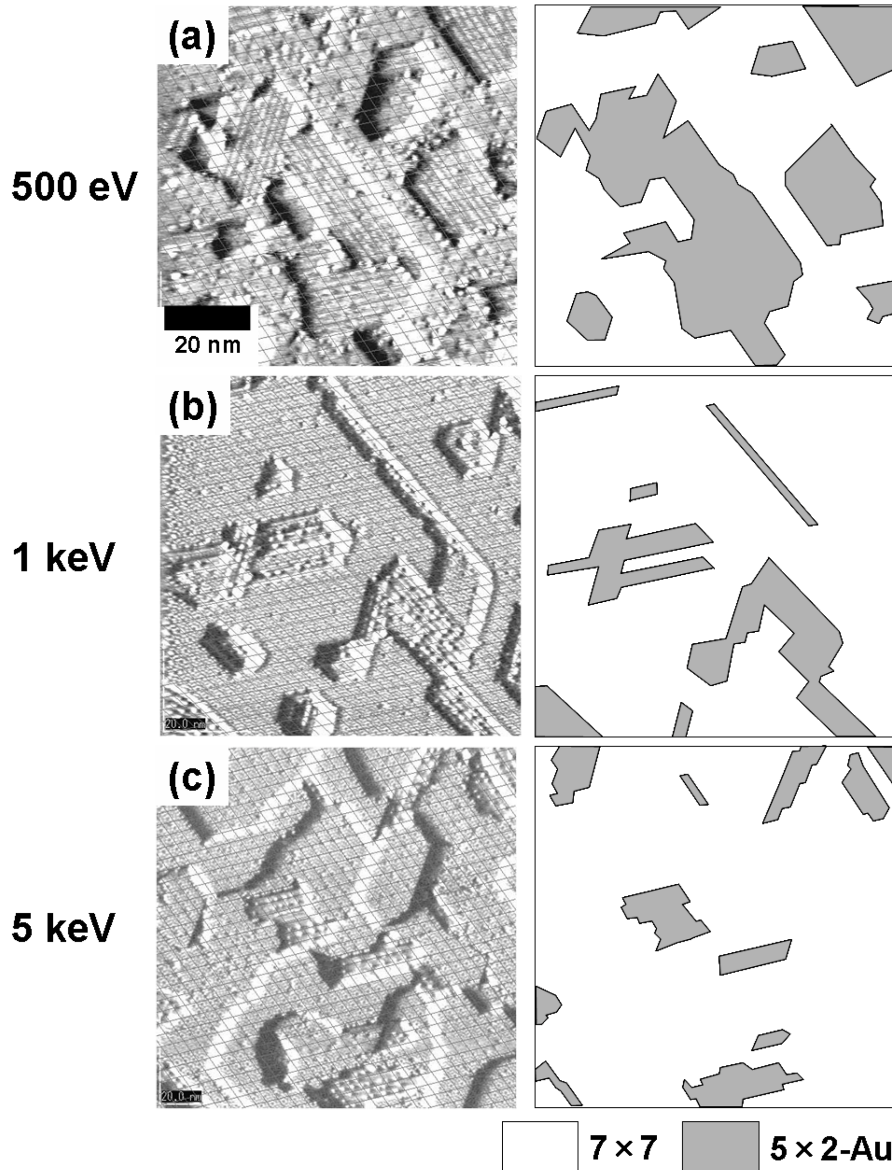

Figure 3.5: Comparison of 5×2-Au area size by ion energy. Au^+ ions are irradiated onto Si(111)-7×7 surfaces kept at 500℃ with different ion energies; (a) 500 eV, (b) 1 keV and (c) 5 keV. The image (a) is taken at 500℃, 10 s after ion irradiation; The images (b) and (c) are taken at R.T. after being quenched 10 s after ion irradiation. Each ion dose is about $2\times10^{14}cm^{-2}$. Below each STM image ($80nm\times80nm$), 7×7 and 5×2-Au areas are indicated as white area and hatched area, respectively.

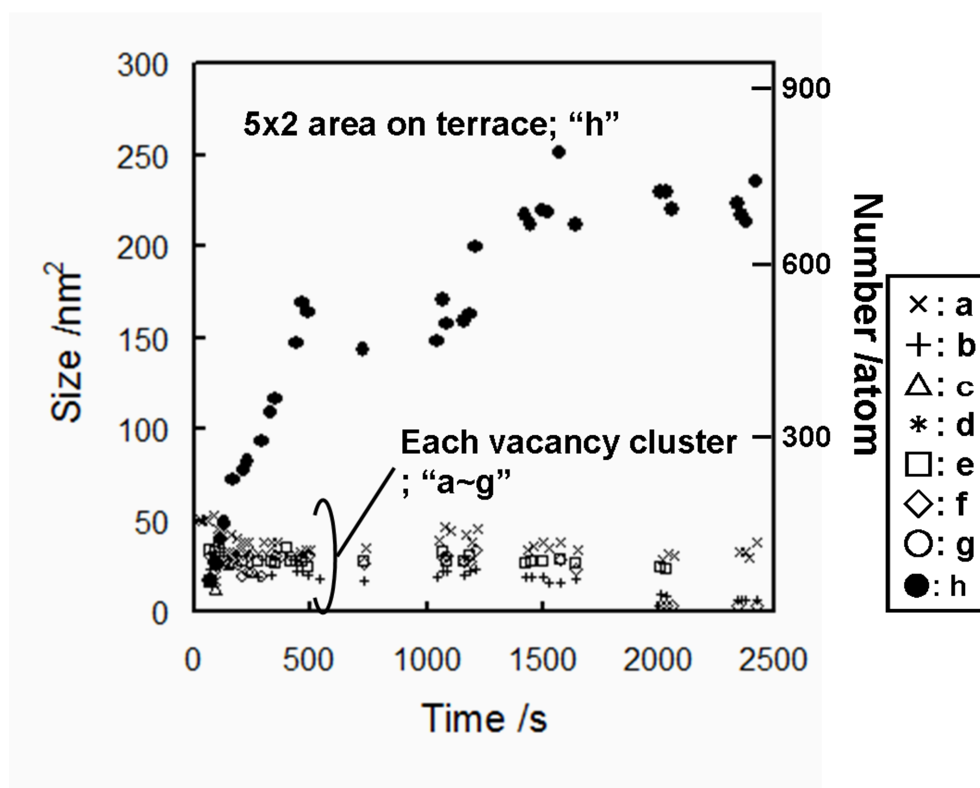

Figure 3.6: Time evolution of size of a 5×2-Au area and each vacancy cluster after ion irradiation. The origin of the time scale corresponds to the beginning of the ion irradiation. Circle mark indicates the 5×2-Au area on terrace corresponding the structure " h " in Fig. 3.2(a), and the other marks indicates each vacancy cluster corresponding to the defects " a "~ "g " in Fig. 3.2(a), respectively.

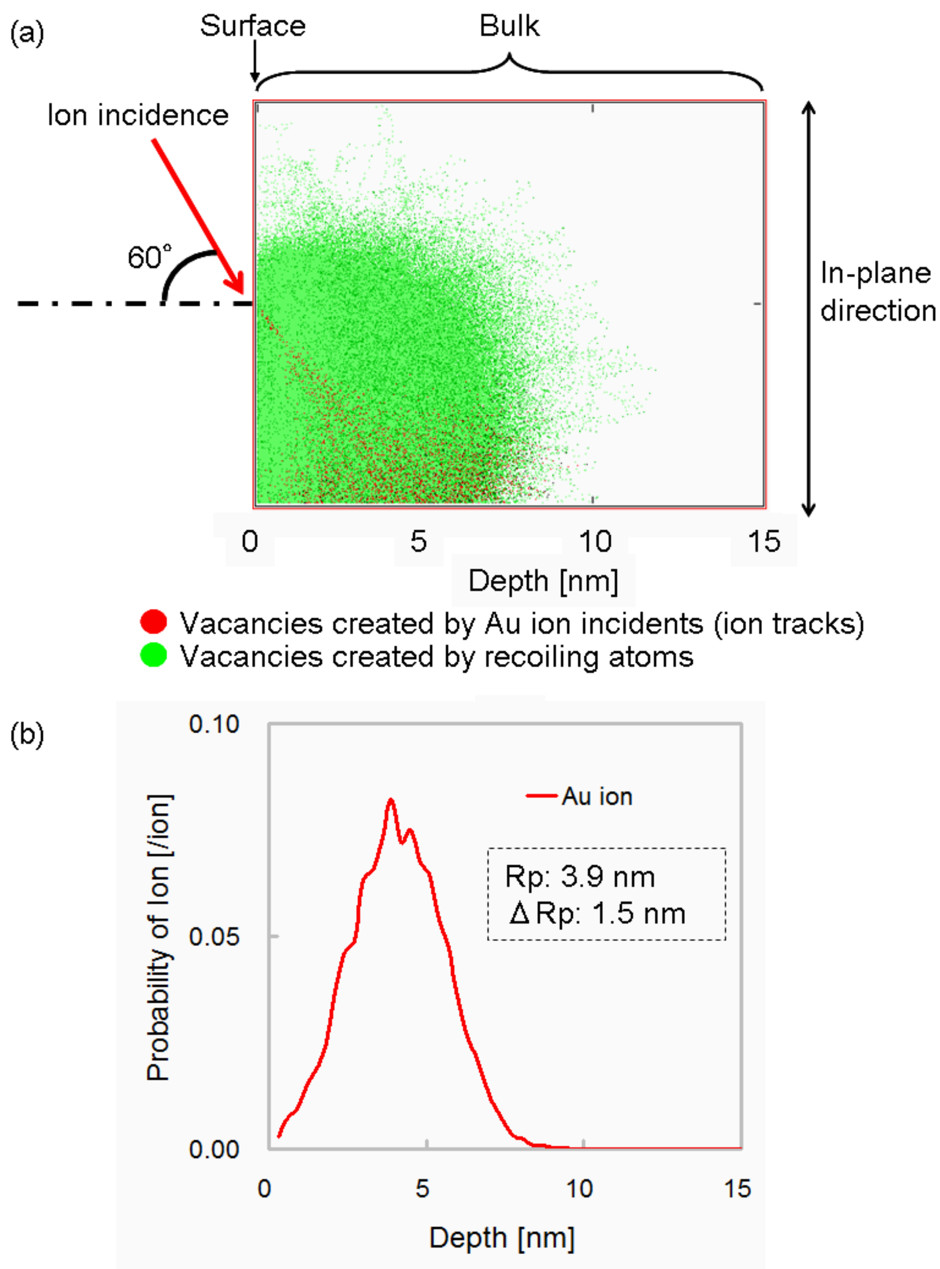

Figure 3.7: Distribution of Au ion calculated by TRIM (ref. [27]). (a) Ion tracks formed by Au ion implantation; Target material: amorphus-Si, Incident angle of ions: 60°, Ion energy: 3 keV, Numer of incident ions (simulated times of ion incidents): 10000. (b) Existing probability of Au ion as a function of depth.

3.4 Summary of Chapter 3

In order to investigate the behaviors of Au atoms as impurities in nano-scale, we performed real-time STM observation of the low-energy Au ion irradiation effects on high-temperature Si(111)-7 $\times$ 7 surface. We obtained sequential STM images of Si(111)-7 $\times$ 7 surfaces kept at 500 ℃ before, during, and after the 3 keV Au^+ ion irradiation. Vacancy islands and 5 $\times$ 2-Au structures were formed on the sample surface, and changed their size during the heat treatment after the ion irradiation. Number of surface Au atoms reached surface during heat treatment is estimated from 5$\times$2 area size. The growth rate of the 5$\times$2-Au domain suggests that implanted Au atoms reached the surface almost without interacting with defects in the bulk Si generated by the ion irradiation. Although our method here is limited to observe the topmost surface, the elemental steps of surface modifications can be directly clarified with the time resolution of the STM scan period. Moreover, this method can be extended to understand the atomistic picture of the other impurities such as dopants just after the ion irradiation.

References

[1] W. M. Bullis: Solid-State Electron. 9 (1966) 143.

[2] S. M. Sze: *Physics of Semiconductor Devices* (Wiley, New York, 1985) 2nd ed., Chap. 3, p. 175.

[3] S. Christiansen, R. Schneider, R. Scholz, U. Gosele, Th. Stelzner, G. Andra, E. Wendler, and W. Wesch: J. Appl. Phys. 100 (2006) 084323.

[4] Th. Stelzner, G. Andra, F. Falk, E. Wendler, W. Wesch, R. Scholz, and S. Christian: Nucl. Instrum. Methods Phys. Res., Sect. B 257, 172 (2007).

[5] L. A. Gilifalco: *Atomic Migration in Crystals* (Blaisdell, New York, 1964), Chap. 5 [in Japanese].

[6] F. C. Frank and D. Turnbull: Phys. Rev. 104 (1956) 617.

[7] U. Gosele, W. Frank, and A Seeger: Appl. Phys. 23 (1980) 361.

[8] N. A. Stolwijk, J. Holzl, W. Frank, E. R. Weber, and H. Mehrer: Appl. Phys. A 39 (1986) 37.

[9] J. S. Williams, M. C. Ridgway, M. J. Conway, J. Wong-Leung, X. F. Zhu, M. Petravic, F. Fortuna, M. O. Ruault, H. Bernas, A. Kinomura, Y. Nakano, and Y. Hayashi: Nucl. Instrum. Methods Phys. Res., Sect. B 178 (2001) 33.

[10] S. M. Myers and G. A. Petersen: Phys. Rev. B 57 (1998) 7015.

[11] J. Wong-Leung, E. Nygren, and J. S. Williams: Appl. Phys. Lett. 67 (1995) 416.

[12] J. Wong-Leung, J. S. Williams, A. Kinomura, Y. Nakano, Y. Hayashi, and D. J. Eaglesham: Phys. Rev. B 59 (1999) 7990.

[13] S. Mohapatra, J. Ghatak, B. Joseph, H. P. Lenka, P. K. Kuiri, and D. P. Mahapatra: J. Appl. Phys. 101 (2007) 063542.

[14] M. Msimanga and M. McPherson: Mater. Sci. Eng. B 127 (2006) 47.

[15] M. Uchigasaki, T. Kamioka, T. Hirata, T. Shimizu, F. Lin, T. Shinada, and I. Ohdomari: Rev. Sci. Instrum. 76 (2005) 126109.

[16] D. Grozea, E. Bengu, and L.D. Marks: Surf. Sci. 461 (2000) 23.

[17] K. Shimada, T. Ishimaru, T. Yamawaki, M. Uchigasaki, K. Tomiki, T. Matsukawa, and I. Ohdomari: J. Vac. Sci. Technol. 19 (2001) 1989.

[18] R. Plass and L. D. Marks: Surf. Sci. 380 (1997) 497

[19] . S. C. Erwin: Phys. Rev. Lett. 91 (2003) 206101.

[20] S. Riikonen and, D. Sanchez-Portal: Phys. Rev. B 71, 235423 (2005).

[21] F. C. Chuang, C. H. Hsu, C. Z. Wang, and K. M. Ho: Phys. Rev. B 77 (2008) 153409.

[22] T. Hasegawa, K. Takata, S. Hosaka and S. Hosoki: J. Vac. Sci. Technol. B 9 (1991) 758.

[23] T. Hasegawa, S. Hosaka and S. Hosoki: Jpn. J. Appl. Phys. 31 (1992) L1492.

[24] M. Shibata, I. Sumita and M. Nakajima: Phys. Rev. B 53 (1996) 3856.

[25] J. Slezak, M. Ondrejcek, Z. Chvoj, V. Chab, H. Conrad, S. Heun, T. Schmidt, B. Ressel, and K. C. Prince: Phys. Rev. B 61 (2000) 16121.

[26] S. Coffa, J. M. Poate, D. C. Jacobson, W. Frank, and W. Gustin: Phys. Rev. B 45 (1992) 8355.

[27] J. P. Biersack and J. F. Ziegler: Nucl. Instrum. Methods 194 (1982) 93.

[28] M. Morgenstern, T. Michely, and G. Comsa: Phys. Rev. Lett. 79 (1997) 1305.

.

Chapter 4

Real-Time Scanning Tunneling Microscope Observation of Silicon Surface Modified by Phosphorus Ion Irradiation

Dopants in Si interact with host Si atoms and point defects. In order to better control the behavior of dopants, it is important to clarify the behavior of point defects as well as that of dopants themselves. To observe point defects directly in real-space is believed to be impossible. However, if point defects diffuse in substrate and appear on surface, we can observe them as surface vacancies, surface atoms, and other atomic or nano-scale changes in the surface morphology. It is therefore expected that detailed and cautious investigation of surface nano-modificaiton will open a discussion on the behavior of point defects near surfaces.

STM is one of the most powerful tools to observe surface modification in atomic and nm scale. Actually, several pioneering works [1–5], followed by our group [6, 7], reported surface defects induced by ion irradiation. However, ion species

used in these works were rare gas such as argon (Ar) [1,2,6,7] and xeon (Xe) [3–5], or Si (self implantation) [8]. There is no report on surface modification with dopant ions actually used in Si LSI technology.

In this chapter, in order to understand what happens actually in the dopant ion irradiation process, real-time STM observation of P ion irradiation on Si substrate has been performed. Si(001) and Si(111) substrate are used as samples. The author tries to discuss on the behavior of point defects involved in the surface morphology change.

4.1 Experiment

The experiment was performed as shown in Fig. 4.1. A sample cut from a n-type Si(111) or Si(001) wafer was installed in the STM unit in UHV after chemical cleaning. The sample was degassed at 600℃ for more than 12 h, and was flashed repeatedly until the surface was covered with reconstruction structure (7×7 for Si(111) sample, 2×1 for Si(001) sample). The sample was then kept at observation temperature of R.T., 500℃ and 600℃ for over 1 h until they reached thermal equilibrium with a STM tip. After preparation of the sample surface, STM observation was started. STM images of the surface were taken with constant-height mode. During the STM observation, P^+ ions with 5 keV were irradiated and the observation was continued in the same area. The ion doses are estimated by the following equation: $I/e \times t/S$, where I is the average absorbed current, e the elementary charge, t the irradiation time, and S the scan area size.

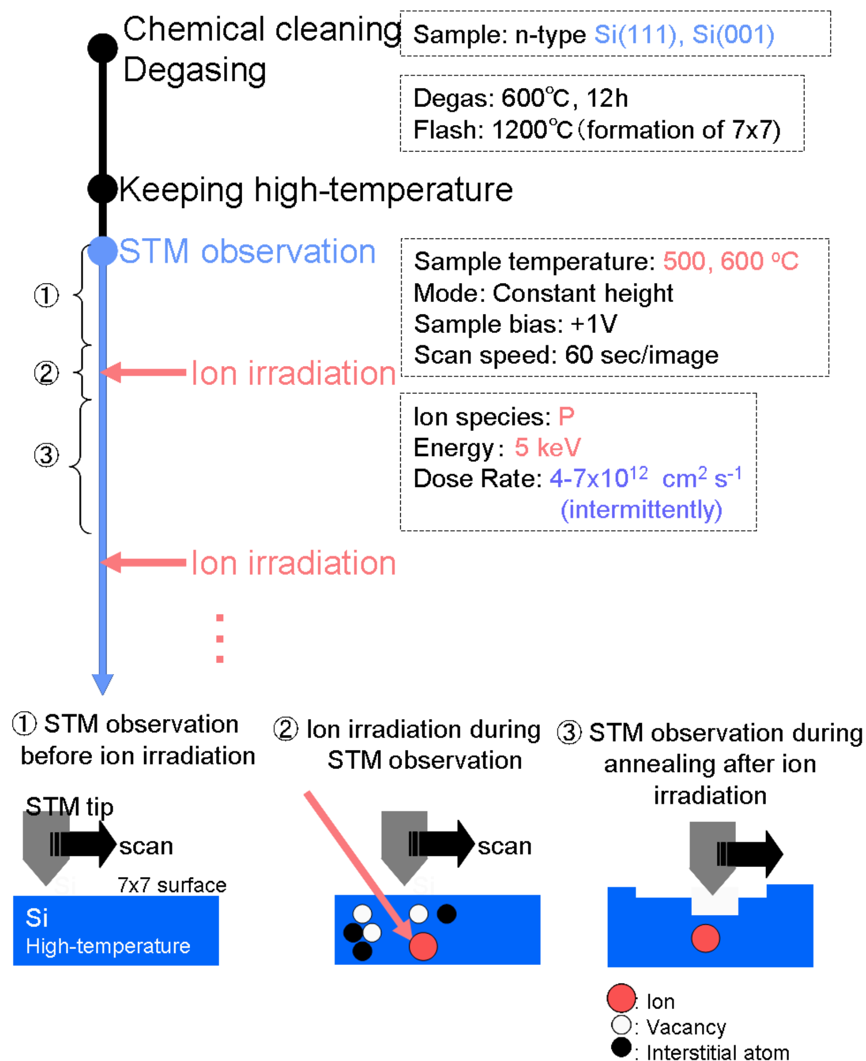

Figure 4.1: Experimental procedure of real-time STM observation of P^+ ion irradiation effects on high-temperature Si surface.

4.2 Modification on Si(111) Surface

4.2.1 Morphological Change by Ion Irradiation and During Heat Treatment

Figure 4.2 shows a sequential STM images of 600℃-Si(111) surface taken (a) before, (b) during, and (c) after the ion irradiation. Figure 4.2(a) is the initial surface, in which atomic steps and 7×7 terraces are observed. During the next scan of Fig. 4.2(b), P^+ ions were irradiated for 6 s. Just after the ion irradiation, many small patches with 20-30 nm in diameter appeared on the terraces. Judged by the scan direction and the width of the black region at the periphery of the vacancy island as shown in the Fig. 4.2(d), these structures are identified to be vacancy islands, which are indentations with 7×7 DAS structure of one bilayer depth. The number density of vacancy islands ($2.7 \times 10^{10} cm^{-2}$) is much smaller than the ion dose ($5.4 \times 10^{13} cm^{-2}$) by three-order of magnitude. This is because that most of the ion-induced defects already recovered before the STM observation reopened.

This is supported by the comparison of ion-irradiated surfaces taken at R.T. and high-temperature. STM images shown in Fig. 4.3 were taken in the separate experiment with almost the same dose but at different temperatures. At R.T. the initial 7×7 surface are fully roughened after the ion irradiation. It is, therefore, indicated that the heat treatment at high-temperature leads to the recovery of the crystal.

Based on a TRIM calculation [9], sputtered atoms and generated vacancies in the observation area are estimated to be 2.4×10^6 vacancies and 4.4×10^7 atoms, respectively. These values are estimated by assuming the sputtering yield of 5.5 atom/ion, the vacancy production rate of 126 atom/ion, and the number of incident ions in the observation area of 3.5×10^4 ion. On the other hand, the average size of each vacancy island is about $285 nm^2$. The estimated number of vacancies corre-

sponds to 4,480, which is calculated based on the assumption that 98 Si atoms are involved in each 7×7 DAS unit cell [10]. This value is about ten times as much as that of TRIM simulation, so that we can not explain that each vacancy island is induced by single-ion-incidence. More than one single-ion-induced defects are responsible to form a vacancy island.

Figure 4.4 shows a sequential STM images of 600℃-Si(111)-7×7 surface taken (a) 108 s after, (b) 466 s, (c) 1576 s after the ion irradiation. During the heat treatment, the vacancy islands tend to shrink and some of them disappeared, which results in the decrement of the number density as shown in Fig. 4.5. The shape of steps edges appear to change. Figure 4.6 shows the step edges and vacancy islands before and after the ion irradiation. From the figure, the steps are found to be retreated during the heat treatment between at 108 s and 1576 s after the ion irradiation. Since the attachment and detachment of atoms (or vacancies) causes the motion of steps and the changes in size of vacancy islands, these results mean that the migration of surface atoms and surface vacancies occurs during the heat treatment. In addition to the surface migration, diffusion of vacancies and interstitials from the substrate to the surface could lead to morphology changes.

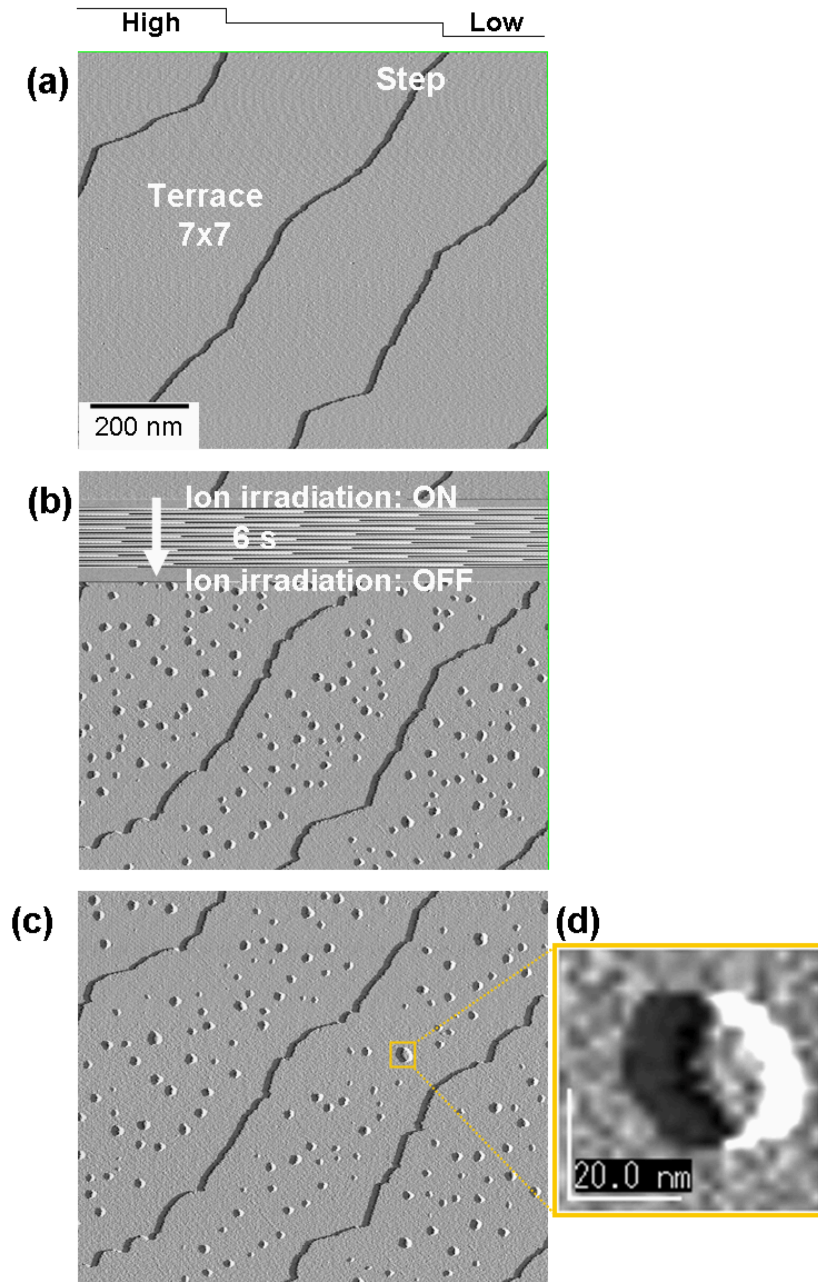

Figure 4.2: Sequential STM images of 600℃-Si(111)-7 × 7 surface taken (a) before, (b) during, and (c) after the ion irradiation. Ion species is P^+ with 5 keV and dose is $5.4 \times 10^{13} cm^{-2}$. Each image was scanned with constant height mode at a scan speed of 60 s/image. Sample bias is +1 V and tunneling current is 0.2 nA.

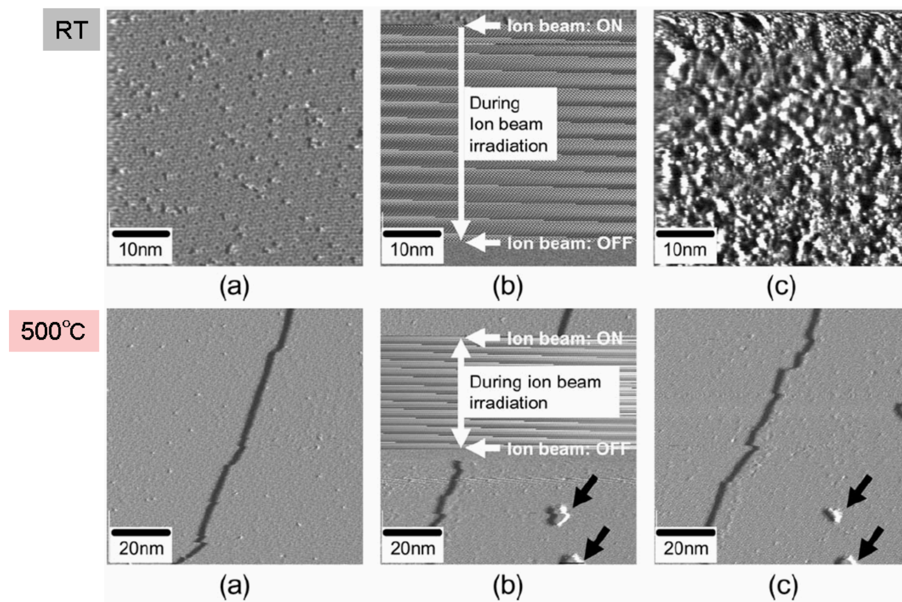

Figure 4.3: Comparison of ion-irradiated surfaces between R.T. and high-temperature [Referred in *T. Kamioka et al., Rev. Sci. Technol.* ***79*** *(2008) 073707*]. Ion species: 5 keV-P^+, Dose: $2.5 \times 10^{14} cm^{-2}$ at R.T. and $2 \times 10^{14} cm^{-2}$ at 500℃.

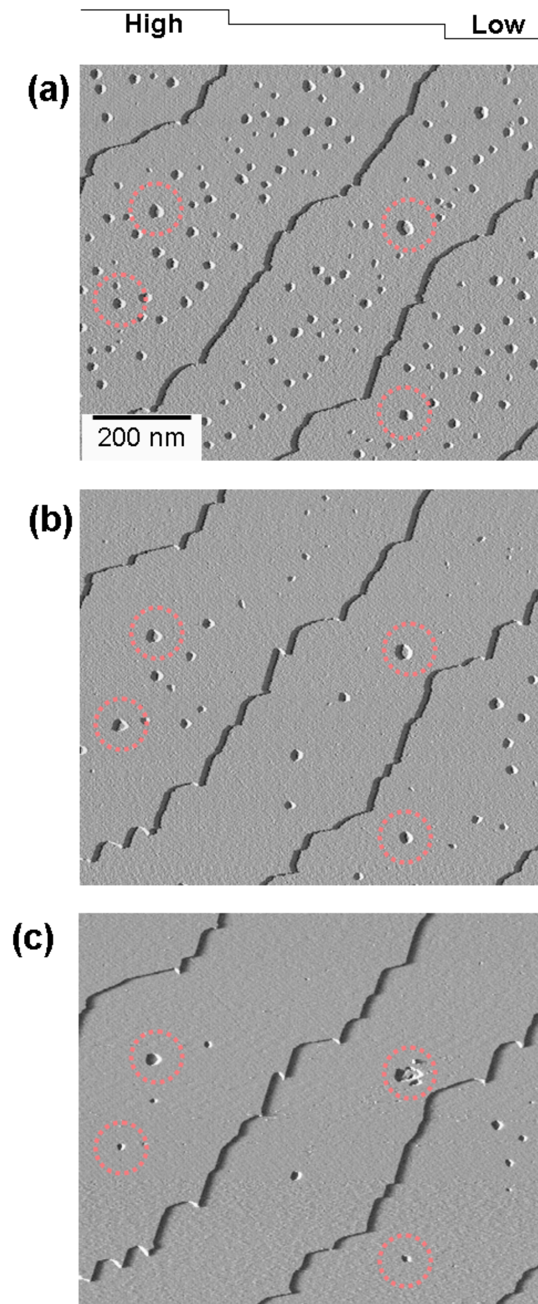

Figure 4.4: Sequential STM images of 600℃-Si(111)-7×7 surface taken at (a) 108 s after, (b) 466 s after, and (c) 1576 s after the ion irradiation. Each image was scanned with constant height mode at a scan speed of 60 s/image. Sample bias is +1 V and tunneling current is 0.2 nA.

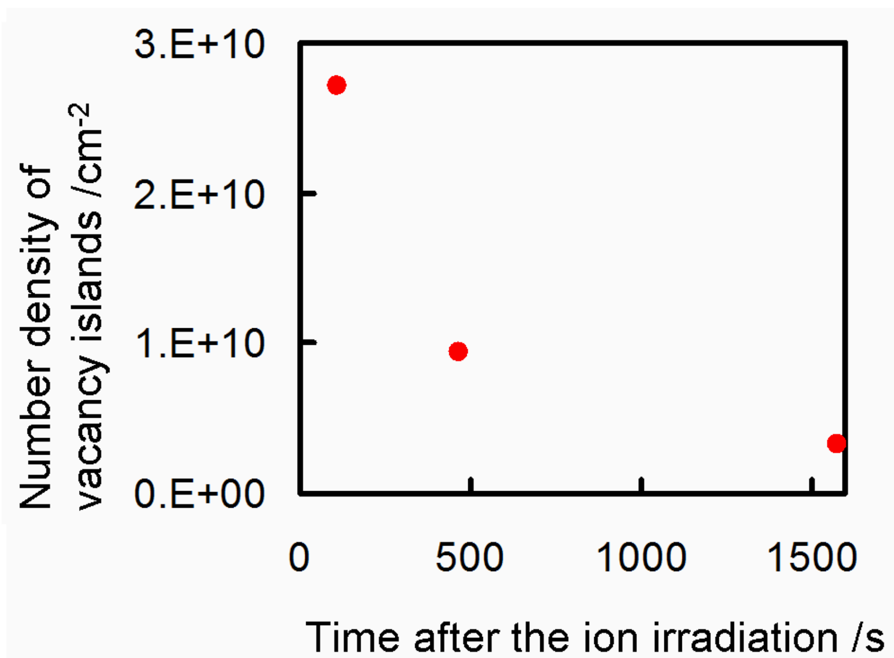

Figure 4.5: Time development of the number density of vacancy islands. The sample area size is $734nm \times 867nm$. Vacancy islands smaller than about $10nm^2$ are not counted.

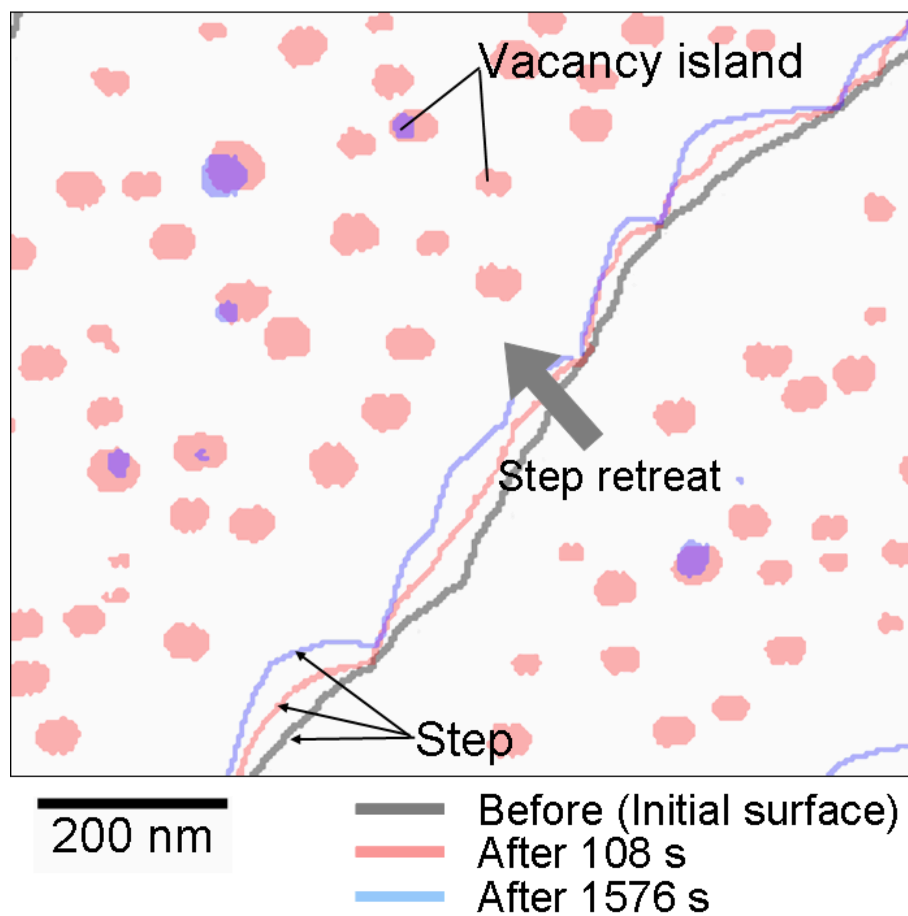

Figure 4.6: Step motion and evolution of vacancy islands before, after ion irradiation.

4.2.2 Surface Modification by Additional Ion Irradiation onto the Same Surface

In order to better understand the effect of ion irradiation on surface morphological change, we additionally irradiated P^+ ions onto the same sample surface. As shown in Fig. 4.7(a), vacancy islands are hardly observed and step edges are roughened at 1576 s after the first ion irradiation. When P^+ ions are additionally irradiated on the surface, vacancy islands newly appeared. As indicated arrows in Fig. 4.7(a) and 4.7(b), the number of step kinks increases so that step edges are more roughened by the ion irradiations. It is noted that the vacancy islands remaining before the second ion irradiation are enlarged by the ion irradiation, which are indicated by dotted circles in Fig. 4.8. It is suggested that the vacancy clusters act as a sink for surface vacancies. During the heat treatment after the second ion irradiation, these vacancy islands shrink and some disappeared and the step edges are retreated and become smooth, in the similar way as the first irradiation and subsequent heat treatment.

These phenomena can be observed at different high-temperatures. Figure 4.9 shows Si(111) surface kept at 500℃ with almost the same dose and time. At 500℃, the number density of residual vacancy islands after the first ion irradiation is larger than those at 600℃. The roughness of the step edges is smaller. The width of denuded zone in terms of vacancies near the step edges is narrower than those at 600℃. These results are ascribed to the difference in the diffusivity of point defects in substrate and on surface. At high temperature, the diffusivity of interstitial atoms is high enough for the recovery of vacancy islands. The diffusivity of vacancies is also high for long distance surface migration to be annihilated at the step edge, which leads to widen the denuded zone near the step edges.

As described above, ion irradiation at high-temperatures induces surface modification as a result of diffusion of point defects. Figure 4.10 shows the STM images of Si(111) surface kept at 500℃ modified with intermittent ion irradiations. As the

ion dose increase, the mean size of vacancy island increases and the retreat and roughness of step edges increase. For clarity, transition of step edges and vacancy islands are indicated as shown Fig. 4.11. In the image of Fig. 4.11(b), we can see the overlap in the distribution of vacancy islands between at 56 s after the 2nd irradiation (green circles) and at 64 s after the 4the irradiation (red circles). We can also distinguish the coalescence of the vacancy islands to form large ones.

Our real-time STM observation reveals the microscopic aspects of elemental steps of surface modification. As shown in Fig. 4.12, we directly observe the coalescence of neighboring vacancy islands just after the ion irradiation, resulting in the expansion of the vacancy island. Also observed is incorporation of a vacancy island into a retreated step edge, resulting in the enhancement of step roughness.

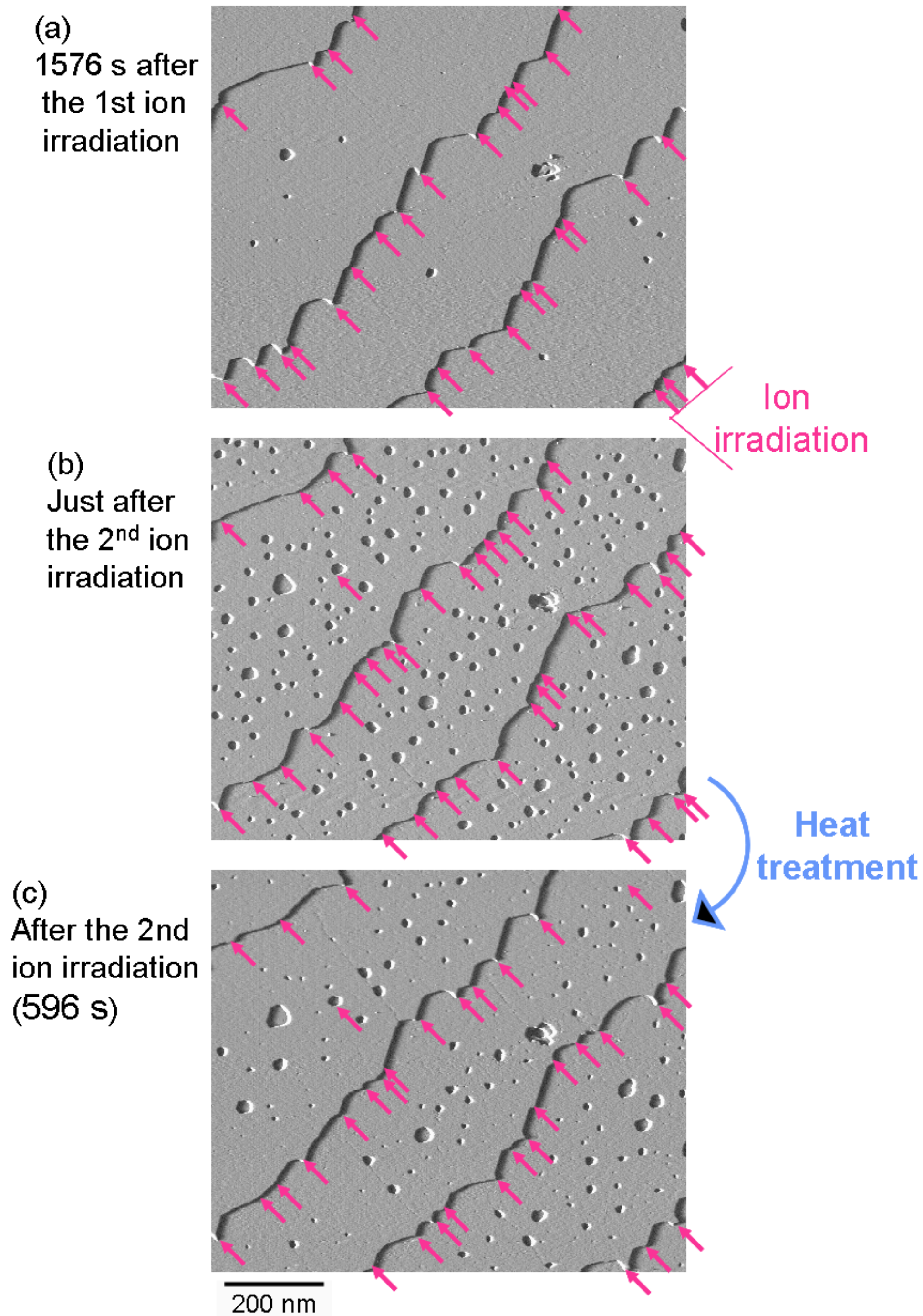

Figure 4.7: STM images of Si(111) surface at 600℃ before and after the second ion irradiation. Dose is $5.4 \times 10^{13} cm^{-2}$. Kinks sites are indicated by arrows.

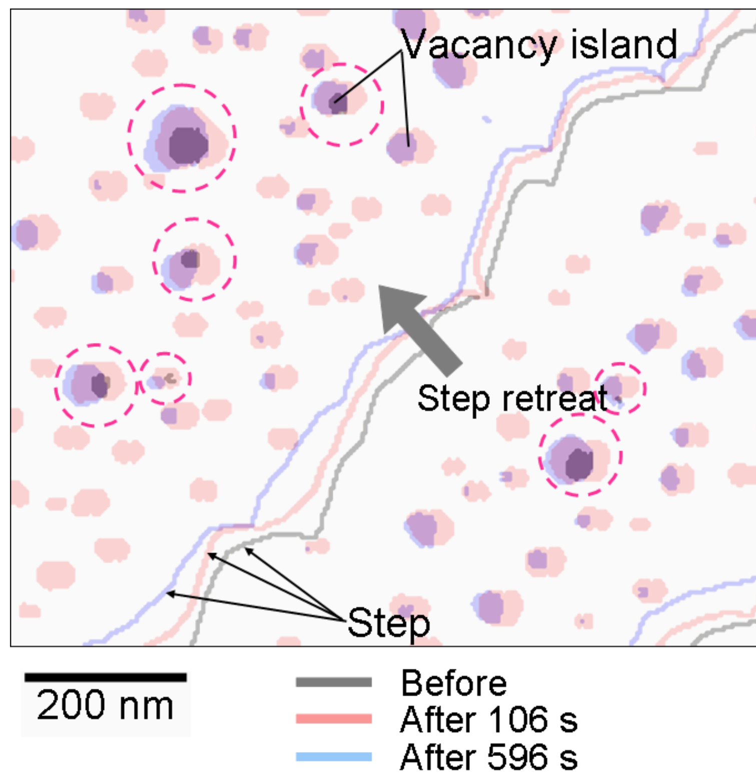

Figure 4.8: Step motion and evolution of vacancy islands before, after the second ion irradiation. Dotted circle indicates the overlapped vacancy islands between before and after the ion irradiation.

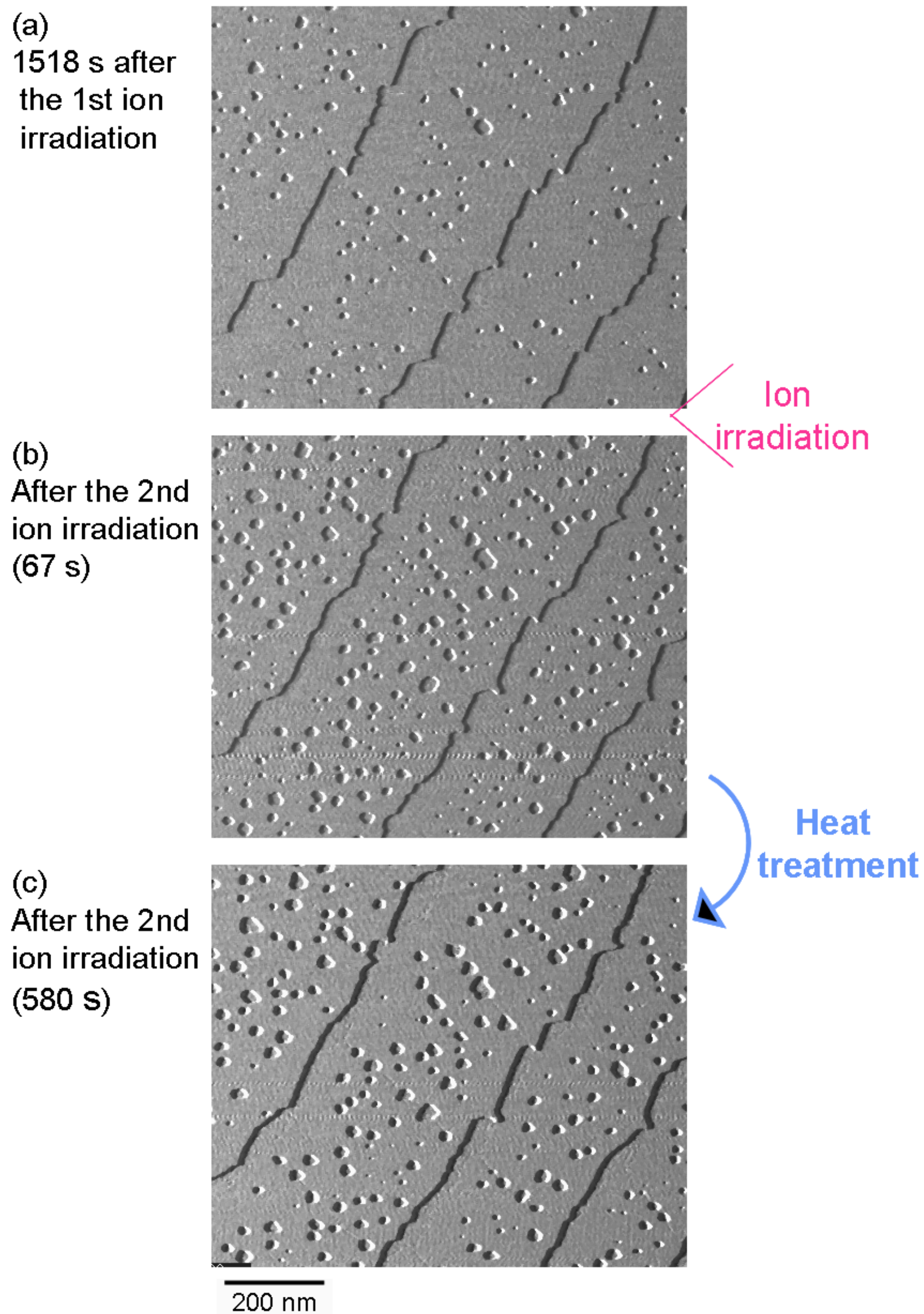

Figure 4.9: STM images of Si(111) surface at 500℃ before and after the second ion irradiation. Dose is $6.3 \times 10^{13} cm^{-2}$.

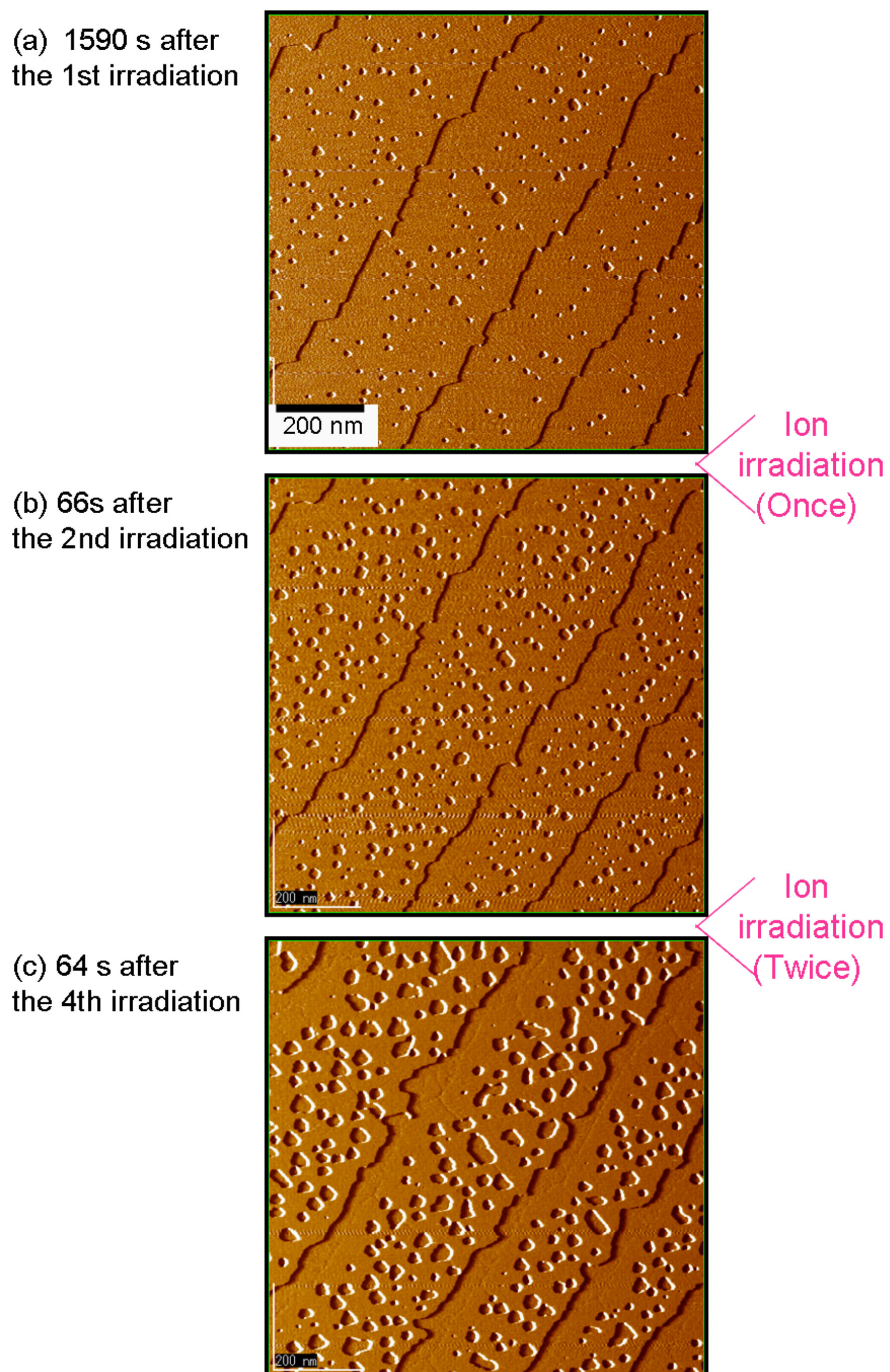

Figure 4.10: STM images of Si(111) surface kept at 500℃ modified with intermittent ion irradiations. Dose at each time: $6.3 \times 10^{13} cm^{-2}$, Vs: +1 V, It: 0.2 nA.

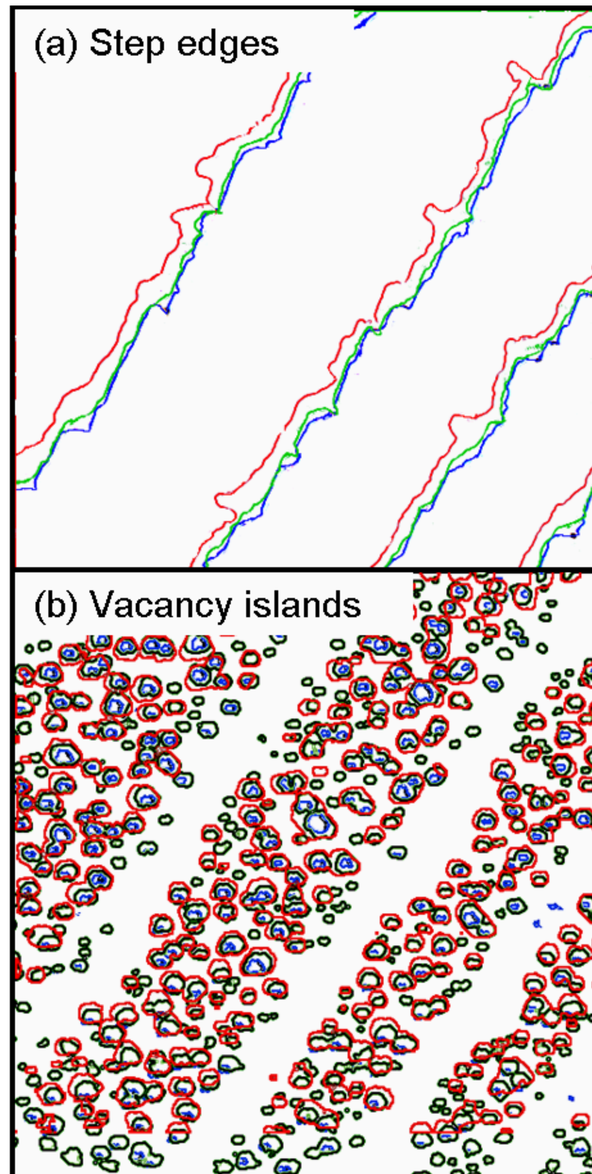

Figure 4.11: Transition of the step edges and vacancy islands just after each ion irradiation. (a) 1590 s after the first ion irradiation, (b) 56 s after the second ion irradiation, and (c) 64 s after the fourth ion irradiation.

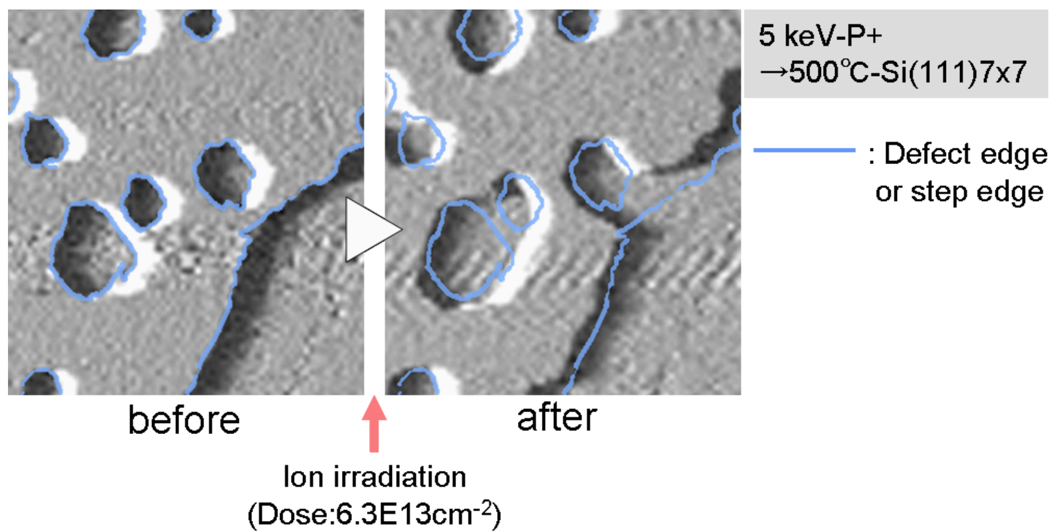

Figure 4.12: Magnified images of vacancy islands near the step edge taken before and after the ion irradiation. Scan area size is $141nm \times 141nm$. 5 keV-P^+ ions were irradiated on to 500℃-Si(111) surface to a dose of $6.3 \times 10^{13} cm^{-2}$.

4.2.3 Behavior of Point Defects

In this way, surface modification by ion irradiation occurs as the nucleation and growth (or decay) of vacancy islands and the retreat of step edges, resulting in the removal of surface atoms. However, although these phenomena are apparently caused by the vacancy diffusion and sputtering, we have to also consider the interstitials diffusion toward surface. In order to explain the behavior of vacancy islands and step edges, we compare the number of surface vacancies in the experiment and in the simulation.

In the temperature range between 500 and 600℃, sublimation of atoms from the surface hardly occurs. Thus, evolution of vacancy islands and step motion are attributed to the sputtering and the diffusion of point defects from the bulk toward the surface. Figure 4.13 shows the number of vacancies appeared on the surface at 600℃ as a function of time after the first ion irradiation. Just after the ion irradiation, surface vacancies increases a lot due to the nucleation of vacancy islands and the retreat of the step edges. The ion dose is $5.4 \times 10^{13} ion/cm^2$, and therefore sputtered atoms calculated by TRIM are 3×10^{14} atoms (sputtering yield is 5.5 atom/ion). However, density of total surface vacancies is about $1.6 \times 10^{14} atom/cm^2$, which is less than those of the simulation as listed in Table 4.2.3. Upon each irradiation (the second, the third, and the fourth irradiation) at each temperature (600℃ and 500℃), it appears to be similar as shown in Fig. 4.14 and Fig. 4.15, respectively. At 500℃, unfortunately we could not extract the data between just after the first ion irradiation and the second ion irradiation, so that we focus on the time after the second ion irradiation (Note that the origin of the time scale corresponds to the time just after the second ion irradiation).

As shown in Fig. 4.16, number of vacancies newly appeared on the surface ($\Delta N_{surfvac}$) upon each irradiation could be determined by the equation: $\Delta N_{surfvac} = N_{sput} + N_{vac} - N_{int}$, where N_{sput} denotes number of sputtered atoms by each ion

irradiation, N_{vac} and N_{int} denotes number of vacancies and interstitials reached the surface within the next scan of each ion irradiation. Now $\Delta N_{surfvac}$ is less than N_{sput}, so that $N_{vac} - N_{int} < 0$. That is, interstitials diffuse from the substrate to the surface much more than vacancies. Figure 4.17 shows the density of atoms reached surface as a function of ion dose. Both at 500℃ and 600℃, observed surface vacancies is less than sputtered atoms, and about 3-3.5 excess interstitials per ion diffuse toward surface.

During the heat treatment after each irradiation, vacancies involved in the step retreat gradually increase at both temperatures. On the other hand, size of vacancy islands tends to decrease at both temperatures at low dose. As the temperature increases, the rate of step retreat and size change of vacancy islands increase. This is attributed to the high diffusivity of point defects at high temperature. As a result, the total number of surface vacancies changes.

In this way, diffusion of point defects toward the surface leads to retreat of step edges and evolution of vacancy islands. On the surface, there is an interaction between steps and vacancy islands, which results in the formation of the denuded zone in terms of vacancies. The density of surface vacancies depends on the distance from the step edge as shown in Fig. 4.18. Both after each ion irradiation and after each heat treatment, the density of surface vacancies in the middle region of the terrace (region “ B ”) is higher than those of near the step edges (region “ A ” and “ C ”). This indicates that the step edges affect the behavior of vacancy islands. Also, the density of surface vacancies in region “ A ”, which is adjacent to the upper terrace, is a little higher than those of in region “ C ”, which is adjacent to the lower terrace. The reason for this may be the decrease of the denuded zone width caused by step retreat, or the asymmetry of the kinetic coefficient of incorporation into a step from the upper and from the lower terrace, which is known as the Ehrlich-Schwoebel effect [11]. In the middle region of the terrace, the morphology

change in size of vacancy islands is less affected by the step edges.

The atomistic picture for growth and decay of vacancy islands are proposed as shown in Fig. 4.19. When a vacancy island shrinks, as shown in the present experiment, possible mechanisms are; (a) supply of adatoms from the step edge, (b) emission of vacancies from the vacancy island, and (c) supply of interstitials from the bulk. It is generally accepted that most of the point defects generated by ion irradiation annihilate by recombination within ps order. Only a few percent of point defects survive and clusterize. Then, these clusters dissolve to release point defects during heat treatment. This is suggested by the gradual increase and decrease of the number of surface vacancies during heat treatment in Fig. 4.14 and Fig. 4.15.

Finally, we show a preliminary result using cross-section TEM of ion-irradiated sample. The experimental procedure is described in Fig. 4.20. A Si(001) substrate was irradiated with 5 keV-P^+ ions at 500℃. Then sample was quenched at 180 s after the ion irradiation. As shown in Fig. 4.21 and Fig. 4.22, within 10 nm depth, the lattice images of (110) plane is observed and defects are hardly observed. However, in the end-of-range, which is the deeper region than the projected range of P ions, we can see a band of defects. These defects have a few nm scale in size so that they indicates clusters of point defects. Although the substrate is different and the ion dose is much higher than those in the STM experiment, similar phenomena may occur in the STM experiment. In order to know the detail information on diffusion of point defects in bulk toward surface, further analysis such as simulation of point defect diffusion and other observation methods such as TEM study are needed.

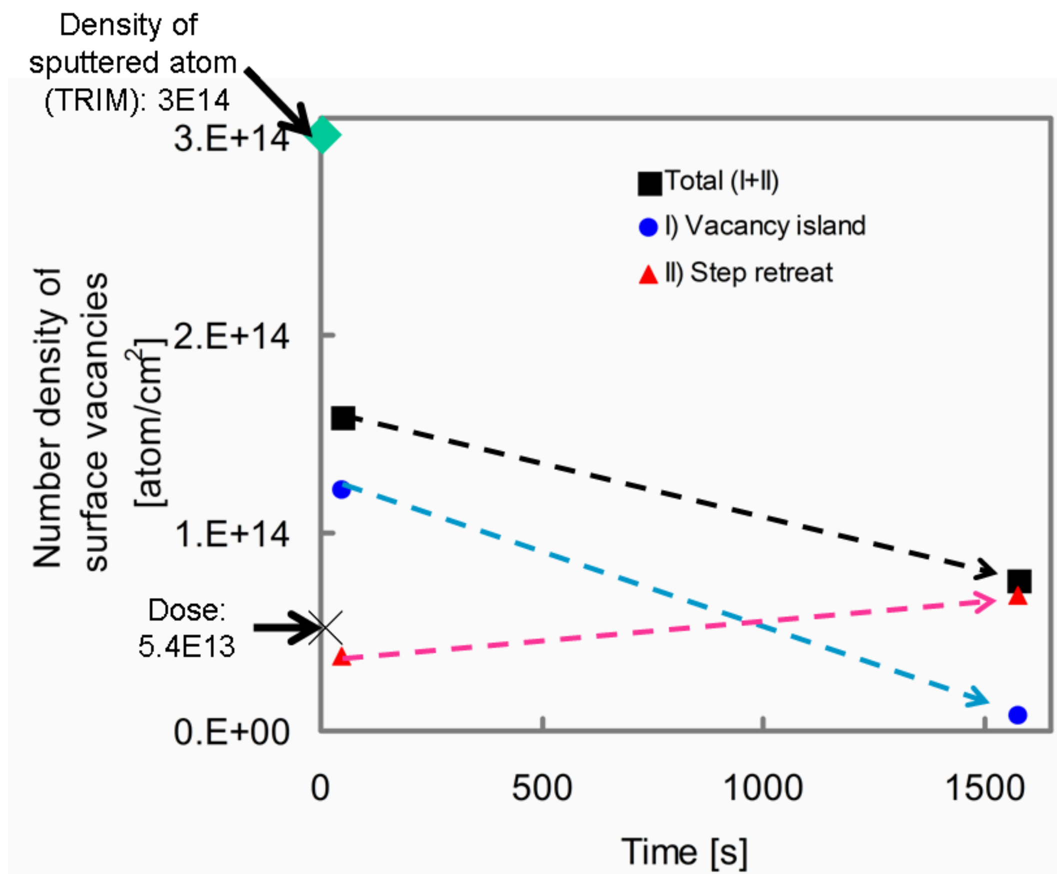

Figure 4.13: Time evolution of surface vacancies after the first ion irradiation at 600℃.

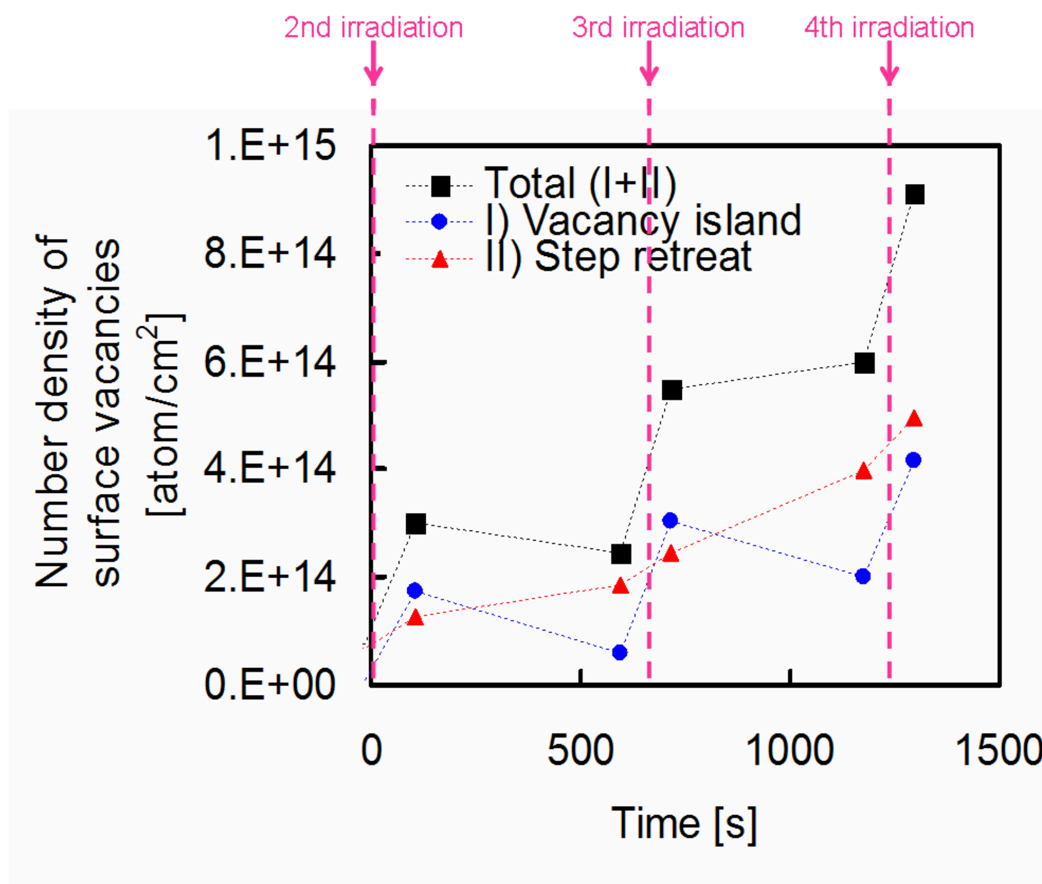

Figure 4.14: Time evolution of surface vacancies after ion irradiation at 600℃. Note that $t = 0$ corresponds to at the end of the second ion irradiation.

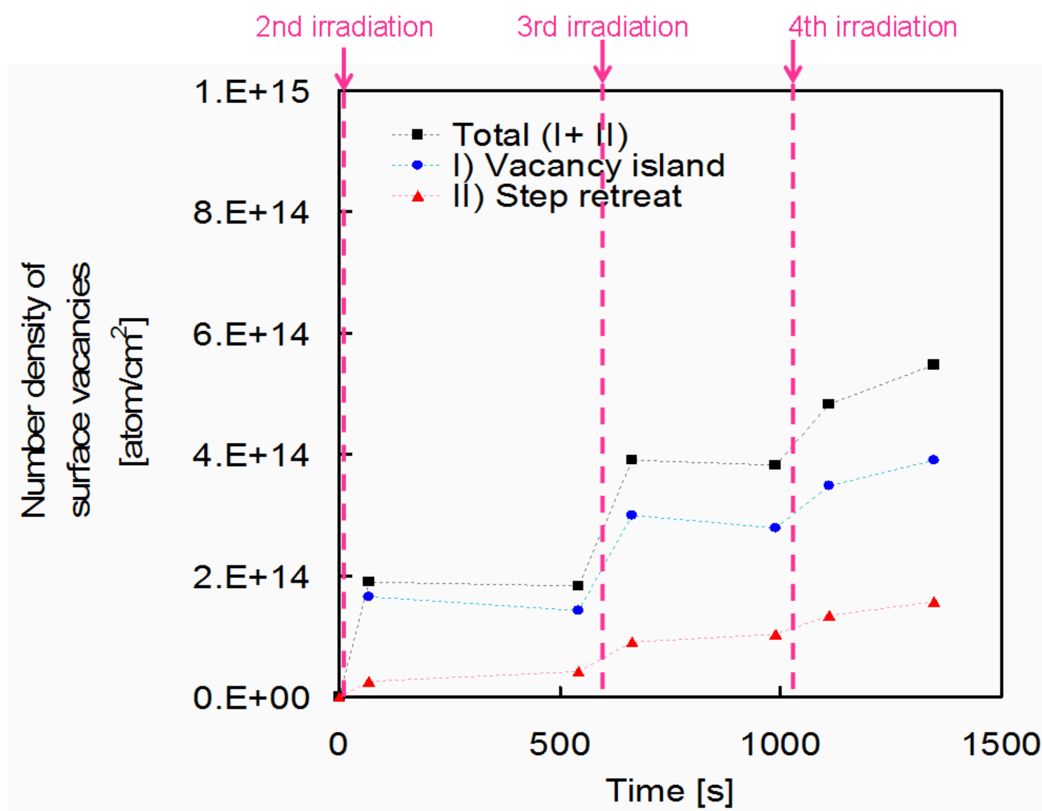

Figure 4.15: Time evolution of surface vacancies after ion irradiation at 500℃. Note that $t = 0$ corresponds to at the end of the second ion irradiation.

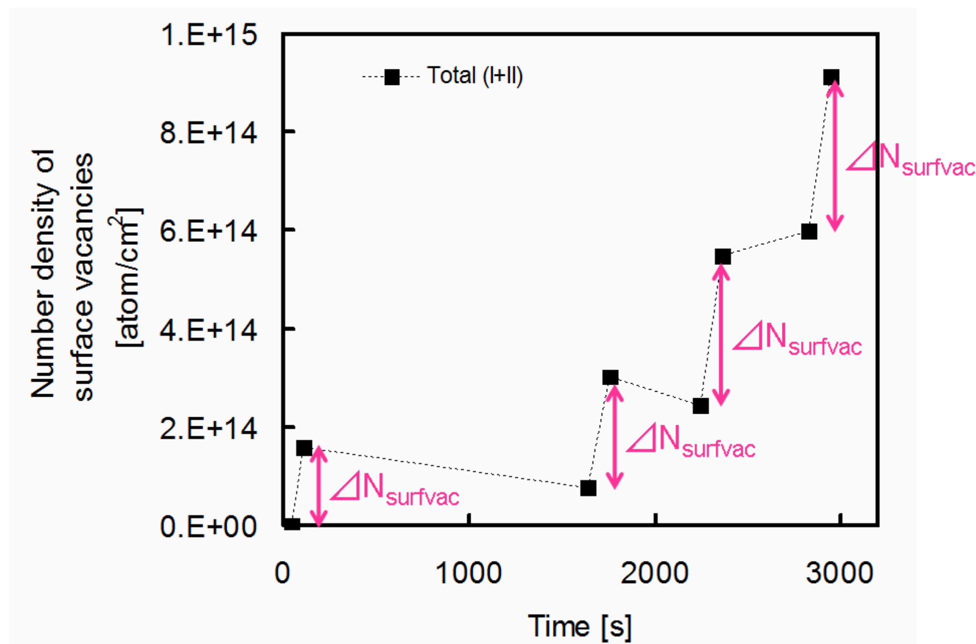

Figure 4.16: $\mathit{\Delta N}_{surfvac}$ denotes the net increase in the number of surface vacancies introduced by each ion irradiation. This value eliminates the variation in the number of surface vacancies during the time interval between each ion irradiation.

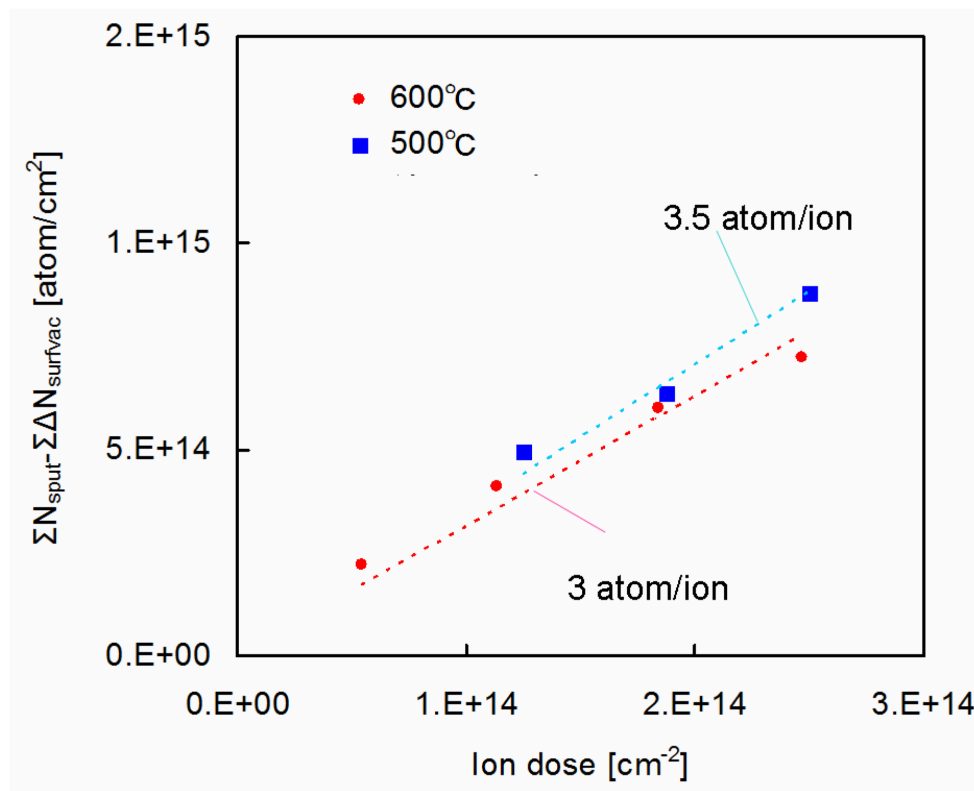

Figure 4.17: Density of atoms reached surface as a function of ion dose.

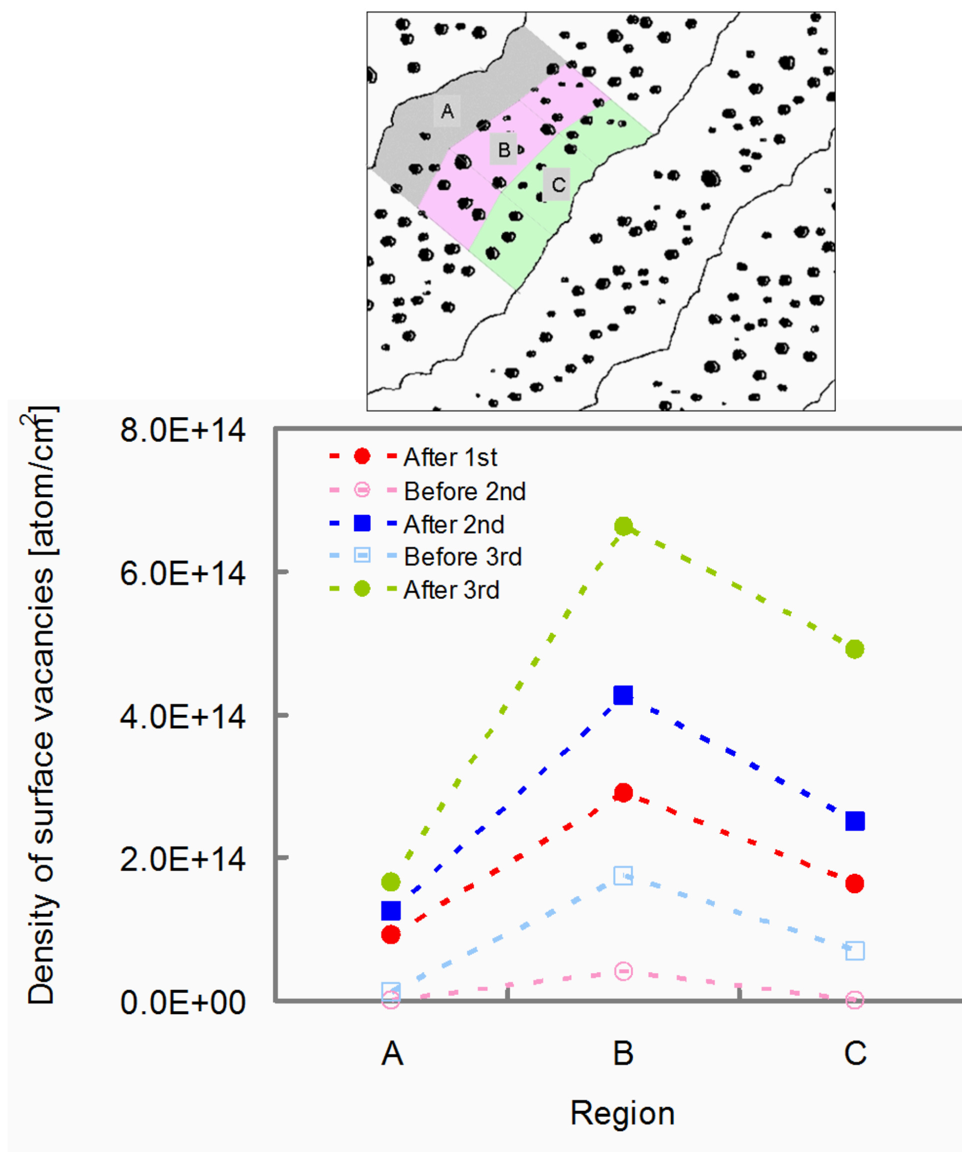

Figure 4.18: The density of surface vacancies in each segment on the terrace. Regions " A ", " B ", and "C " correspond to the regions in the above image, respectively.

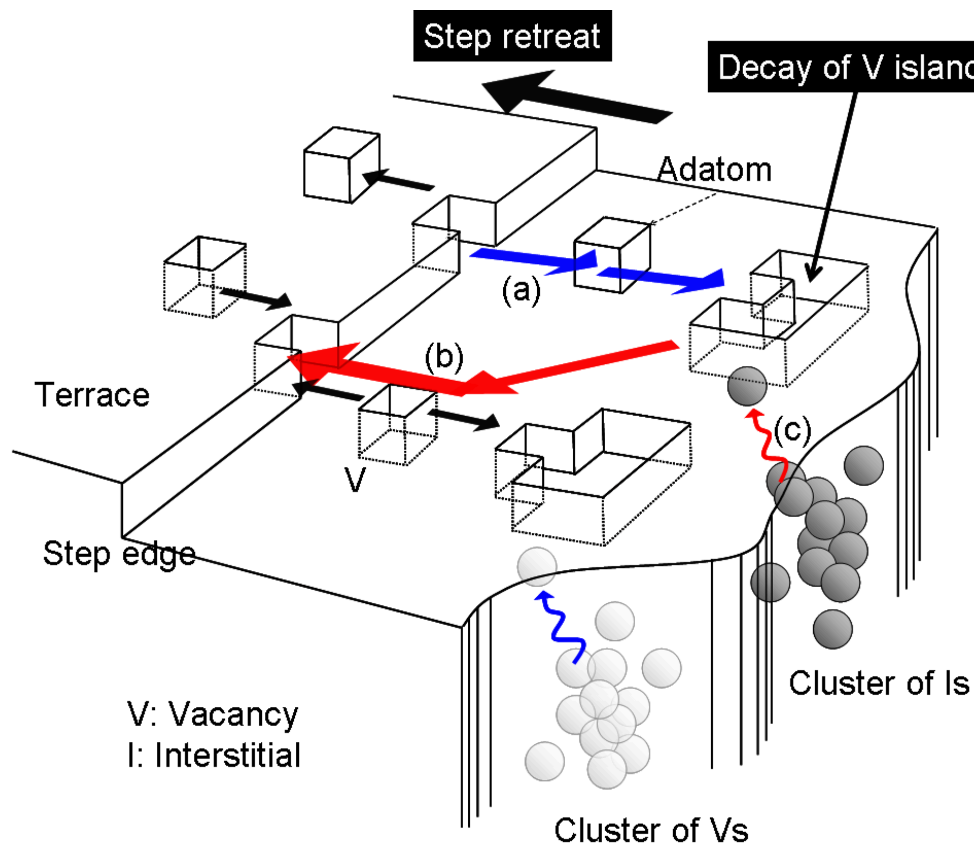

Figure 4.19: Possible mechanisms of decay of vacancy islands; (a) supply of adatoms from the step edge, (b) emission of vacancies from the vacancy island, and (c) supply of interstitials from the bulk.

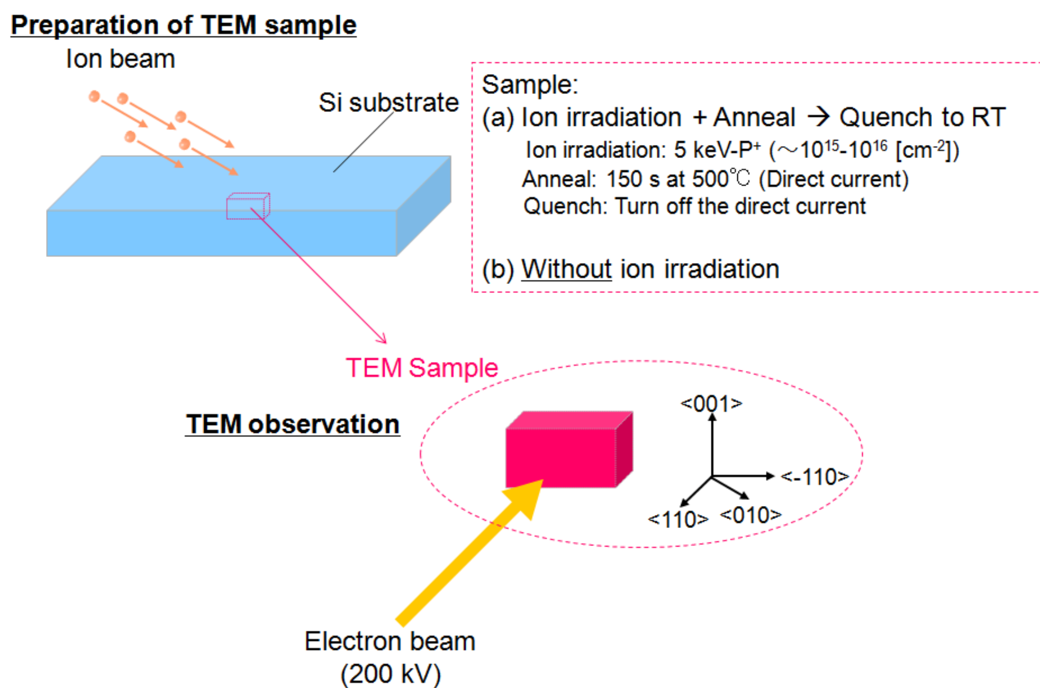

Figure 4.20: Preparation of TEM sample. A Si(001) substrate is irradiated with 5keV-P^+ ions at 500℃ and then quenched at 180 s after the ion irradiation.

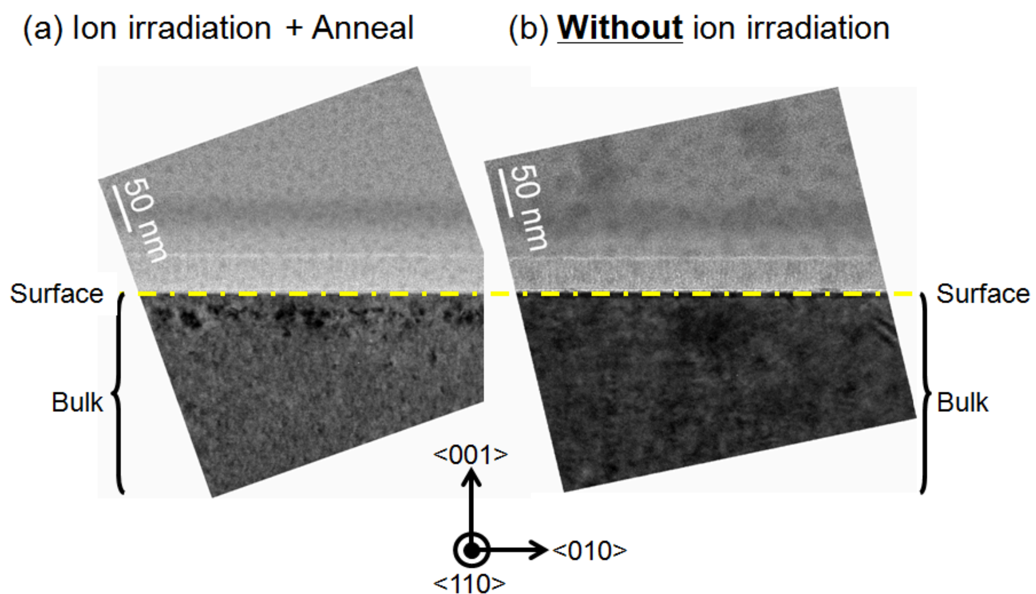

Figure 4.21: Cross-section TEM images of (110) plane of Si(001) substrate. (a) Ion-irradiated sample with 5 keV-P^+ ions to a dose of about $10^{15} - 10^{16} cm^{-2}$ at 500℃. The sample was quenched at 150 s after the ion irradiation. (b) Sample without ion irradiation.

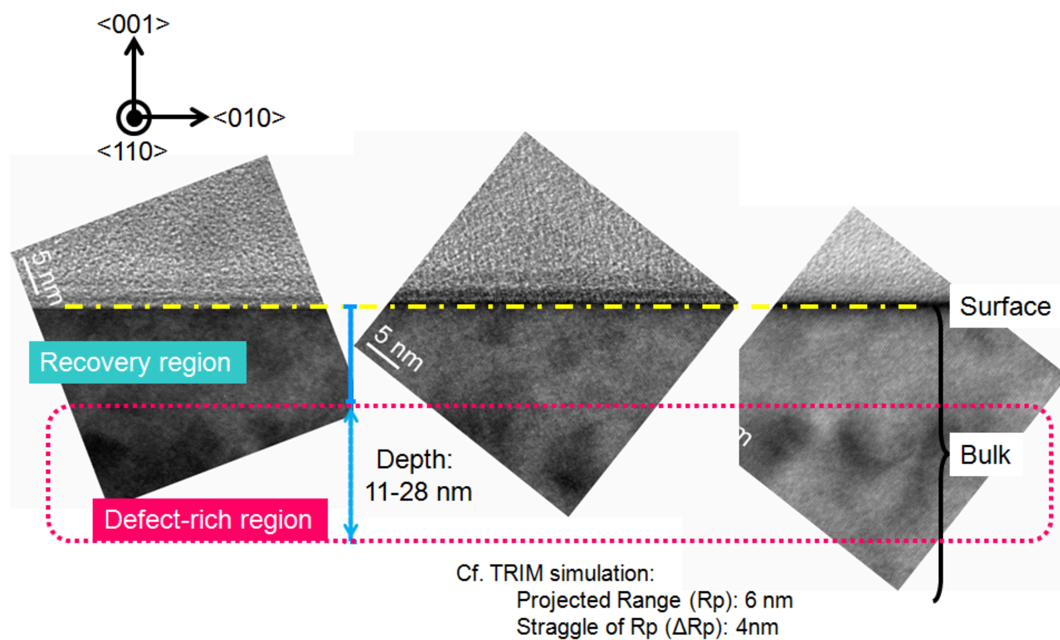

Figure 4.22: Magnified cross-section TEM images of (110) plane of the ion-irradiated Si(001) substrate. The sample was irradiated with 5 keV-P^+ ions to a dose of about $10^{15} - 10^{16} cm^{-2}$ at 500℃, then was quenched at 150 s after the ion irradiation.

Table 4.1: Comparison of density of observed surface vacancies after the ion irradiation with ion dose and estimated sputtered atoms.

Ion dose		5.4×10^{13} [cm^{-2}]
Density of sputtered atoms (TRIM)		3×10^{14} [cm^{-2}]
Density of surface vacancies involved in the formation of vacancy islands and the retreat of steps at 108 s after the ion irradiation	I)+II) Total	1.6×10^{14} [cm^{-2}]
	I) Vacancy islands	1.2×10^{14} [cm^{-2}]
	II) Step retreat	3.8×10^{14} [cm^{-2}]

4.3 Modification on Si(001) surface

4.3.1 Morphological Change by Ion Irradiation and During Heat Treatment

Figure 4.23 shows sequential STM images of 500 ℃-Si(001)-2 × 1 surface taken (a) before, (b) during, and (c) after 5 keV-P^+ ion irradiation. Although the initial surface before the ion irradiation has many vacancy type point defects, there are no clusters of them. During the next scan of Fig. 4.23(b), P^+ ions were irradiated onto the sample surface. After the ion irradiation as shown in Fig. 4.23(c), vacancy islands, which is two dimensional clusters of surface vacancies, are formed on the terrace and step edges are roughened. Vacancy islands are observed only on the lower 1×2 terrace between S_A (the step edges is perpendicular to the dimmer rows) and S_B step (the step edges is perpendicular to the dimmer rows). S_B steps are more roughened than S_A step since vacancies prefer to annihilate at S_B step [12].

The number density of vacancy islands ($5.8 \times 10^9 cm^{-2}$) is much smaller than the ion dose ($4 \times 10^{13} cm^{-2}$) by four-order of magnitude. In addition, the average number of vacancies which consist of each vacancy island is about 1,100 and this is about ten times as much as the TRIM estimation. These features are seen in vacancy islands on Si(111). Most of the ion-induced defects already recovered before the STM observation reopened, and more than one single-ion-induced defect is considered to form a vacancy island.

Figure 4.24 shows sequential STM images of Si(001)-2 × 1 surface during heat treatment at 500℃ after the ion irradiation. During the heat treatment, surface morphology gradually changes so as to shrink vacancy islands. As shown in Fig. 4.24(b), vacancy islands on terraces almost disappear at 1631 s after the ion irradiation. Some vacancy islands enlarge and the others shrink. Steps are gradually retreated during the heat treatment.

In is noted that the growth rate of size of vacancy islands is anisotropic. The growth parallel to the dimmer rows increases faster than those of perpendicular to the dimmer rows. Figure 4.25 shows growth rate of vacancy island size perpendicular and parallel to Si(001)-2 $\times$ 1 dimmer in the separate experiment with the same experimental condition. Vacancy islands exhibit a large expansion in the parallel direction to the dimmer rows compared to perpendicular direction by 2-3 times. Considering the pioneering report on the anisotropic kinetics step retreat, in which S_B steps (the step edges is perpendicular to the dimmer rows) retreat 1.8 times faster than S_A steps (parallel to the dimmer rows) [12], this result reflects anisotropic surface diffusivity of point defects.

The evolution of surface morphology could change by the different experimental conditions such as temperature and dose, and is now under investigation.

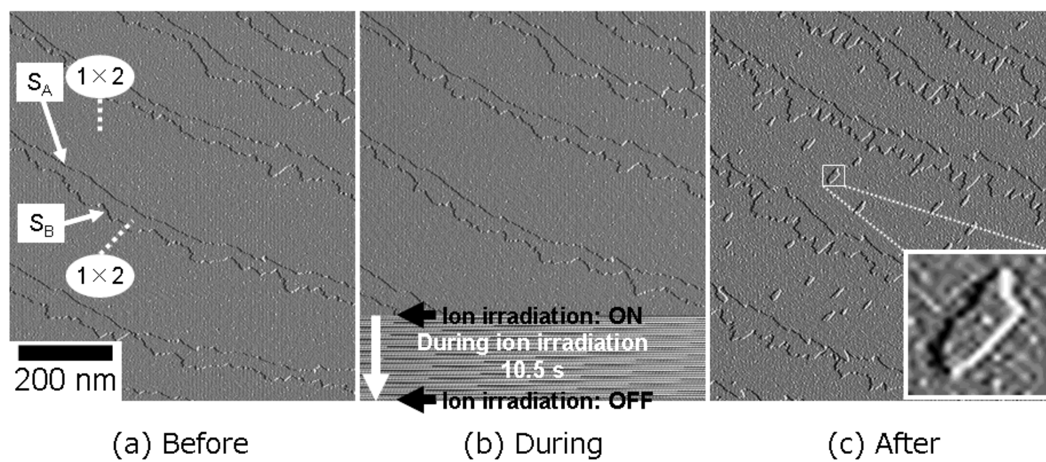

Figure 4.23: Sequential STM images of 500℃-Si(001)-2×1 surface taken (a) before, (b) during, and (c) after the ion irradiation. Ion species is P^+ with 5 keV and dose is $4 \times 10^{13} cm^{-2}$. Each image was scanned with constant height mode at a scan speed of 60 s/image. Sample bias is -2.6 V, and tunneling current is 0.08 nA.

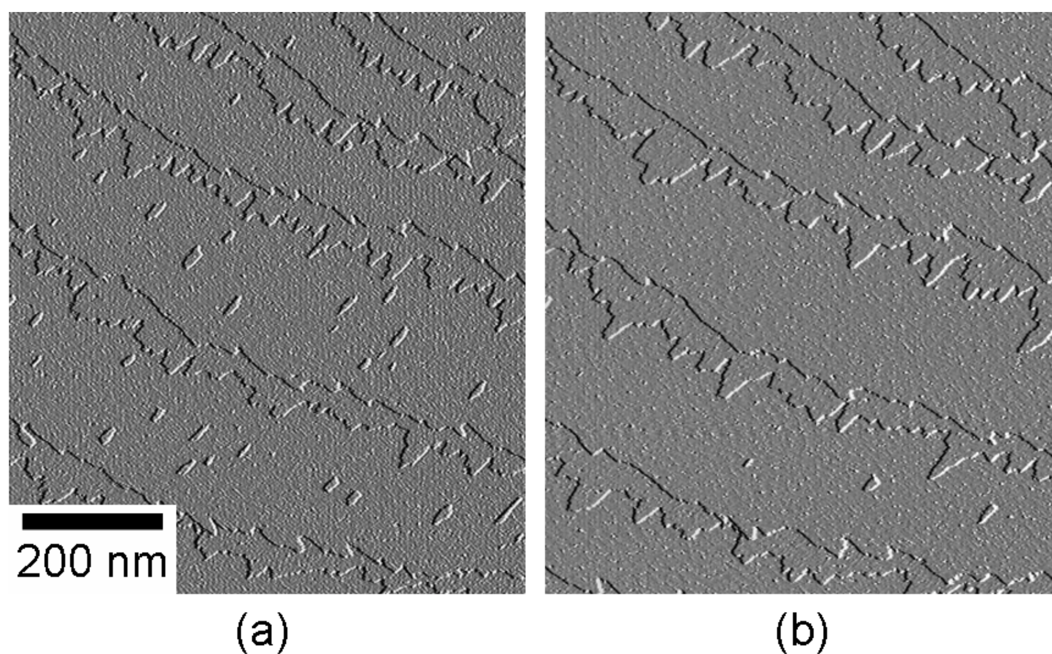

Figure 4.24: Sequential STM images of 500℃-Si(001)-7 × 7 surface taken (a) 60 s after, and (b) 1631 s after the ion irradiation. Each image was scanned with constant height mode at a scan speed of 60 s/image. Sample bias is +1 V and tunneling current is 0.08 nA.

4.3.2 Segregation of Phosphorus Atoms toward Surface

In addition with the atomistic behaviors of point defects, those of dopants need to be addressed. There exist fundamental questions regarding the interaction between point defects and implanted dopants in the vicinity of surface. For instance, are both the segregation of P atoms at the topmost surface and activation of P atoms in the vicinity of the surface related to the behavior of implantation-induced surface defects such as vacancy islands? Segregation of P atoms at surface has attracted significant interest since this could degrade device performance. Electrical activation of P atoms is also important since this determines conductivity of devices.

Figure 4.26 shows an STM image of Si(001) surface after quenching from 500℃ after 3 keV-P^+ ion irradiation as a preliminary result. In the figure, some bright sites are observed. “ Y-shape ” structure can be seen in the solid circle line, which could be Si-P heterodimmer. This structure is often observed when P atom exsit on Si(001)-2×1 [13, 14]. In this experiment, this P atom is considered to diffuse from the substrate.

The result in Fig. 4.26 demonstrates that our system has an ability to observe segregated P atoms during ion irradiation. In order to observe activation process of implanted P atoms in the vicinity of surface, hydrogen-termination of surface [15, 16] after ion irradiation and using Pt-Ir tip [17] would be effective. These are the future challenges.

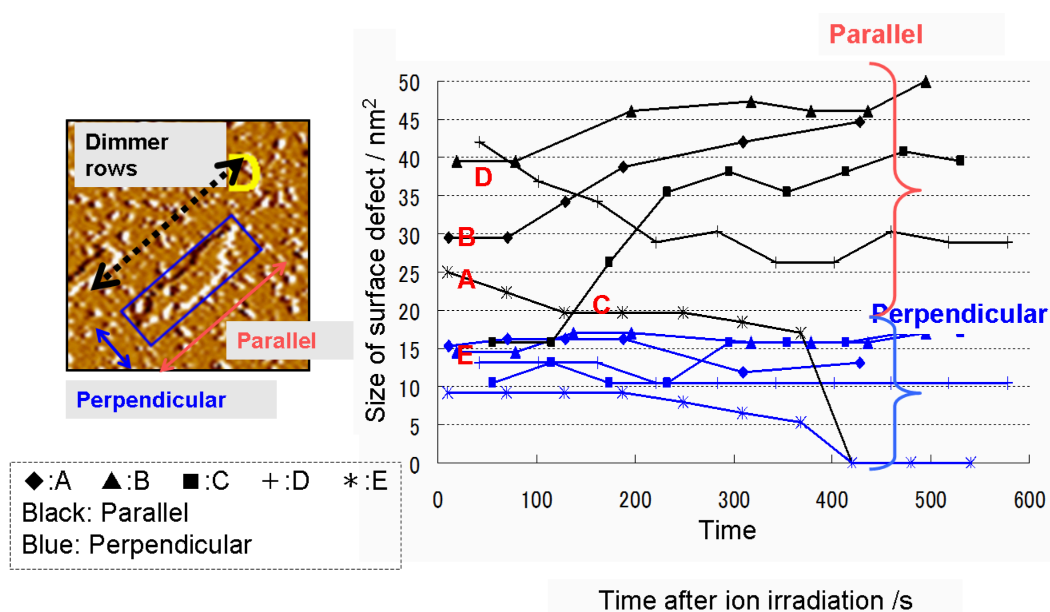

Figure 4.25: Growth rate of surface defect size along perpendicular and parallel to Si(001)-2 × 1 dimmer. " A "- "E " are sampled vacancy islands in the observation area. The Black and blue lines correspond to the components of each vacancy size parallel and perpendicular to the dimmer on the terrace.

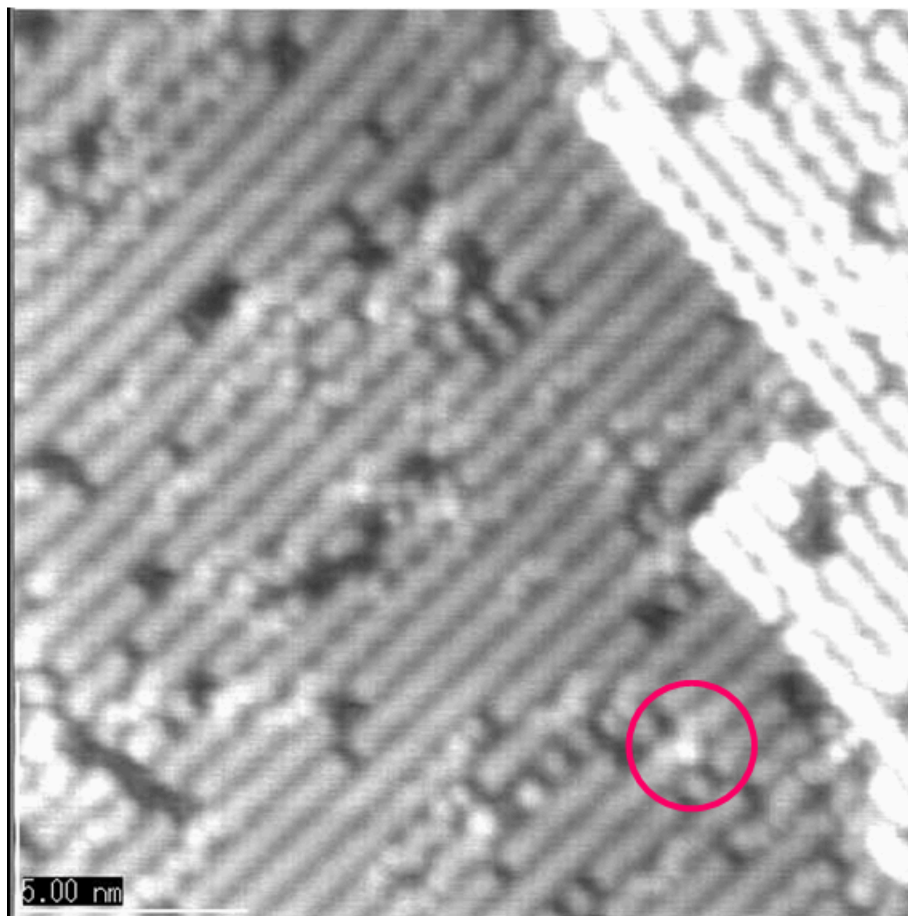

Figure 4.26: Si(001) surface modified with 3 keV-P^+ ions taken at R.T. Sample surface was first irradiated at 500℃ and annealed at the same temperature, then was quenching to R.T. Observation mode: Topography, Vs: -2.4 V, It: 0.5 nA.

4.4 Summary of Chapter 4

In this chapter, some of our results on surface nano-modification with phosphorus ion irradiation using Si(111) and Si(001) substrates are described.

First, surface modification of Si(111)-7$times$7 surface with P ions are reported. Real-time STM observation of P ion irradiation effects are shown for the first time. Ion irradiation causes nucleation of vacancy islands and retreat of step edges, resulting in removal of surface atoms. Behavior of point defects is discussed in terms of number of diffused point defects toward surface.

Then, surface modification of Si(001)-2$times$1 with P ions are reported. In addition to surface vacancy island, Si-P hetero-dimer seems to appear on the surface. Since there is no signature of P on the initial surface, the observed P atoms is supplied from the substrate after the ion irradiation. Segregation of P atoms at surface and interface is generally supposed to degrade of device performance so that the mechanism needs to be clear from the technological view point.

References

[1] Y. Wei, L. Li, and I. S. T. Tsong: Nucl. Instrum. Meth. B **115** (1996) 572.

[2] K. Yoneyama and K. Ogawa: Jpn. J. Appl. Phys. **35** (1996) 3719.

[3] P. Bedrossian: Surf. Sci. **301** (1994) 223.

[4] B. S. Swartzentruber, C. M. Matzke, D. L. Kendall, and J. E. Houston: Surf. Sci. **329** (1995) 83.

[5] P. J. Bedrossian, M. -J. Caturla, and T. Diaz de la Rubia: Appl. Phys. Lett. **70** (1997) 176.

[6] K. Shimada, T. Ishimaru, T. Yamawaki, M. Uchigasaki, K. Tomiki, T. Matsukawa, and I. Ohdomari: J. Vac. Sci. Technol. B **19** (2001) 1989.

[7] M. Uchigasaki, K. Tomiki, T. Kamioka, E. Nakayama, T. Watanabe, and I. Ohdomari: Jpn. J. Appl. Phys. Part 2 **44** (2005) L313.

[8] M. Uchigasaki, T. Kamioka, T. Hirata, T. Shimizu, F. Lin, T. Shinada, and I. Ohdomari: Rev. Sci. Instrum **76** (2005) 126109.

[9] J. P. Biersack and J. F. Ziegler: Nucl. Instrum. Methods **194** (1982) 93.

[10] K. Takayanagi, Y. Tanishiro, S. Takahashi, and M. Takahashi: Surf. Sci. **164** (1985) 367.

[11] R. L. Schwoebel, E. J. Shipsey: J. Appl. Phys. **37** (1966) 3682.

[12] H. Watanabe and M. Ichikawa: Phys. Rev. B **55** (1997) 9699.

[13] N. J. Curson, S. R. Schofield, M. Y. Simmons, L. Oberbeck, J. L. O'Brien, and R. G. Clark: Phys. Rev. B **69** (2004) 195303.

[14] G. W. Brown, B. P. Uberuaga, H. Grube, M. E. Hawley, S. R. Schofield, N. J. Curson, M. Y. Simmons, and R. G. Clark: Phys. Rev. B **72** (2005) 195323.

[15] M. Nishizawa, L. Bolotov, and T. Kanayama: Jpn. J. Appl. Phys. **44** (2005) L1436.

[16] S. Kurokawa, T. Takei, and A. Sakai: Jpn. J. Appl. Phys. **42** (2003) 4655.

[17] G. W. Brown, H. Grube, and M. E. Hawley: Phys. Rev. B **70** (2004) 121301.

.

Chapter 5

Conclusion

In order to address the atomistic behavior of implanted atoms and point defects, surface nano-modification by dopant ion irradiation was studied by performing real-time STM observation.

First, combining the LMIS/IG-STM and the new beam alignment procedure with the developed system enabled us to observe surface modification in real-time at almost every experiment. Morphological changes of Si(111)-7×7 surfaces caused by P^+ ion irradiation were observed just after the ion irradiation. Considering that in the conventional procedure 20-30 times of ion beam alignment was needed until some ion-irradiation effects was observed in real-time, the developed system has drastically improved the accuracy of the ion beam alignment. The developed system can be applicable to various types of LMISs. The LMIS-IG/STM equipped with the developed ion beam alignment system would be a powerful tool for microscopic investigation of the dynamic processes of ion irradiation effects.

Second, in order to demonstrate that the developed real-time observation system is actually an effective tool for addressing the atomistic picture of implant atoms, real-time STM observation of Si(111)-7×7 surface irradiated with Au^+ ions was performed. By using the reconstructions such as 7×7, 5×2 as rulers in nature, the

number of Au atoms on the surface was estimated from the size of reconstructed domains involving them. Although our method here is limited to observe the top-most surface, the elemental steps of surface modifications can be directly clarified with the time resolution of the STM scan period. Moreover, this method can be extended to understand the atomistic picture of the other impurities just after the ion irradiation.

Third, in order to discuss the behavior of point defects in the vicinity of solid surfaces which are irradiated with dopant ions, real-time STM observations of P^+ ion irradiation effects were shown for the first time. Ion irradiations on Si surfaces at high temperature induce nucleation of vacancy islands and retreat of step edges. During the heat treatment after the ion irradiations, the step edges continue to retreat and the vacancy islands tends to shrink and disappear. Additional irradiations increase surface vacancies, which lead to evolution of vacancy islands, coalescence of neighboring vacancy islands, and incorporation of vacancy islands into step edges. Behavior of point defects was discussed in terms of number of diffused point defects toward surface. The evolution of surface morphology would change in the different experimental conditions such as dose, temperature, and ion energy. Therefore, systematic investigation of surface modification is needed in order to extract some physical parameters such as activation energy of diffusion of point defects in the vicinity of surface.

Remarkable differences in the surface defects induced by ion irradiation have not been found yet between P and other implant species such as Si and Ar. However, some irradiation-induced structures, which may be derived from existence of P atoms, are observed. Another future challenge is to observe directly the behavior of dopants such as segregation and activation process in the vicinity of surface.

ACKNOWLEDGMENTS

The author would like to acknowledge and thank Prof. Iwao Ohdomari, who helped me find this avenue of research to begin with, and provided me with many opportunities of various activities related to the research. The author would like to thank Prof. Chuhei Ooshima, Prof. Takanobu Watanabe for their great assistance in developing this document. The author would like to thank Prof. Takashi Tanii, and Takahiro Shinada for their helpful suggestions.

Special thanks to Makoto Uchigasaki for and Kennichi Tomiki as seniors in my group for opening way of my doctor course. Also special thanks to Kou Sato for his grateful effort on his CAD and mechanical skills, as well as STM observation. Also special thanks to Yutaka Kazama for his drawing skill, as well as analysis of STM images. I would like to special thank Katsuaki Uta (UNSYS) for me developing the special ion gun installed in LMIS-IG/STM.

The author would like to very thank Hideaki Yamamoto for his care and diligence. His perfect office work saved me a number of times.

For research assistance of STM observation, preparation of tips and samples, very thanks to Eiji Nakayama, Takashi Hirata, Takuya Shimizu, Mutsuko Aoki, and Naohiro Yoshida.

Also grateful thanks to Aya Seike, Kosuke Tatsumura for giving me useful comments. I would also like to thank to the Prof. Ohdomari ’s students, in particular, Iwao Matsuya, Takeo Miyake, Yuki Sugiura.

Very special thanks to Ms. Atsuko Kobayashi, secretary for Prof. I. Ohdomari. Her kindness and tenderness bring a ray of light in this laboratory.

The author would like to express my gratitude to the late my grand mother. The author would sincerely thanks to my mother and father, Hatsue and Hideo Kamioka, my brother Takuya Kamioka.

List of Publications

Articles

1. **T. Kamioka**, K. Sato, Y. Kazama, T. Watanabe, and I. Ohdomari, " Development of an ion beam alignment system for real-time scanning tunneling microscope observation of dopant-ion irradiation ", Rev. Sci. Instrum. **79** (2008) 0730707.

2. I. Ohdomari and **T. Kamioka**, " Surface modification of silicon with single ion irradiation ", Appl. Surf. Sci. **254** (2007) 242.

3. M. Uchigasaki, **T. Kamioka**, T. Hirata, T. Shimizu, F. Lin, T. Shinada, and I. Ohdomari, " Development of liquid-metal-ion source low-energy ion gun/high-temperature ultrahigh vacuum scanning tunneling microscope combined system ", Rev. Sci. Instrum **76** (2005) 126109.

4. M. Uchigasaki, K. Tomiki, **T. Kamioka**, E. Nakayama, T. Watanabe, and I. Ohdomari, " Si island formation on domain boundaries induced by Ar ion irradiation on high-temperature Si(111)-7 $\times$ 7 dimer-adatom-stacking fault surfaces ", Jpn. J. Appl. Phys. **44** (2005) L313.

International Conference

1. **T. Kamioka**, K. Sato, Y. Kazama, T. Watanabe, and I. Ohdomari, "Real-time STM observation of Si(111)-7 $\times$ 7 surface modified by Au ion irradiation", International Symposium on Surface Science and Nanotechnology (ISSS-5), 9th-13th Nov. (2008) Tokyo, Japan.

2. Y. Kazama, **T. Kamioka**, K. Sato, T. Watanabe, and I. Ohdomari, "Real-time STM observation of defects induced by low-energy dopant ion irradiation on high-temperature Si surface", International Symposium on Surface Science and Nanotechnology (ISSS-5), 9th-13th Nov. (2008) Tokyo, Japan.

3. **T. Kamioka**, K. Sato, Y. Kazama, T. Watanabe, and I. Ohdomari, "Real-time STM observation of surface modification with low-energy dopant ion irradiation", 14th International Conference on Solid Films and Surfaces (ICSFS-14), 29th Jun.-4th Jul. (2008) Dublin, Ireland.

4. **T. Kamioka**, Iwao Ohdomari, "Real-time STM observation of surface modification with accelerated ions", International Workshop on Materials Life Science using Nuclear Probes from Heavy-ion Accelerators (SAKURA Workshop), 1st-3rd Apr. (2008) RIKEN (Wako), Japan.

5. **T. Kamioka**, M. Uchigasaki, E. Nakayama, T. Hirata, T. Shinada, J. Kurosawa, K. Uta, and I. Ohdomari, "Development of Liquid Metal Ion Gun / UHV Scanning Tunneling Microscope Combined System (LM-IG / UHV-STM)", 8th International Conference on Atomically Controlled Surfaces, Interfaces and Nanostructures (ACSIN 8), 21th Jun. (2005) Stockholm, Sweden.

6. **T. Kamioka**, M. Uchigasaki, E. Nakayama, T. Hirata, and I. Ohdomari, "Real-time high-temperature STM observation of defects induced by Si ion

irradiation on Si(111)-7×7 surface ", International Symposium on Molecular Nano-Engneering and its Development into Microsystems: Semiconductor Nanotechnology, 20th-21th Dec. (2004) Tokyo, Japan.

7. **T. Kamioka**, M. Uchigasaki, E. Nakayama, T. Hirata, and I. Ohdomari, " Nanoscale Modification of Si Surface: Dynamics of Defects Induced by Ar^+ Ion Irradiation ", Ext. Abst. 21COE International Symposium on ' Practical Nano-Chemistry ', 10th-11th Dec. (2003) Tokyo, Japan.

8. M. Uchigasaki, **T. Kamioka**, E. Nakayama, T. Hirata, and I. Ohdomari," Fundamental process of nanoscale modification with ion irradiation on solid surface ", Ext. Abst. International Symposium on Molecular Nano-Engneering and Its Development into MicrosystemsMolecular Nano-engineering for Bio-Science and Technology Applications, p.19 (2003).

9. M. Uchigasaki, **T. Kamioka**, E. Nakayama, T. Hirata, T. Watanabe, and I. Ohdomari, " Real-time high-temperature STM observation of Ar ion induced surface voids on Si(111) : dependence on ion irradiation energy ", Ext. Abst. The 7th International Conference on Atomically Controlled Surfaces, Interfaces and Nanostructures (ACSIN-7), p.375 (2003).

10. M. Uchigasaki, **T. Kamioka**, E. Nakayama, T. Tanii, T. Watanabe, and I. Ohdomari, " Real-time high-temperature STM observation of Ar ion induced surface defects on Si(111) ", Ext. Abst. The 9th International Conference on the Formation of Semiconductor Interfaces (ICFSI-9), p.149 (2003).

11. K. Tomiki, M. Uchigasaki, **T. Kamioka**, T. Watanabe, and I. Ohdomari, " High-temperature in-situ STM observation of Si(111) surfaces with steps for studying nanoscale modification with ion irradiation ", Ext. Abst. 13th International Conference on Ion Beam Modification of Materials (IBMM-13), 004 (2002).

12. **T. Kamioka**, M. Uchigasaki, K. Tomiki, T. Watanabe, and I. Ohdomari, " High-temperature in-situ STM observation of surface defects induced by Ar ion irradiation on flat Si(111) surface ", Ext. Abst. 11th International Conference on Solid Films and Surfaces (ICSFS-11), p.71 (2002), Marseille, France.

Domestic Confernce

1. K. Sato, **T. Kamioka**, Y. Kazama, and I. Ohdomari, " Real-time STM observation of surface nano-modification by dopant ion irradiation on Si(001) ", The 69th Autumn Meeting of Japanese Society of Applied Physics and Related Societies, Sep. (2008) Nagoya, Japan.

2. **T. Kamioka**, K. Sato, Y. Kazama, and I. Ohdomari, " Annealing time dependency of low-energy ion irradiation effects on high-temperature Si(111) surface ", The 69th Autumn Meeting of Japanese Society of Applied Physics and Related Societies, Sep. (2008) Nagoya, Japan.

3. **T. Kamioka**, K. Sato, Y. Kazama, and I. Ohdomari," In-situ STM observation of defects induced by low-energy dopant-ion irradiation on high-temperature Si surface ", The 55th Spring Meeting of Society of Applied Physics, Mar. (2008) Chiba, Japan.

4. K. Sato, **T. Kamioka**, Y. Kazama, and I. Ohdomari, " Development of an ion beam alignment system for real-time STM observation of dopant-ion irradiation process ", The 55th Spring Meeting of Society of Applied Physics, Mar. (2008) Chiba, Japan.

5. **T. Kamioka**, K. Sato, and I. Ohdomari, " In-situ STM observation of Si surface modified by low-energy dopant-ion beam ", The 68th Autumn Meeting

of Japanese Society of Applied Physics and Related Societies, Sep. (2007) Hokkaido, Japan.

6. **T. Kamioka**, M. Uchigasaki, and I. Ohdomari, " Real-time STM observation of low-energy metal-ion irradiation on high-temperature Si(111) surface (II) ", The 54th Spring Meeting of Japan Society of Applied Physics, Mar. (2007), Tokyo, Japan.

7. **T. Kamioka**, M. Uchigasaki, and I. Ohdomari, " Real-time STM observation of low-energy metal-ion irradiation on high-temperature Si(111) surface ", The 67th Autumn Meeting of Japan Society of Applied Physics and Related Societies, Aug.- Sep. (2006), Shiga, Japan.

8. **T. Kamioka**, F. Lin, M. Uchigasaki, T. Hirata, T. Shimizu, and I. Ohdomari, " STM observation of low-energy dopant-ion irradiation effect on high-temperature Si(001) surface ", The 53rd Spring Meeting of Japan Society of Applied Physics, Mar. (2006), Tokyo, Japan.

9. **T. Kamioka**, M. Uchigasaki, T. Hirata, and I. Ohdomari, " Formation of Si(111)5 $\times$ 2-Au in vacancy clusters induced by Au^+ irradiation onto high-temperture Si(111)7$\times$7 surface ", The 66th Autumn Meeting of Japan Society of Applied Physics and Related Societies, Sep. (2005), Tokushima, Japan.

10. T. Hirata, M. Uchigasaki, **T. Kamioka**, I. Ohdomari, " Real-time STM observation of nano modification dynamics on ion-irradiated semiconductor surface ", The 66th Autumn Meeting of Japan Society of Applied Physics and Related Societies, Sep. (2005), Tokushima, Japan.

11. **T. Kamioka**, M. Uchigasaki, E. Nakayama, T. Hirata, and I. Ohdomari, " Real-time STM observation of defects formed on domain boundary induced

by Si ion irradiation on Si(111)-7 × 7 surface ”, The 52nd Spring Meeting of Japan Society of Applied Physics, Apr. (2004), Saitama, Japan.

12. **T. Kamioka**, M. Uchigasaki, E. Nakayama, T. Hirata, and I. Ohdomari, “ Real-time high-temperature STM observation of defects induced by Si ion irradiation on Si(111)-7×7 surface ”, The 65th Autumn Meeting of Japan Society of Applied Physics and Related Societies, Sep. (2004), Miyagi, Japan.

13. **T. Kamioka**, M. Uchigasaki, E. Nakayama, T. Hirata, T. Shinada, J. Kurosawa, I. Ohdomari, and K. Uta, “ Development of Liquid Metal Ion Gun / UHV Scanning Tunneling Microscope Combined System (LM-IG / UHV-STM) ”, The 51st Spring Meeting of Japan Society of Applied Physics, Mar. (2004), Tokyo, Japan.

14. M. Uchigasaki, **T. Kamioka**, E. Nakayama, T. Hirata, and I. Ohdomari,“ Fundamental formation process of surface vacancy induced by Ar ion irradiation on high temperature Si(111) ”, The 51st Spring Meeting of Japan Society of Applied Physics, Mar. (2004), Tokyo, Japan.

15. M. Uchigasaki, **T. Kamioka**, E. Nakayama, T. Hirata, T. Watanabe, and I. Ohdomari, “ Area extension of Si island induced by Ar ion irradiation on high temperature Si(111) ”, The 64th Autmun Meeting of Japan Society of Applied Physics and Related Societies, Aug. (2003) Fukuoka, Japan.

16. M. Uchigasaki, K. Tomiki, **T. Kamioka**, E. Nakayama, T. Watanabe, and I. Ohdomari, “ Temperature dependence on early-stage expansion of surface vacancy induced by Ar ion irradiation on Si(111) ”, The 50th Spring Meeting of Japan Society of Applied Physics, Mar. (2003), Kanagawa, Japan.

17. M. Uchigasaki, K. Tomiki, **T. Kamioka**, T. Watanabe, and I. Ohdomari, “ Real-time STM observations of process of Ar ion hot implantation on Si(111)

(III) ”, The 49th Spring Meeting of Japan Society of Applied Physics, Mar. (2002), Kanagawa, Japan.

18. K. Tomiki, M. Uchigasaki, **T. Kamioka**, T. Watanabe, and I. Ohdomari, “ Real-time STM observations of process of Ar ion hot implantation on Si(111) (II) ”, The 49th Spring Meeting of Japan Society of Applied Physics, Mar. (2002), Kanagawa, Japan.

19. **T. Kamioka**, M. Uchigasaki, K. Tomiki, T. Watanabe, and I. Ohdomari, “ Real-time STM observations of process of Ar ion hot implantation on Si(111) (I) ”, The 49th Spring Meeting of Japan Society of Applied Physics, Mar. (2002), Kanagawa, Japan.

20. **T. Kamioka**, M. Uchigasaki, K. Tomiki, T. Watanabe, and I. Ohdomari, “ Real-time STM Observation of surface defects induced by Ar ion irradiation on Si(111) (In Japanese) ”, The 9th Micro Technology Laboratory Symposium, Mar. (2002) Tokyo, Japan.

21. M. Uchigasaki, K. Shimada, T. Ishimaru, K. Tomiki, **T. Kamioka**, T. Watanabe, and I. Ohdomari, “ Real-time high-temperature STM observation of defects induced by Ar ion irradiation on Si(111)7 $\times$ 7 surface ”, The 62nd Autumn Meeting of Japan Society of Applied Physics and Related Societies, Sep. (2001), Nagoya, Japan.